Optimal energy management strategy for the Honda Civic IMA

van Baalen, J.

Award date:
2006

Optimal Energy Management Strategy for the Honda Civic IMA

J.v.Baalen

DCT 2005.148

Master's thesis

Coach(es): ir. T.Hofman

Supervisor: Prof.dr.ir. M.Steinbuch

Technische Universiteit Eindhoven
Department Mechanical Engineering
Dynamics and Control Technology Group

Eindhoven, January, 2006

Preface

This report is the crowning glory of the work that I have delivered during my study on the TU/e. I have had bad times in which I wished I never started this study but I have had a lot of very nice times as well. I've learned many things, also besides my study, that I can and will use in the future. I've learned to know new people which are now close friends and I would like to thank everyone who has contributed to the very nice time I have had during my study.

Additionally I would like to thank Theo Hofman, who has made me enthusiastic and has coached me very intensively while we were working on the same subject. Many thanks to Maarten Steinbuch as well, who always had time for a personal talk while he was supervising me during the last years of my study. I would never have finished this report without the support of my parents and my boyfriend. Thanks!

Samenvatting

De vraag naar energiezuinige auto's neemt snel toe door de mondiale milieuproblematiek en naderende uitputting van traditionele energiebronnen. Door voertuigen te hybridiseren neemt het brandstof verbruik aanzienlijk af. Onder hybridizeren verstaat men het toevoegen van een tweede vermogensbron, waardoor de eerste vermogensbron in optimalere werkpunten kan worden bedreven en rem-energie kan worden gerecupereerd en hergebruikt. Een regelstrategie, de *Energy Management Strategy (EMS)*, is nodig om de vermogens uit beide bronnen te regelen. Door het optimaliseren van de EMS wordt het brandstofverbruik van een hybride voertuig gereduceerd. De Honda Civic IMA, een parallel-hybride auto, is in dit verslag gebruikt als een case study. Dit voertuig is volledig gemodelleerd, de modellen zijn gevalideerd en later gebruikt in *Dynamic Programming (DP)*. Deze optimalisatie-methode is gebruikt om de meest optimale EMS voor de IMA te bepalen. Omdat DP niet geschikt is voor online implementatie, zijn de resultaten van DP geanalyseerd en is een *rule based controller* ontworpen. Deze regelt aan de hand van een eenvoudige strategie, bestaande uit heuristische regels, de vermogensstroom in het voertuig.

De doelstelling van het onderzoek luidt:

Ontwerp een optimale Energy Management Strategy voor de Honda Civic IMA met behulp van Dynamic Programming

Uit de DP-simulaties kunnen een aantal conclusies worden getrokken over het gebruik van de componenten (elektromotor, verbrandingsmotor en batterij) en de bijbehorende efficiencies. Het gebruik van de hybride modes en de brandstofbesparing die het oplevert is duidelijk te zien, net als de manier waarop het vermogen wordt verdeeld over de verbrandings- en elektromotor. De resultaten uit DP zijn geanalyseerd en een *power split rule based controller* is hiervan afgeleid. Het brandstofverbruik blijkt goed overeen te komen met de resultaten van DP. Deze strategie is echter gevoelig voor een andere cyclus (hoger brandstofverbuik en andere *power split* strategie). De *torque split* resulterend uit DP lijkt minder gevoelig te zijn voor voor het verschil in cyclus. Daarom is deze ook vertaald naar een *rule based controller*. Deze regelstrategie geeft in alle bovengenoemde opzichten goede resultaten.

Het totale brandstof verbruik van deze geïmplementeerde regelstragie komt uit op $4.77\ l/100km$ op de Europese rijcyclus. Ten opzichte van een conventioneel voertuig is dit een besparing van 29.4 %. Vergeleken met het huidige gebruik van de Honda Civic IMA wordt slechts 2.5 % bezuinigd. Aangezien het onderzoeksprogramma "Impulse drive" -waar deze studie een onderdeel van is- zich een brandstofvermindering van 50 tot 75 % ten opzichte van een conventioneel voertuig ten doel heeft gesteld, moeten andere methoden dan de optimalisatie van de EMS worden gebruikt om dit te realiseren.

Onderzoek naar frequenter of langer gebruik van *idle stop mode* kan een aanzienlijke brandstofbesparing opleveren. Verder kan het systeem rendement (en dus de brandstofbesparing) verhoogd worden door het ontwerp van nieuwe componenten of het gebruik van bestaande componenten in nieuwe systeemconfiguraties. De keuze van de component grootte speelt hierin ook een rol. DP is een handig hulpmiddel om inzicht te krijgen in de meest optimale EMS voor deze nieuwe configuraties.

Abstract

Due to environmental pollution and approaching exhaustion of traditional energy sources, the demand for fuel economic cars has grown. Fuel consumption reduces considerably by hybridizing the vehicle, which implies adding a secondary power source to a vehicle. The primary power source can then be used at more optimal operating points and brake energy can be recuperated and re-used. A control strategy is necessary to control the power flow from both sources. This specific type of control strategy is called an Energy Management Strategy (EMS). The fuel consumption can be reduced by optimizing the EMS. The Honda Civic IMA, a parallel hybrid car, is used as a case study in this report. This vehicle is completely modelled, this model is validated and has been used in Dynamic Programming (DP) later on. DP is an optimization routine that is used to define the most optimal EMS for the IMA. However, DP can not be used for online implementation. The results of DP have been analyzed and a rule based controller has been derived. This controller controls the power flow in the system with a simple heuristic strategy.

The goal of the thesis can be defined as:

Design an optimized Energy Management Strategy for the Honda Civic IMA with the help of Dynamic Programming.

From the DP simulations, conclusions can be drawn with respect to the usage of the vehicle components (Internal Combustion Engine, Electro Motor and battery) and the corresponding efficiencies. The usage of hybrid modes and the fuel savings that are obtained can be seen clearly, as well as the power split between the electro motor and the internal combustion engine. The results of DP are analyzed and a power split rule based controller is derived. The fuel consumption of this controller resembles the results of DP, however the controller seems to be very sensitive for different drive cycles (higher fuel consumption and other power split). The torque split resulting from DP seems to be less sensitive for different cycles. That is why a torque split rule based controller has been designed as well. This controller gives good results in all above mentioned respects.

The total fuel consumption of this controller is $4.77\ l/100km$ on the European drive cycle which is $29,4$ % lower than a comparable conventional vehicle. However, when this result is compared to the fuel usage of the Honda Civic IMA, a decrease of only 2.5 % is achieved. This study is a part of the research programme "Impulse Drive". The goal for this program is to decrease the fuel consumption with 50 - 75 %, with respect to comparable conventional vehicles . Another method than optimizing the EMS has to be used to achieve this goal.

Investigation to more frequent or longer usage of the idle stop mode can result in a significant fuel consumption. Furthermore, the system efficiency (so the fuel savings as well) can be increased by the design of new components or the usage of existing components in new system configurations. The choice for the component size is relevant in this design as well. DP is a helpful tool to get more insights in the optimal EMS for these new configurations.

Contents

Introduction

The number of cars in the world has tripled in the last twenty years. This has caused an enormous growth of fossil fuel consumption which leads to large-scale environmental pollution. For this reason, the demand for fuel economic vehicles and cleaner alternatives has grown. One way to improve the fuel economy of a vehicle is to hybridize it by adding a secondary power source to the car. Due to hybridization, brake energy can be recuperated and more optimal operating points can be used. A control strategy is needed to control the power flow from primary and secondary power source to the vehicle. This specific type of control strategy is also called an **Energy Management Strategy (EMS)**. The fuel consumption of existing **Hybrid Electric Vehicles (HEV's)** has already been reduced with $\pm$ 25% compared to a conventional vehicle. The NWO (The Dutch Organization for Scientific Research) research programme "Impulse Drive" focusses on the generic design process of a hybrid vehicle with more significant reduction of fuel consumption (50 % - 75 %) on a representative drive cycle. This thesis is a part of that research programme: the reduction of fuel consumption for hybrid vehicles due to the optimization of the Energy Management Strategy. A case study of the energy flow in hybrid vehicles is made for the **Honda Civic IMA**, one of the first commercial available hybrid vehicles. This car has a fuel consumption of $4.9\ l/100km$ on the European drive cycle.

Energy Management Strategies

The main question during Energy Management Strategy optimization for Hybrid Electric Vehicles is: what needs to be the battery power output given a certain vehicle power demand? For this specific problem, an optimal EMS is calculated with the optimization routine **Dynamic Programming (DP)**. The advantage of DP is that the implementation of non-linear behaviour of system component efficiencies and operating point constraints is easy. One of the disadvantages is "the curse of dimensionality". For large grid sizes or more control inputs, the computation time grows exponentially. Furthermore, grid inaccuracy is a problem. DP is an inherently non-causal technique and needs future information about the drive cycle. Therefore DP is found unsuitable for online implementation. In practical implementations, the EMS in controlled by a **Rule Based (RB)** controller which determines the power distribution instantaneously. DP is used to get insights in energy management and by analyzing the results, the rule based controller has been derived.

Problem definition

The goal of this thesis is to design an optimized Energy Management Strategy for the Honda Civic IMA with the help of Dynamic Programming.

Furthermore, the influence of the

- system components (efficiencies, constraints),
- hybrid functions,
- and drive cycles

on the fuel consumption and EMS resulting by DP is investigated. A rule based controller is derived and used to simulate different drive cycles. The outcome gives more insight into the robustness of the designed Rule Based Controller.

Outline

In the first chapter of this report, the general idea of hybrid vehicles is explained. In addition, dynamic programming is highlighted in an overview of the research currently being done on the subject of energy management for HEV's. Since the Honda Civic IMA is used as a case study, a model is developed for further usage in the design of a control strategy in Chapter 2. A backward facing Quasi Static model has been made to model power flow in the vehicle and a dynamic model is constructed to calculate the driving power needed over a prescribed drive cycle in Chapter 3.1. The models have been validated by comparing suppliers data with simulations over a standard drive cycle in Chapter 3.2. These simulations are used as a reference for the results obtained with DP. The theory behind Dynamic Programming and the implementation of the EMS problem into a DP problem are described in Chapter 4. To define the influence of the system components on the strategy, the implementation is done in several steps. The influence of three different subjects (components, mean efficiency and hybrid modes) on the fuel consumption and the EMS resulting from DP are investigated in Chapter 5. The most optimal EMS is analysed and a rule based controller is derived and tested (Chapter 6). Finally, the conclusions and recommendations of this thesis are presented in Chapter 7 and 8.

Chapter 1

Hybrid Electric Vehicles

Hybrid Electric Vehicles (HEV's) are able to reach high fuel economy as well as low emissions without compromising driveability. A hybrid vehicle has a **Primary power source (P)**, which in most cases is an internal combustion engine (ICE), and a **Secondary power source (S)** e.g. an electro motor (see Figure 1.1). S connects to the system P with the help of a **Transmission (T)** [9], [11]. The **Controller (C)** distributes the power flow between P, S and the **Vehicle wheels(V)**. The electro motor retrieves its energy from a bidirectional energy accumulator (e.g. super capacitor, a flywheel or battery) and is able to assist the engine. When the car brakes, the electro motor functions as a generator and the recovered energy is stored in the accumulator. This energy can be used later to assist the primary power source. Compared to conventional cars this technology decreases fuel consumption with $\pm$ 25 %.

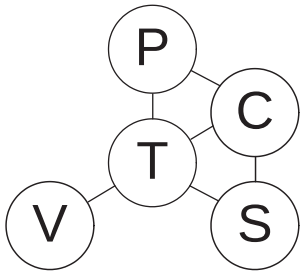

Figure 1.1: Schematic representation of a Hybrid Electric Vehicle, P = Primary power source, S = Secondary power source, T = Transmission technology, C = Controller, V = Vehicle wheels

Several driving functions have been defined for vehicles, such as fuel consumption, emissions, comfort, driveability and safety [10], [9], [6]. A hybrid vehicle improves mainly three driving functions: fuel consumption, emissions and driveability. The fuel consumption and emission can be improved by the possibility to use different hybrid modes while the driveability is improved due to the extra torque delivered by the secondary power source.

In the following sections an introduction is given about the three existing HEV configurations and the hybrid drive modes which describe the usage of the primary and secondary power source for parallel HEV's.

1.1 HEV system configurations

HEV's can have three different system configurations: series, parallel and series-parallel [8], [27] see Figure 1.2.

In the **series** configuration the electro motor drives the vehicle on its one. The power is supplied by an engine-driven generator and/or the battery. TNO has developed a series hybrid car by placing a motor-generator set into a Volkswagen Beetle.

In a **parallel** configuration primary and secondary power source are both mechanically connected to the same drive shaft. This implies that the Internal Combustion Engine (ICE) and the Electro Motor (EM) can power the vehicle individually or simultaneously. The Honda Civic IMA is an example of a parallel hybrid vehicle.

The Toyota Prius is an example of a hybrid car with a **series-parallel** configuration in which the parallel and serial mode occur simultaneously. The power of the engine goes via a planetary gear set through both a mechanical (directly) and an electrical (via a motor-generator set) path to the wheels.

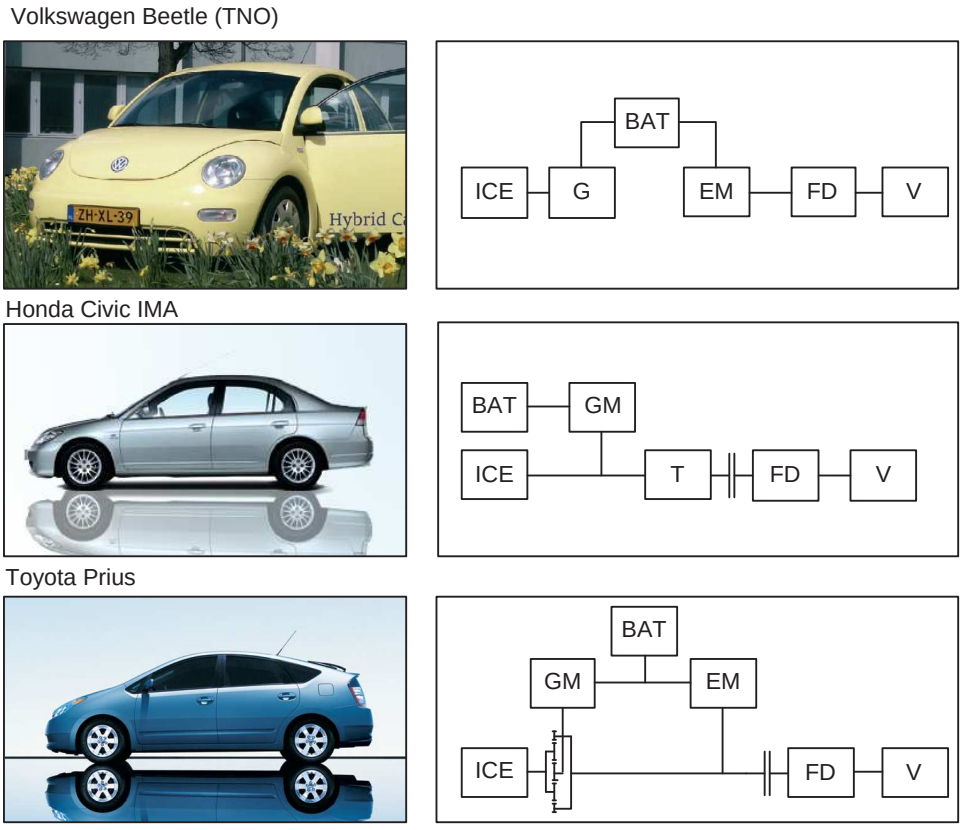

Figure 1.2: The Volkswagen Beetle (series) made by TNO, the Honda Civic IMA (parallel), and the Toyota Prius (series-parallel), ICE = Internal Combustion Engine, BAT = battery, EM = Electro Motor, GM = Generator-Motor, G = Generator, T = Transmission, FD = Final Drive, V = Vehicle

1.2 HEV modes

Due to the hybridization of a vehicle, the power flow inside the vehicle can go through various paths in different directions [4], [27], [23]. Each possibility can be represented by a driving mode. Diverse options are possible for the three configurations. This thesis focuses on the parallel configuration with the Honda Civic IMA as case study. Therefore the 6 different modes for parallel HEV's are described below and can be seen in Figure 1.3.

a. **Engine driving (E)**: the ICE delivers all requested driving power.

b. **Motor Assist (MA)**: both engine and electro motor deliver the requested driving power. The fuel consumption decreases because the engine delivers less power, while the dynamic performance of the vehicle is maintained.

c. **Motor driving (M)**: the requested driving power is delivered by the motor only. This mode avoids very low engine efficiency at low powers. During motor driving the engine is idling or off.

d. **Charging (CH)**: the engine delivers power for both vehicle propulsion and battery recharging. The engine runs at higher power than requested for driving. The power surplus is used to charge the battery.

e. **Brake Energy Recovery (BER)**: when the car decelerates, 60% of the decelerating power, which normally would have been dissipated by the front wheel brakes, is recovered by the electro motor. It is not possible to recover 100 % of the brake power at the front wheels because of unwanted dynamical behaviour [25]. The recovered energy is stored in an accumulator and can be used later. This proces is called Brake Energy Recovery (BER).

f. **Idle Stop (IS)**: when the engine is warm, idle stop can be used to safe fuel. During full vehicle stops, the primary power source shuts down. Meanwhile, the auxiliaries are powered from the battery. In a split second the engine can be started again by the electro motor. This causes a significant reduction of fuel consumption during traffic jams and city driving.

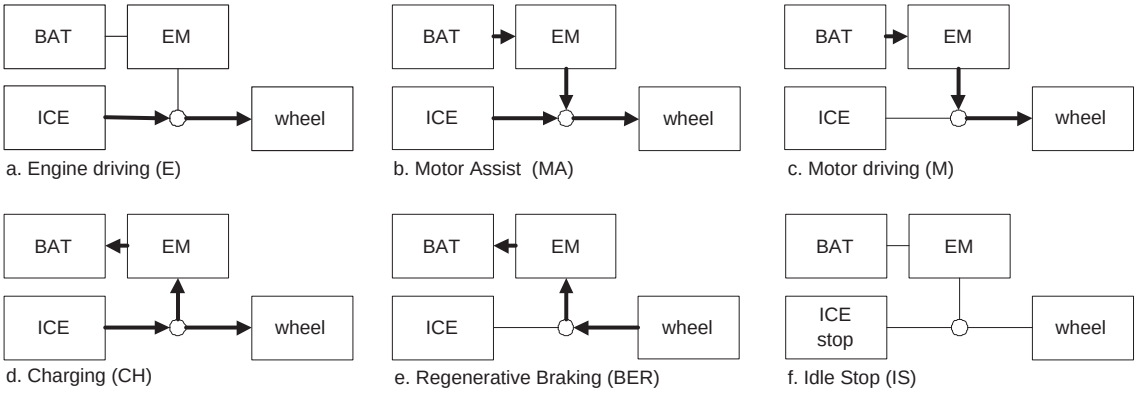

Figure 1.3: The six driving modes of a HEV

The control of the hybrid modes and the power delivered by the ICE and EM during these modes is called the Energy Management Strategy. Optimizing this strategy leads to better fuel consumption. An investigation of methods used for EMS optimization has been made and a summary is given in the next section.

1.3 Energy Management Strategies

Numerous energy management strategies have been developed to control the driving modes and define the power split for HEV's. **The goal of energy management is to lower the fuel consumption by controlling the power flow in the HEV**. In practice, these energy management strategies are rule based controllers. The NREL (the National Renewable Energy Laboratory) has completely measured the Honda Insight, the predecessor of the Honda Civic IMA, and has derived a rule based controller for the energy management in the system. An abstract of the measurement report [13] is given in Appendix C. The energy management strategy of the Honda Insight is based on the requested drive torque. When the torque $T_{drive} > 20\ Nm$, the electro motor assists the ICE ($1.0\ l$) with $T_{em} = 10\ Nm$. The motor assist and motor only mode are not used to avoid bad engine efficiency at low powers. The concept of the IMA is based on engine downsizing which means that the electro motor is used to improve the driveability.

The research area concerned with energy management has grown very fast in the last five years. Many computation methods of all kinds have been used to calculate the optimal Energy Management Strategy, e.g. Adaptive Control [32], Neural Networks, Fuzzy Logic control [27], Quadratic Programming [15], Rule Based Control [18], H_∞ Control [26] and Model Predictive Control [15]. These methods will not be discussed here because this report focuses on another extensively used method: Dynamic Programming.

Dynamic Programming

Dynamic Programming (DP) is a technique that **guarantees a global optimal solution.** This routine optimizes in relation to a time horizon instead of a fixed point in time. It requires heavy computation and a predefined trajectory has to be known to use DP. Consequently, the dynamic optimization algorithm is inherently non-causal and therefore not implementable online. However, it can be used as a benchmark to compare other methods and optimize them. For these reasons DP is used in this EMS study.

In most cases the implementation of DP is more or less the same. The defined control input variable is divided into a grid, which defines the states of the system. For computing the costs from one state to the next, a cost or objective function has to be defined. This cost function consists at least of the fuel consumption rate. Sometimes other aspects are added to the cost function such as a final SOC (State of Charge of the battery) penalty or emission- and driving comfort penalties. At each step, the minimization is performed subject to constraints of the state- and control variables. This ensures that the engine torque and speed, SOC, motor torque and speed, gear shift ratios etc. are all within their corresponding bounds. For every point, only the most optimal cumulative costs are saved in the cost-to-go Matrix. The optimal path can be found by a backward search in this matrix.

The theory of Dynamic Programming is explained further in Chapter 4. Many articles have been written about this subject. The work of three research groups that have used DP extensively is discussed next.

The research group under supervision of Professor Grizzle [16], [17], [20], [21], [19] from the University of Michigan has designed a simple intuitive rule based controller for a hybrid truck in which they define a Normal, Charging and Braking mode. The mode change is a result of the required power demand. A DP controller is designed as well and the outcomes have been used as a benchmark. By analyzing the strategy resulting from DP, the rule based controller has been improved for gear shift, power split and recharging control. Later on, the emissions have been taken into account as well. When this controller was used for a different trajectory, it turned out to be not optimal anymore. To avoid this problem, the power demand from the driver was modelled as a random Markov Process. The new optimal control strategy was obtained by using Stochastic Dynamic Programming (SDP) and

from these results, a new rule based controller was derived. This lead to better results.

Another university that works on optimizing the EMS with DP is the Tsinghua University [34], [35], [36]. They have introduced a four step method to design an EMS for Hybrid vehicles. A hybrid dynamical system theory is formulated for the HEV control system, that incorporates both continuous and discrete dynamics. This model contains different driving modes, e.g. a regeneration mode, a power split mode etc. Then Sequential Quadratic Programming (SQP) is used to optimize the power distribution by optimizing the total system efficiency and an improved DP technique is applied to solve the complex operating mode transition problem. In this DP algorithm, SQP is also used to calculate at each stage the optimal engine torque, which is not a global optimal solution but a good approximation. In doing this, the grid reduced extremely. The final total computation time decreased four times. From the DP results, a rule based and a fuzzy logic based control were designed and finally these rules have been optimized by a Genetic Algorithm.

At the Swiss Federal Institute (ETHZ), the research group of Professor Guzella has been working on hybrid vehicles for a couple of years as well. After comparing various rule based controllers, the major drawback was that all numerical values used in the rules did not have a physical meaning and therefore had to be calibrated for each particular driving condition [29]. In [31] and [28], they propose a method to define and calculate an equivalence factor that weighs the fuel energy with the electrical energy use in order to build a cost function which takes the time variations of both energy forms into account. Selecting the optimal value of the control variable at each time instant lead to an optimal control strategy. The result of this strategy approached the solution of the global optimum defined by DP (which uses an a priori known drive cycle). This real-time controller is called the Equivalent Consumption Minimization Strategy (ECMS) and only needs the current status of the power train to calculate the strategy. In [30] the T-ECMS has been developed. With this method, the control parameters are continuously estimated on-board by using data from static route mapping and telemetry. This real-time controller approaches the global solution very well.

Chapter 2

Modelling of the Honda Civic IMA

A model of the Honda Civic IMA is necessary for the usage in DP. This model exists of two parts: a quasi static model to describe the power flow in the system and a dynamic vehicle model to compute the power needed for driving over a prescribed drive cycle. Both models are presented in this chapter.

The IMA is available with two different transmissions, a manual and a Continuous Variable Transmission (CVT). The version with Manual Transmission (MT) is discussed in this chapter. A similar model has been made for the IMA with CVT in Appendix G and the results obtained for this model with DP are shown as additional information for the interested reader. Due to lack of time is chosen to focus on the MT version in this thesis.

A backward facing quasi static approach is an often used method to model the power flow in vehicles [8]. This method has been used to model the Honda Civic IMA as well (see Figure 2.1). In a Quasi static approach, the velocity and acceleration are assumed to be constant in a certain time interval. A backward facing model implies that the *input* variables are speed v and acceleration a of the vehicle, while the *output* is the input power needed by the ICE, P_{fuel}.

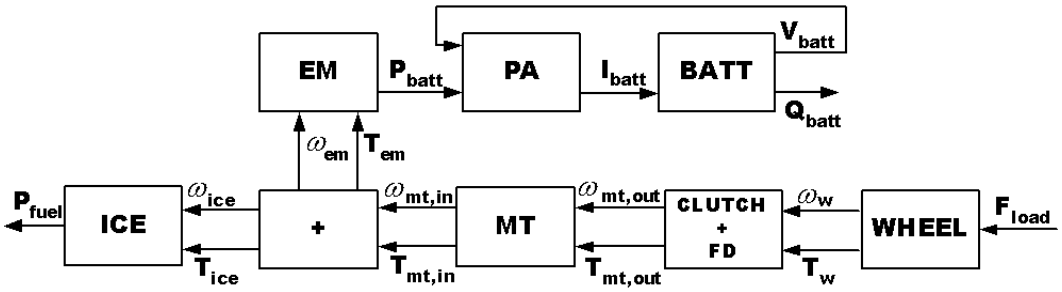

Figure 2.1: The quasi static representation of the parallel layout of the Honda Civic IMA

In the IMA, the Internal Combustion Engine and the electro motor are connected to the input of the Manual Transmission Transmission (MT) through the same shaft. This automatically implies the same shaft speeds for ICE and EM. The electro motor has a bidirectional connection with the battery (BATT) through which energy recuperation can take place as well. The Power Amplifier (PA) controls the voltage V_{batt} and current I_{batt} from and to the battery. The clutch is connected to the output shaft of the MT and via the Final Drive (FD) the torque is transmitted to the wheels.

The vehicle parameters of the IMA can be found in Appendix D. The data are obtained from different sources such as the Advanced Vehicle Simulator (ADVISOR), a Matlab application developed by the National Renewable Energy Laboratory (NREL) [24], the website New-cars.com [3], the website of Honda [1] and the digital encyclopedia of the Honda Insight (the older hybrid model) [2]. Because most of the models (ICE, EM, MT) are not explicitly available, models of other resembling components have been used. In the next sections the models for all components are presented. The wheels are not modelled because the assumption of no wheel slip has been made.

2.1 Primary power source: Internal Combustion Engine

The primary power source in the Honda Civic IMA is a 1.39 l gasoline SI Otto Internal Combustion Engine. The maximum power of this engine is 61 kW at 5700 rpm and the maximum torque is 119 Nm at 3300 rpm. An engine map for this specific engine is not available. A map of a comparable modern 1.4 l engine has been used. The engine has a maximum power of 58 kW at 5700 rpm and a maximum torque of 120 Nm at 3500 rpm. The assumption that this engine map is representative for the IMA is validated in Section 3.2.

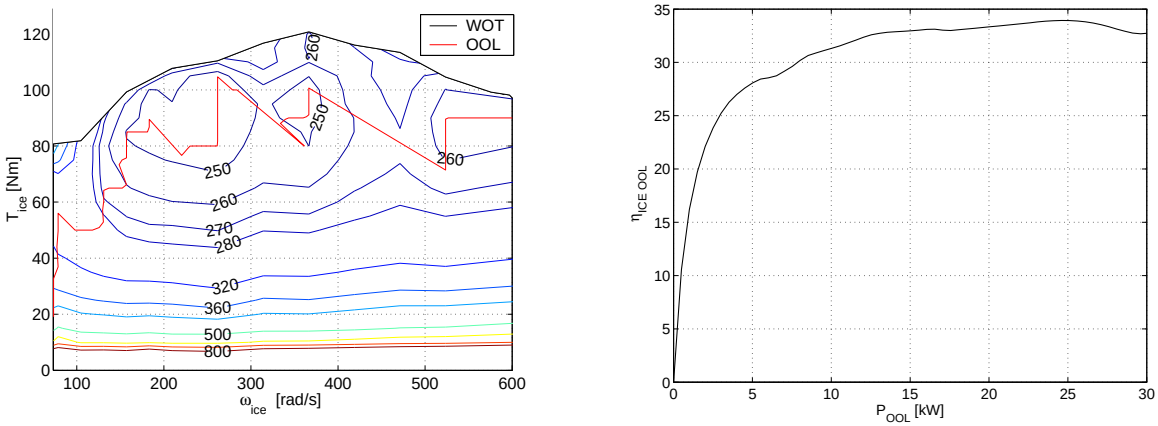

Figure 2.2: *left:* The Brake Specific Fuel Consumption map in g/kWh of a modern 1.4 l engine as function of the engine speed and engine torque. WOT = Wide Open Throttle line, OOL = Optimal Operation line *right:* The efficiency over the Optimal Operating Line of the ICE.

In Figure 2.2, the Brake Specific Fuel Consumption map with corresponding Wide Open Throttle (WOT) line and the Optimal Operating Line (OOL) is shown. The WOT line represents the maximum torque at wide open throttle for every engine speed. The OOL connects all points of minimal fuel consumption for every possible output power at the crank shaft. The efficiency over the OOL is plotted in the right figure.

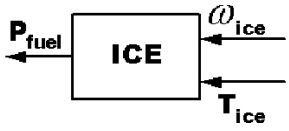

Figure 2.3: The quasi static representation of the ICE

The fuel consumption is given in Brake Specific Fuel Consumption (BSFC) $[g/kWh]$. The relations between the mass flow $\dot{m}$ $[g/s]$, the thermal efficiency η_{ice} $[\%]$, the power at the output shaft P_{ice} $[W]$, the fuel power P_{fuel} $[W]$ and the BSFC $[g/kWh]$ following from the Quasi Static model (Figure 2.3) are [24]

$$P_{ice} = T_{ice} \cdot \omega_{ice}, \tag{2.1}$$

$$\dot{m} = \frac{P_{ice} \cdot BSFC}{3600 \cdot 1000}, \tag{2.2}$$

$$P_{fuel} = \dot{m} \cdot \Delta H, \tag{2.3}$$

$$\eta_{ice}(T_{ice}, \omega_{ice}) = \frac{P_{ice}}{P_{fuel}} = \frac{3600 \cdot 1000}{BSFC \cdot \Delta H}. \tag{2.4}$$

ΔH represents the lower heating value of gasoline (= 44000 $[J/g]$). The fuel consumption map of the ICE is valid in stationary conditions.

Engine friction losses

Engine friction losses such as pumping losses cause a negative torque while decelerating. This means that a part of the braking energy is dissipated by the engine instead of recuperated by the motor. In order to increase the energy recuperation, a Cylinder Idling System (CIS) has been developed. The CIS developed for the IMA reduces pumping losses with approximately 50% by inactivating three of the four valves during deceleration. In Figure 2.4, the drag torque losses with and without CIS are depicted.

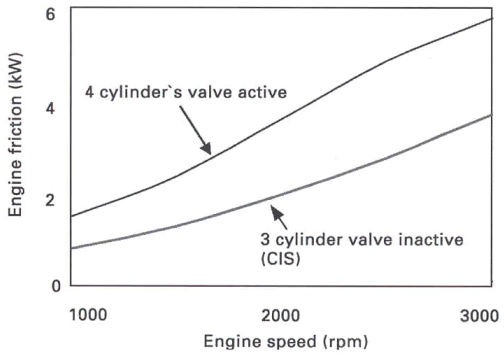

Figure 2.4: The Drag torque of the IMA with and without the CIS

2.2 Secondary power source: Electro Motor

The Integrated Motor Assist (IMA) motor is a permanent-magnet, synchronous AC motor, see Figure 2.5. In synchronous AC motors the permanent magnetic rotor operates at the same speed as the rotating magnetic field. The permanent magnets generate a magnetic field which interacts with the magnetic field of the windings on the stator, which results in motion. The term brushless DC motor is used for this type of motor as well. This is because the machine acts like a brush-type DC motor, only the the brushes are replaced by electronic commutation.

The thin design electric machine (Figure 2.5) is located between the 4-cylinder ICE and the manual transmission. The output shaft from the EM is directly connected to the output shaft from the ICE. The IMA motor serves a number of functions. It assists in vehicle propulsion when needed, allowing the use of a smaller internal combustion engine. It also operates as a generator, allowing braking energy to be used for recharging the IMA Battery Module, which can later be used to provide motor assist. Furthermore, the EM can be used to start the internal combustion engine very quickly and quietly. This allows the internal combustion engine to be shut off when it is not needed without any delay in restarting on demand. Finally, the EM takes the place of the conventional alternator, providing energy that feeds the 12 V electrical system.

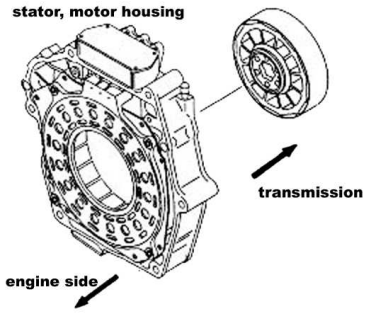

Figure 2.5: The IMA motor/Generator

The EM has a maximum power of 10 kW and maximum torque of 62 Nm. The efficiency map of the EM (including the power electronics) is taken from the Honda Insight model, available in ADVISOR [24]. They have scaled the stationary efficiency map of a 49 kW PM electric motor to a 10 kW EM. This efficiency map is shown in Figure 2.7.

The efficiency of the EM can be derived from the quasi static model for the EM (Figure 2.6).

$$\eta_{em} = \frac{P_{batt}}{\omega_{em} \cdot T_{em}} \tag{2.5}$$

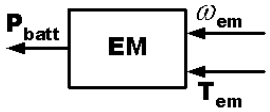

Figure 2.6: The quasi static representation of the EM

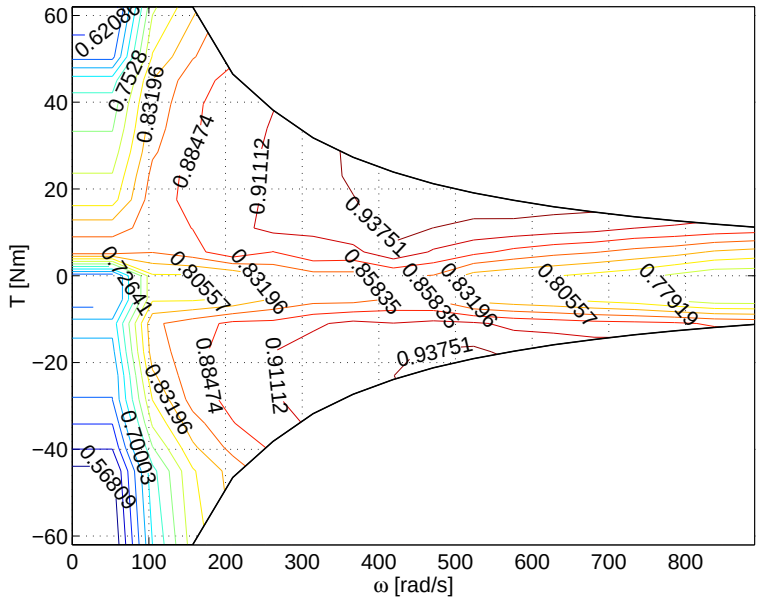

Figure 2.7: The efficiency map of the EM

2.3 Transmission

The transmission of the IMA consists of three parts, the manual transmission, the final drive and the differential. The efficiency of the final drive and differential together is assumed to be $\eta_{fd+d} = 0.98$ and for the manual transmission a constant efficiency η_{mt} of 0.95 is assumed [8]. The values for the gear ratios are given in Appendix D.

Clutch

The clutch is disengaged when the vehicle stands still. The minimum wheel speed required to drive with the clutch closed is $6.02\ rad/s$. Slipping losses due to the difference in final drive and manual transmission output speed occur during the closing of the clutch. These losses can be described by

$$P_{c,loss} = (\omega_{fd} - \omega_{mt,out}) \cdot T_{mt,out} \tag{2.6}$$

Friction clutches only produce substantial losses during the acceleration phase from stand still. There are no more additional losses when the clutch is closed.

2.4 Battery

The Nickel Metal Hydride (NiMh) battery module in the IMA has a high energy density and long service life. It supplies high voltage during motor only (M) or motor assist (MA) mode and the regenerated power during charging (CH) or braking (BER) is stored. The battery module is used to charge the conventional $12\,V$ battery as well. The specifications of the battery pack are in Appendix D and the battery pack is depicted in Figure 2.8.

Figure 2.8: The battery pack of the Honda Civic IMA

2.4.1 Assumptions for the battery model

Battery power characteristics are generally expressed at a temperature of $25°C$, although the battery cells are very sensitive to temperature fluctuations[1]. The available battery data is measured by the NREL at $25°C$ [13]. This means that temperature fluctuations can not be taken into account. It would be interesting to investigate the temperature effect on the battery performance for future research.

There is a dependency between the capacity of the battery and the discharge current. The **Peukert equation** describes this effect [8].

$$t_f = C \cdot I_{dis}^{-n} \tag{2.7}$$

t_f is the discharging time until the cut voltage (+/- 80% of the open circuit voltage) is reached, n is the so-called Peukert coefficient which varies between 1 and 1.5 and C is a constant. If the discharge current is high, the capacity of the battery decreases. This implies a change in SOC (see Equation 2.11). In this case the Peukert effects have not to be taken into account because it is assumed that the charge and discharge currents are low enough so that the charge capacity change is nihil. The charging or coulombic efficiency due to irreversible parasitic reactions in the battery has not been taken into account as well.

2.4.2 The battery model

The equivalent circuit for the battery is depicted in Figure 2.9. The internal battery power P_s and the power at the terminal voltage P_{batt} are described by

$$P_s(t) = V_{oc}(t, SOC) \cdot I(t), \tag{2.8}$$

$$P_{batt}(t) = P_s(t) - P_{loss}(t), \tag{2.9}$$

$$= V_{oc}(t, SOC) \cdot I(t) - I(t)^2 \cdot R_i(t, SOC), \tag{2.10}$$

[1] The charge conduction of the electrolyte is very sensitive to temperature fluctuations.

with V_{oc} the open circuit voltage and R_i the internal battery resistance both dependent on the SOC. To keep the equations clear, these dependencies are omitted in the next equations.

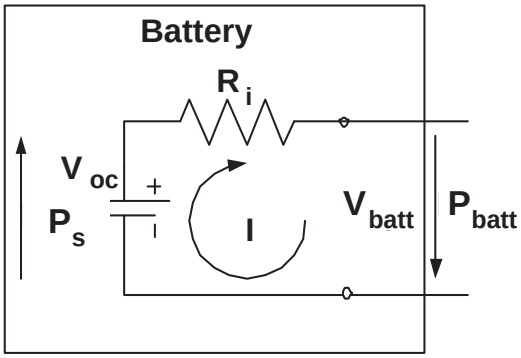

Figure 2.9: The equivalent circuit for a battery

Figure 2.10 shows the quasi static model for the battery module. The Power Amplifier (PA) efficiency is assumed to be 100%. When the electro motor generates power, the PA transforms the voltage V_{batt} to 144 V and the current I_{batt} increases the amount of electric energy available in the battery $Q_{batt}(t)$

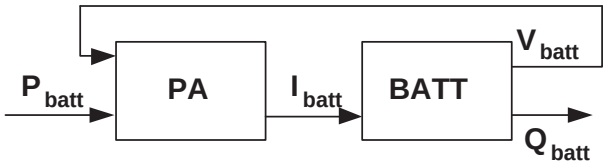

Figure 2.10: The quasi static representation of the battery

The SOC represents the normalized charge level (between 0 and 1) in the battery: the amount of electric charge available $Q(t)$, related to the nominal battery capacity Q_0 [8]

$$SOC(t) = \frac{Q(t)}{Q_0}, \quad \dot{Q}(t) = I(t). \tag{2.11}$$

The change in SOC during operation can be expressed as [28]

$$\frac{d\,SOC}{dt} = \frac{I(t)}{Q_0}. \tag{2.12}$$

Solving $I(t)$ from Eqn. 2.10 and substituting this into 2.12 gives [20]

$$\frac{d\,SOC}{dt} = -\frac{V_{oc} - \sqrt{V_{oc}^2 - 4R_i P_{batt}(t)}}{2R_i Q_b}. \tag{2.13}$$

Using the balance of power, the charge and discharge current can be calculated

$$P_{loss}(t) - P_s(t) + P_{batt}(t) = 0, \tag{2.14}$$

which means respectively for charge and discharge

$$R_i \cdot I(t)^2 + V_{oc} \cdot I(t) - P_{in}(t) = 0, \tag{2.15}$$

$$R_i \cdot I(t)^2 - V_{oc} \cdot I(t) + P_{out}(t) = 0. \tag{2.16}$$

Solving these equations for I gives

$$I_{chg}(t) = \frac{-V_{oc} + \sqrt{V_{oc}^2 + 4R_i \cdot P_{in}(t)}}{2R_i}, \tag{2.17}$$

$$I_{dis}(t) = \frac{V_{oc} - \sqrt{V_{oc}^2 - 4R_i \cdot P_{out}(t)}}{2R_i}, \tag{2.18}$$

in which $I_{chg}(t)$ always has a positive and $I_{dis}(t)$ a negative value.

2.4.3 The battery efficiency

The definition of the battery efficiency follows from Eqn. 2.8 and 2.10

$$\eta_{batt}(t) = \frac{P_s(t)}{P_{batt}(t)} = \frac{V_{oc}I(t)}{V_{oc}I(t) + I(t)^2 R_i}. \tag{2.19}$$

In accordance with the definition, the efficiency for discharge is higher than one.

The internal resistance of the battery changes when the SOC changes, see Figure 2.11. Therefore, the efficiency depends on the SOC as well. The efficiency for charge and discharge is depicted as a function of the battery power in Figure 2.12.

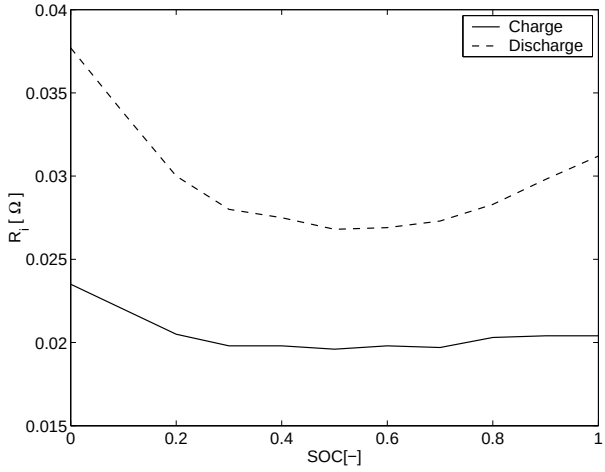

Figure 2.11: The internal resistance as a function of the SOC. These data are obtained from ADVISOR [24].

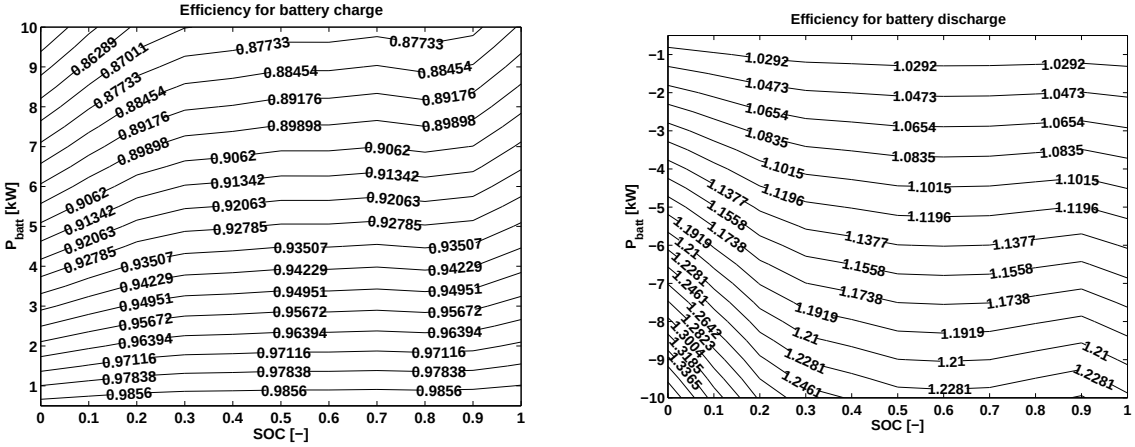

Figure 2.12: The efficiency for charge (left) and discharge (right) as a function of the battery power

The SOC is kept in the range of [0.3 - 0.8] for an optimal efficiency and to avoid damage to the battery. When the efficiency is plotted for SOC = 0.4, 0.5 and 0.6 (Figure 2.13), it is evident that the efficiency is not very sensitive for these SOC levels. An initial SOC of 0.5 is used further in this study. Consequently it is assumed that the battery efficiency is independent of the SOC level.

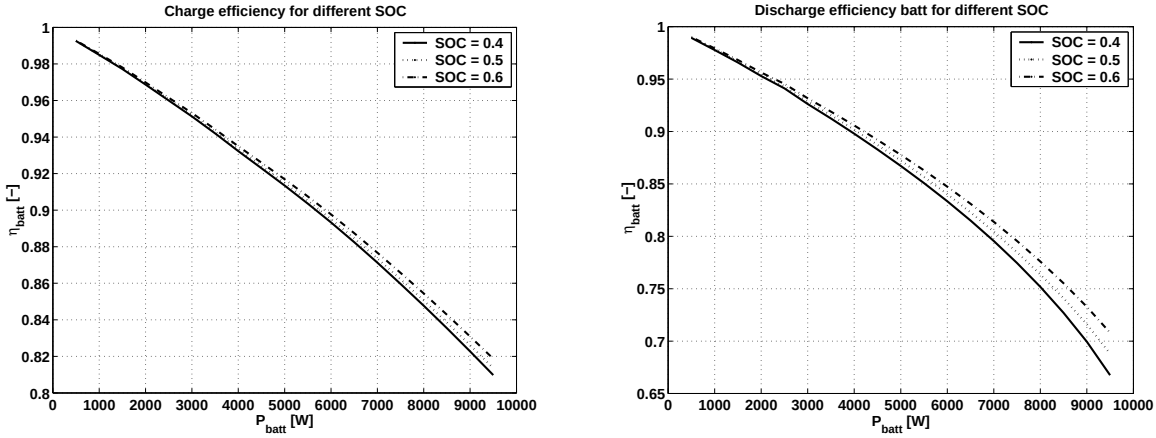

Figure 2.13: The efficiencies for different SOC for charge (left) and discharge (right)

2.5 Dynamic vehicle model

Now the models needed to describe the power flow in the vehicle are available, the power needed to drive the vehicle has to be computed. For this purpose a dynamic model of the IMA has been made which is presented in this section.

When a vehicle is driving, different forces are acting on the system which are shown in Figure 2.14.

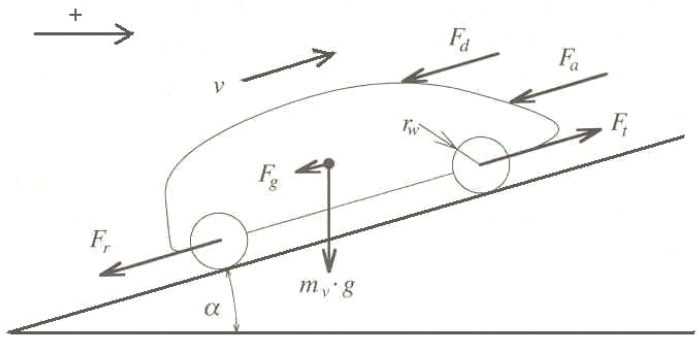

Figure 2.14: The forces working on the entire system

The **longitudinal dynamics** following from the 2^{nd} law of Newton can be described by Eqn. 2.20, assuming there is no wheel slip [8].

$$m \cdot a(t) = F_t(t) - (F_a(t) + F_r(t) + F_g(t) + F_d(t)) \tag{2.20}$$

In this equation, F_t represents the tracking force at the front wheels, F_a is the aerodynamic drag force, the rolling resistance force F_r is caused by the rolling friction of the wheels, F_g is the grade resistance force when driving on a non-horizontal road and finally the disturbance force F_d is defined for all non specified disturbances on the vehicle. The inertia forces caused by the rotating parts in the system have been lumped into the system as an additional mass, i.e. $m = m_v + m_{rot}$. This additional term will be derived later in this section.

The assumption is made that no disturbance forces F_d are working on the system. Further, the grade resistance force F_g is not present because the road grade is 0%. The remaining forces can be described as

$$F_t = \frac{T_{load}}{r_w} = F_{load} = F_a + F_r + m \cdot a, \tag{2.21}$$

$$F_a = \frac{\rho_{air}}{2} \cdot A_f \cdot c_d \cdot v^2, \tag{2.22}$$

$$F_r = m \cdot g \cdot c_r, \tag{2.23}$$

in which T represents the torque, r_w the wheel radius. With respect to the air drag force, A_f is the frontal surface area of the vehicle, ρ_{air} is the air density and c_d the air drag coefficient of the car. Finally, g represents the gravity constant and c_r the rolling resistance coefficient. [7]

In Figure 2.15, the free body diagram for the Honda Civic IMA drive train is depicted in which all forces and torques acting on the system are shown. The driving axles are assumed to be rigid.

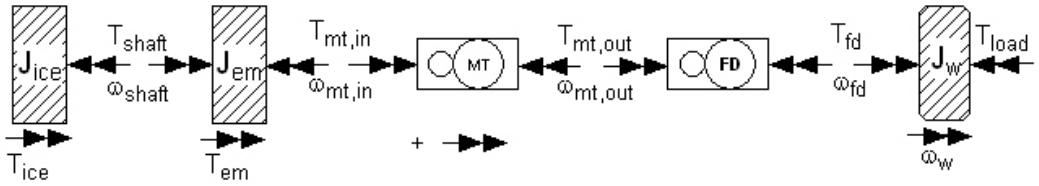

Figure 2.15: The fores and torques working on the entire system

The following equations express the moments of equilibria of the subsystems

$$\begin{aligned} T_{ice} - T_{shaft} &= J_{ice}\,\dot{\omega}_{shaft}, && (2.24)\\ T_{shaft} + T_{em} - T_{mt,in} &= J_{em}\,\dot{\omega}_{shaft}, && (2.25)\\ T_{mt,in} \cdot i_{mt} \cdot \eta_{mt} - T_{mt,out} &= 0, && (2.26)\\ T_{mt,out} \cdot i_{fd} \cdot \eta_{fd} - T_{fd} &= 0, && (2.27)\\ T_{fd} - T_{load} &= J_w \cdot \dot{\omega}_w, && (2.28)\\ & && (2.29) \end{aligned}$$

in which i_{mt} and i_{fd} are respectively the MT and final drive ratio. The efficiency of both transmissions $\eta_{mt} \cdot \eta_{fd}$ is replaced by η_t in the following equations. When all intermediate variables are eliminated, the relation between the torque of the ICE + EM and the load forces follows (Eqn. 2.30)

$$(T_{ice} + T_{em})\, i_{mt} \cdot i_{fd} \cdot \eta_t - F_{load} \cdot r_w = J_{tot} \cdot \dot{\omega}_w, \tag{2.30}$$

in which

$$\begin{aligned} J_{tot} &= J_w + (J_{ice} + J_{em})\, i_{mt}^2 \cdot i_{fd}^2, && (2.31)\\ \dot{w}_w &= \frac{a}{r_w} && (2.32) \end{aligned}$$

Inserting F_{load} and $\dot{w}_w$ in Eqn. 2.30, dividing by r_w and isolating a leads to

$$a = \frac{(T_{ice} + T_{em}) \cdot \frac{i_{mt} \cdot i_{fd}}{r_w} \cdot \eta_t - (F_a + F_r)}{\frac{J_{tot}}{r_w^2} + m}, \tag{2.33}$$

in which the previously mentioned additional mass factor can be described by the term $\frac{J_{tot}}{r_w^2}$. This equation is implemented in the simulink file to compute the driving power needed over a drive cycle in chapter 3.1. With this model for the vehicle dynamics some acceleration performance simulations have been made. The results are incorporated in a paper for the Electric Vehicle Symposium (EVS) [11] which can be found in Appendix F.

Chapter 3

The Conventional Vehicle Model

Before the model is used in DP, the model of the ICE has to be validated in a conventional vehicle model. The efficiency map of the ICE of the IMA was not available and an efficiency map of a modern 1.4 l ICE was used instead. To validate this engine map, the fuel consumption for the IMA over a prescribed drive cycle was compared to the suppliers data. In Section 3.1, the used drive cycle is described. Then the needed drive power is computed with a simulink model and with a second simulink model, the fuel consumption is computed in section 3.2. As an extra study, the effect of downsizing the engine is shown as well by implementing a 1.6 l engine the the IMA model at the end of the section.

3.1 Drive cycle

During the years, test cycles of standardized speed profiles have been developed in which fuel consumption and emissions of various vehicles can be compared with each other. The vehicle is placed on a dynamo meter and a driver follows the speed profile while measurements are made. The drive cycles are also very widely used to simulate emissions and fuel consumption of vehicles for research purposes.

When using DP, the vehicle power to drive the IMA over a predefined trajectory has to be known. A **European drive cycle (NEDC)** has been used to calculate this power. This cycle repeats the speed profile of an urban cycle (ECE) four times and adds a highway cycle (EUCD) to the driving profile. The first ECE cycle is driven in cold-soak conditions. The cold start is important to assess the pollutant emissions (engine and catalyst warming up) but the fuel consumption is also influenced by the cold start conditions (higher engine friction), although not as dramatically as the pollutant emissions [8]. Given this cycle and the longitudinal dynamics of the IMA, the power P_v needed for the desired speed ω_v of the vehicle can be computed (See Figure 3.1).

To investigate the sensitivity of the DP results for other drive cycles, the **Federal Test Procedure** (**FTP-75**) is used. This cycle is commonly used in the United States and has a typical warm-up phase as well. The speed profile is depicted in Figure 3.2. For both cycles, the shifting moments are prescribed.

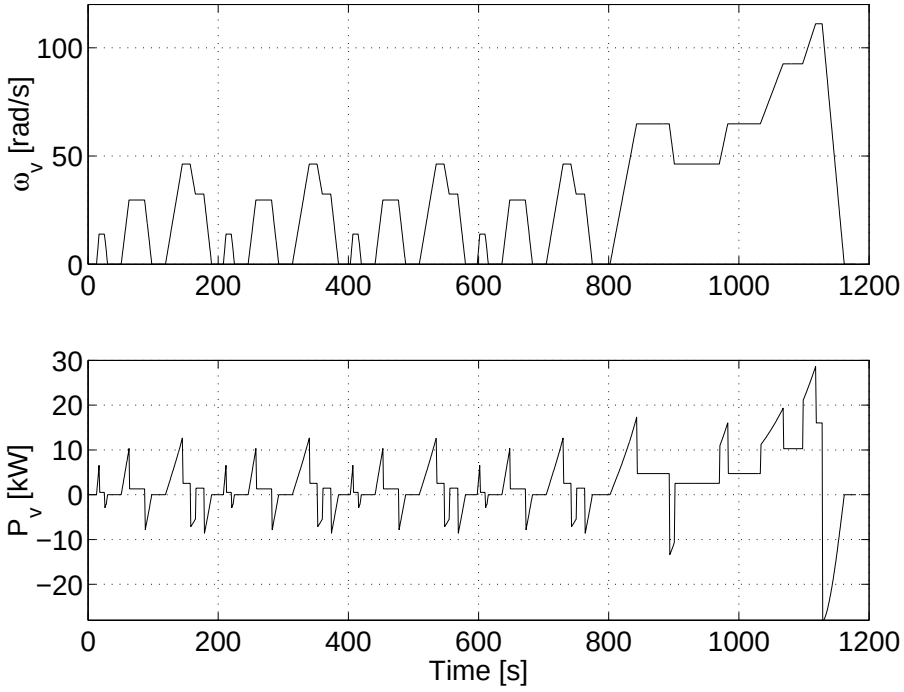

Figure 3.1: The power P_v needed for the Honda Civic IMA to follow the NEDC speed profile ω_v.

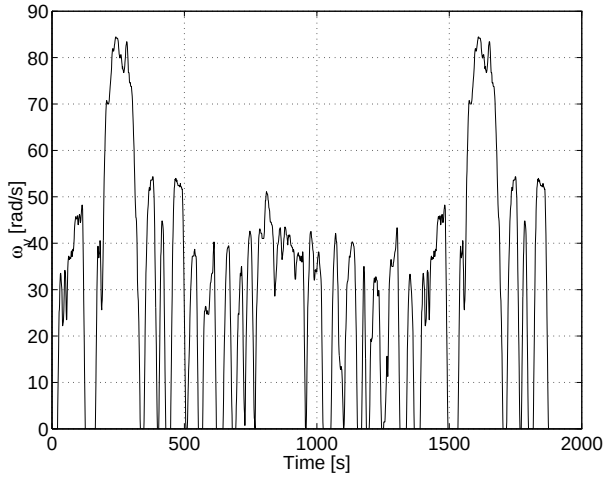

Figure 3.2: The FTP cycle is a test cycle commonly used in the USA

The Simulink file used to compute the driving power, is shown in Figure 3.3. Equation 2.20 has been implemented in the block "vehicle dynamics". The speed and gear ratio are looked up. In the block "inertia" the additional mass due to the rotational inertia is computed. A constant power of 300 W is added to the tracking power to take the auxiliary power into account.

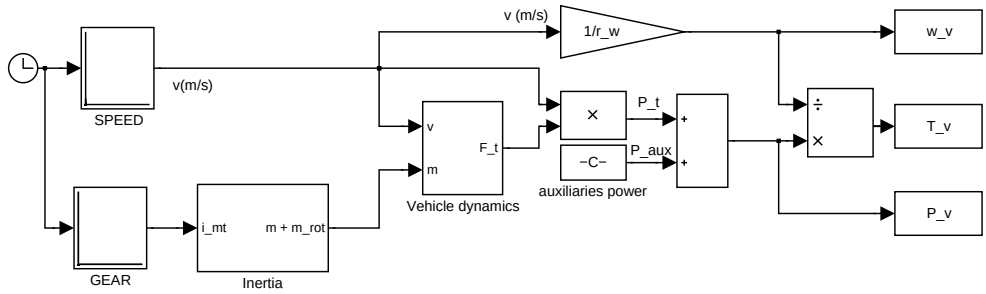

Figure 3.3: The Simulink File to compute the driving power P_v and torque T_v.

3.2 Validation ICE model

A backward facing Simulink model shown in Figure 3.4 is used to compute the fuel consumption of a conventional vehicle over the NEDC cycle. All inertia forces, component efficiencies, clutch losses, and auxiliaries have been taken into account.

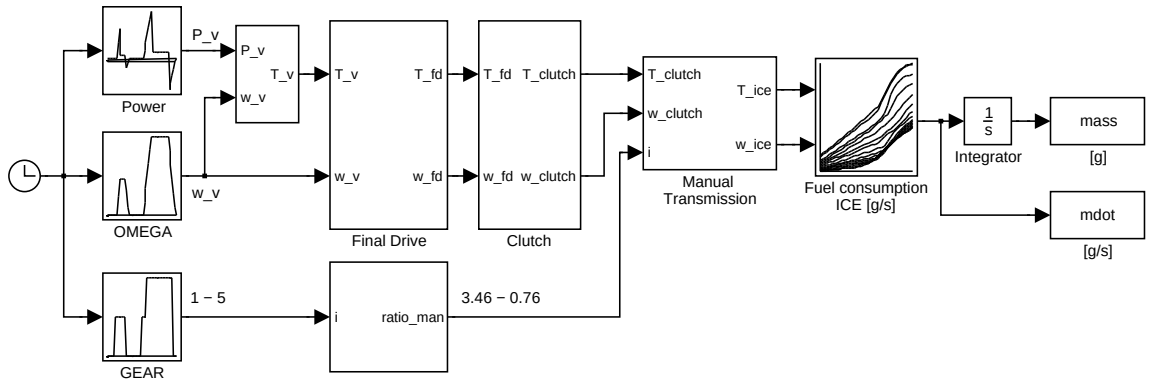

Figure 3.4: The Simulink file to compute the fuel consumption over the NEDC.

The Honda Civic exists as a conventional vehicle. However, the ICE of the conventional Civic differs from the IMA. Consequently it is impossible to validate the model with the catalogue. The **Honda Jazz** is a conventional vehicle available with the same ICE as the Honda Civic IMA. The relevant vehicle data are in Appendix E. The model of the ICE is validated by exchanging the vehicle parameters of the IMA with those of the Honda Jazz. The fuel consumption for highway, city and combined cycle are compared with the data from the catalogue and can be found in Table 3.2 (the catalogue values are between the brackets).

model	City [$l/100\ km$]	Highway [$l/100\ km$]	Combi [$l/100\ km$]
MT Jazz	7.0 (7.3)	5.0 (5.1)	5.6 (5.8)
MT Civic	7.1	5.1	5.8

Table 3.1: Fuel consumption for the conventional Jazz and Civic. The catalogue values are between brackets.

The modelled consumption is somewhat lower than the catalogue values. This difference can be explained by the different methods to measure the fuel consumption. During efficiency map measurements the engine is warm while the engine has a cold start when driving over a drive cycle. This leads to a higher fuel consumption up to 4% for the city cycle. For the highway usage, the fuel consumption differs only 2 %. Because the highway cycle is at the end of the NEDC, the motor has warmed up which can be an explanation for the better corresponding fuel consumption. The difference for the combined cycle is 3.4 %. Taking this into account, the conclusion is that the fuel consumption of the available 1.4 l engine corresponds good to the 1.3 l Honda IMA engine. When the IMA parameters are substituted into this model a reliable benchmark for a conventional Honda Civic with 1.3 l engine is created. The influence on hybridization can be seen very clearly when the outcomes of DP are compared to this benchmark.

3.3 The effect of engine downsizing

The maximum torque line of the 1.3 l engine and the maximum torque line of the IMA system (electro motor and ICE together) are shown in Figure 3.5 (published by Honda [22]). Honda claims that the overall dynamic performance of the IMA is comparable with a 1.6 l engine. To quantify the fuel reduction due to engine downsizing, the fuel consumption over the NEDC for a 1.6 l engine (Table 3.2) has been compared with the benchmark of the IMA. The fuel usage improvement resulting from down scaling is 10.7 % for the combined cycle. Catalogue values for the conventional Honda Civic with 1.6 l engine are also available. Again, the same phenomenon of lower fuel consumption can be seen.

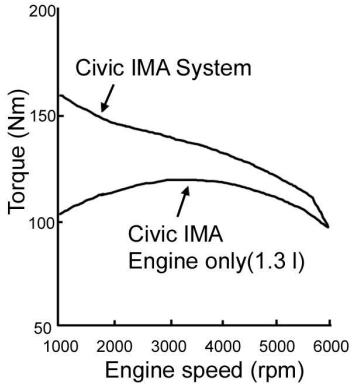

Figure 3.5: The maximum torque line of the IMA with and without motor assist

model	City [$l/100\ km$]	Highway [$l/100\ km$]	Combi [$l/100\ km$]
MT Civic 1.6 l	8.4 (8.7)	5.4 (5.5)	6.5 (6.7)
MT Civic 1.3 l	7.1	5.1	5.8

Table 3.2: Fuel consumption for the conventional 1.6 l Civic. The catalogue values are between brackets.

Chapter 4

Dynamic Programming

Dynamic Programming (DP) is a mathematical technique developed by R. Bellman in the 50's [5]. The most important advantage of using DP is that a global optimal solution is guaranteed to be found. A great disadvantage is that the computational time scales exponentially with the system order. When more state or control variables are implemented or the grid size is being enlarged, the time needed to compute the DP problem grows explosively.

DP can not be used online because of two reasons. First of all, the trajectory has to be known beforehand and secondly, the computational time is too extensive for online calculation. A rule based control law has to be derived from the offline results obtained with DP which then can be used for online implementation.

In this chapter the theory of dynamic programming and the implementation for this specific EMS problem are described.

4.1 The principle of optimality

A key aspect of dynamic programming is that decisions cannot be viewed in isolation since one must balance the desire for low present cost with the undesirability of high future costs. The DP technique captures this trade off. At each stage decisions are ranked, based on the sum of the present cost and the expected future cost, assuming optimal decision making for subsequent stages. This is known as the *Principle of Optimality* [5].

Definition 6.1 (Principle of Optimality) From any point on an optimal trajectory, the remaining trajectory is optimal for the corresponding problem initiated at that point.

This principle states that if a trajectory from $x(0)$ to $x(p)$ is optimal, every single sub trajectory $x(k)$ to $x(k+1)$ has to be optimal as well, see Figure 4.1. This principle has been used while calculating the cost-to-go matrix, which contains all optimal costs to come from state $x(k)$ to state $x(k+1)$.

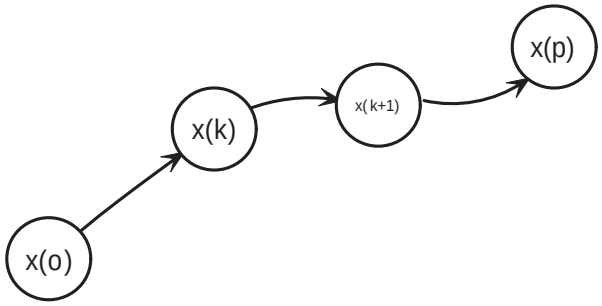

Figure 4.1: If the trajectory from $x(0)$ to $x(p)$ is optimal, the trajectory from $x(k)$ to $x(k+1)$ has to be optimal as well

4.2 Problem formulation

A discrete-time dynamic system is given

$$x_{k+1} = f(x_k, u_k), \tag{4.1}$$

where the state x_k is an element of a space S_k, the control variable u_k is an element of a space C_k. The control variable is constrained to take values in a given non-empty subset $U(x_k) \subset C_k$, which depends on the current state x_k

$$u_k \ \in \ U_k(x_k) \, \forall \, x_k \ \in \ S_k, \tag{4.2}$$

so that the new state $x(k+1)$ will be an element of the state space S_k. The optimization problem has to find a set of control variables $u(0), ..., u(p-1)$ that brings the system from state $x(0) = 0$ to $x(p) = x_p$ and minimizes the cost criterium J

$$J = \sum_{k=0}^{p-1} L(x(k), u(k)), \tag{4.3}$$

so that the cumulative costs from $t = t_0$ until $t = t_p$ are minimal. L is the cost-to-go matrix in which the optimal costs to come from state $x(k)$ to the next state $x(k+1)$ by applying control $u(k)$ are saved.

The Energy Management Problem of this study can be described as an optimization problem in which the cost criterium $J(x)$ is described by L, which is the cumulative fuel consumption $\dot{m}$ in $[g/s]$ over a drive cycle.

$$\min_x J(x) \text{ subject to }, \tag{4.4}$$

$$h(x) = 0, \tag{4.5}$$

$$g(x) \leq 0. \tag{4.6}$$

$$\tag{4.7}$$

The state variable x is the battery state of charge and the control variable u is the power requested from the battery which can be described by the ΔSOC of the battery. The cost function can now be described by

$$J(x) = \int_{t_0}^{t_f} \dot{m}(x(t), u(t)) \, dt, \tag{4.8}$$

$$= \int_{t_0}^{t_f} \dot{m}(SOC, \Delta SOC) \, dt. \tag{4.9}$$

The constraints of the problem are given by the maximum and minimum power, torque and speed requirements of the engine, transmission, electro motor and the battery.

$$\begin{aligned}
\omega_{ice\ min} \leq \quad & \omega_{ice}, \omega_{em} && \leq \omega_{ice\ max}, && (4.10)\\
0 \leq \quad & T_{ice} && \leq T_{ice\ max}, && (4.11)\\
T_{em\ min} \leq \quad & T_{em} && \leq T_{em\ max}, && (4.12)\\
P_{em\ min} \leq \quad & P_{em} && \leq P_{em\ max}, && (4.13)\\
0 \leq \quad & P_{ice} && \leq P_{ice\ max}, && (4.14)\\
\Delta SOC_{min} \leq \quad & \Delta SOC && \leq \Delta SOC_{max}, && (4.15)\\
SOC_{min} \leq \quad & SOC && \leq SOC_{max}, && (4.16)\\
\omega_{ice} \quad & = && \omega_{em}. && (4.17)
\end{aligned}$$

Furthermore, this problem is subject to an integral constraint for the SOC balance

$$E_{batt}(t)|_{t_0}^{t_f} = \int_{t_0}^{t_f} P_{batt}(t)dt = 0, \tag{4.18}$$

so that the initial state of charge is equal to the final state of charge. If this constraint wouldn't have been applied, the difference in SOC at the end of the cycle would have ended up in an additional fuel usage term for the entire problem. To avoid this additional term, the integral constraint has been set active.

4.3 Problem implementation

The implementation of the IMA power split optimization problem is described in this section. The method to calculate the cost matrix, the grid choice for control and state variables and the algorithm to compute the optimal route in the cost matrix are explained.

Calculation cost matrix

The battery power $\overline{P}_{batt}$ is the control vector u (see Figure 4.2). This vector is defined between $-10\ kW < P_{batt} < 10\ kW$ with steps of $100\ W$. When the requested battery power is positive, the battery SOC increases which corresponds to the regeneration mode. When P_{batt} is negative, the system is in the motoring mode. The electro motor power $\overline{P}_{em}$ depends on the control vector and the corresponding battery efficiency.

$$\overline{P}_{em} = \overline{P}_{batt} \cdot \eta_{batt}(\overline{P}_{batt}) \tag{4.19}$$

The required driving power at every time step is inserted into a vector $\overline{P}_{drive}$ with the length of the control vector. Via the final drive, clutch and MT, the power goes to the input shaft of the MT, $\overline{P}_{mt,in}$. At every time step, $\overline{P}_{mt,in}$ and $\overline{P}_{em}$ are known vectors which means the power required from the ICE depending on the control input can be calculated as well.

$$\overline{P}_{ice} = \overline{P}_{em} + \overline{P}_{mt,in} \tag{4.20}$$

For each control step u at time step t, the required engine power is known and the corresponding fuel consumption vector $\overline{\dot{m}}_{fuel}$ can be calculated and saved in the cost matrix C. When one of the constraints of the components is exceeded, e.g. the torque of the EM, an infinitive value is inserted in the cost matrix at the corresponding place. This avoids solutions in the infeasible domain. A somewhat simplified M-file of this cost matrix calculation is in Appendix H

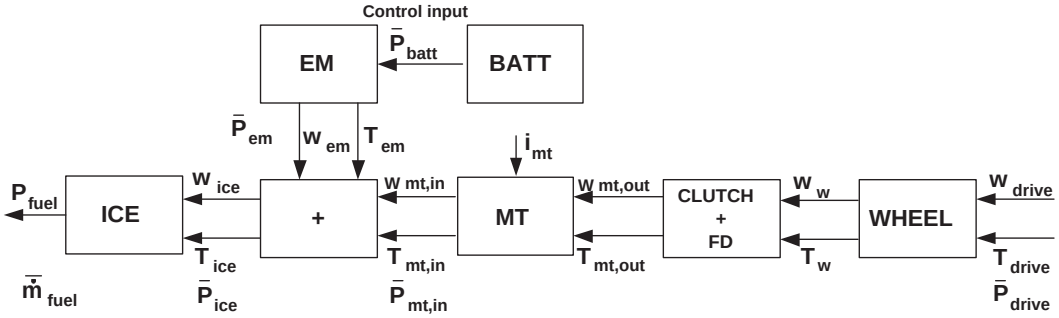

Figure 4.2: A schematic representation of the calculation of the cost matrix

Grid

Three grids have to be defined for the DP problem: the time, control and state grid. The time grid t has a length n_t of 1180, which is the exact duration of the drive cycle. The control grid u has a size of n_u = 201 because P_{batt} is between + and -10 kW and a step size P_{step} of 100 W is used.

The battery SOC is the state variable x. The maximum energy level of the battery equals E_{max} = 3.1 MJ. The value at $t = 0$, $E(0)$ = 0.5 E_{max}. This value changes during the simulation between 0.3 - 0.8 E_{max}. The relation between the control u and state variable x is

$$E_{batt}(t+1) = E_{batt}(t) + P_{batt}(t) \cdot \delta t, \tag{4.21}$$

in which δt = 1 and E is the energy from the battery. The number of steps n_x in the state grid can be calculated by

$$n_x = \frac{E_{max} - E_{min}}{P_{step} \cdot \delta t} = \frac{2.48e6 - 0.93e6}{100} = 15500. \tag{4.22}$$

The grid can be visualized and is seen in figure 4.3.

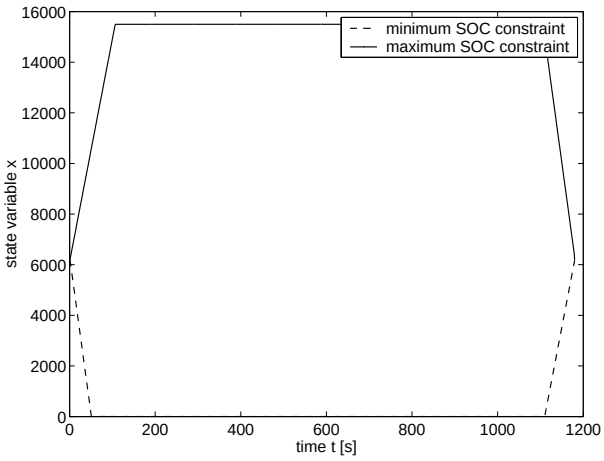

Figure 4.3: The grid of the DP problem

When the battery is fully charged/discharged, the SOC reaches its maximum/minimum constraint. These two constraints take care that at $t = t_{end}$, the final state is equal to the state at t = 0.

Routine

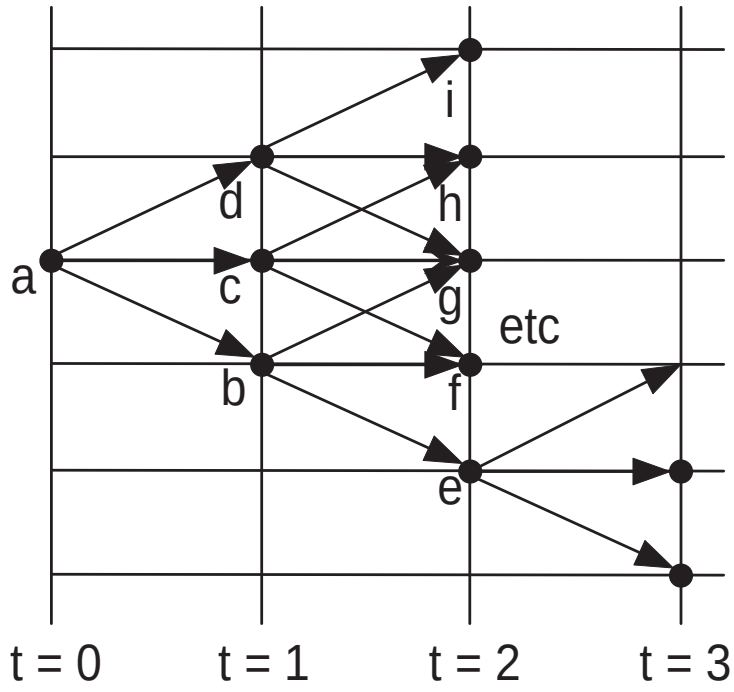

Figure 4.4: Dynamic Programming route

For every time step t, the costs for every control step u are saved into the cost matrix C with size n_u x n_t. The nodes in the cost-to-go matrix L (n_x x n_t) represent the state space and the costs at the nodes in the matrix represent the costs to come from the start position to the node. The first three time steps of the this matrix are shown in Figure 4.4. The cost-to-go matrix is initialized with infinitively large values only. Exclusively at the begin state (node a), a value of 0 has been inserted. At t = 0 all the allowed control steps are made and when the costs to come to the new nodes b,c, and d are lower than the costs that were already present in the cost-to-go matrix at these nodes, the new lower costs are saved in the cost-to-go matrix L at nodes b, c, and d. At t = 1, the same thing has been done for every node in the state space, starting from the lowest position, node b. For b, all the control steps lead to lower costs at place e, f and g. The costs at node b are added to the costs to go from b to e, f or g and are saved at these three nodes. Now we can go one step higher in the state space, node c, and the same procedure can be followed. When the costs to reach node f via node c are lower than the costs to reach node f via node b, the costs coming from node c are saved and the costs from node b are thrown away. This routine goes on until all possibilities have been checked to come from t = 1 to t = 2. Then the same routine is done for t = 2 until $t = t_{end}$. During this routine, the constraints of the state space are not allowed to be violated. This means that if a control input leads to a node in the infeasible domain (outside the allowable region), the routine skips this calculation and goes to the next step. During this routine, a node matrix N is saved as well. The most optimal path is saved in this matrix by saving the most optimal node to node route.

This procedure can be described by the following routine:

1. Initialize
2. Time loop (k)
    3. State variable loop (i)
        4. Control input loop (j)
            5. State (i) reachable applying control input (j)?

            $\Rightarrow$ NO:

            - Next control input

            $\Rightarrow$ YES:

            - Compute cost for node (i,j)
            - Check if costs for this control input to come to node (i,j) are lower than costs for this node that were already present in the cost-to-go matrix L

            $\Rightarrow$ NO:

            - Next control input

            $\Rightarrow$ YES:

            - Save the new costs at node (i,j) in the cost-to-go matrix L
            - Save the node x(k) that is responsible for the most optimal costs at node (i,j) at x(k+1) in the node matrix N
        6. Next control input (j)
    7. Next state (i)
8. Next time (k)
9. End

The Matlab script with the used DP routine is in Appendix H

Chapter 5

Results of DP for the Manual Transmission

The energy management problem for the Honda Civic IMA is implemented in DP and the results are presented in this chapter. Different models are necessary to investigate the influence of the components (Section 5.3), the mean efficiency of S (Section 5.4) and the modes idle stop, charge and BER (Section 5.5) on the fuel consumption and the strategy. In Section 5.1, an overview of these models is given. Before the optimization is started, a founded decision for the grid step size and a validation of the DP algorithm are made in Section 5.2. The NEDC is used to compute the drive power in all simulations, except for the last section in which the influence of the drive cycle is investigated. A summary of the main results is given in this chapter while the complete overview of the results is included in Appendix I. The results give insights in the most optimal power split strategy resulting from DP. These insights are used to define a rule based controller in next chapter.

5.1 Overview used models

The influence of three different subjects (components, mean efficiency and hybrid modes) on the fuel consumption and the EMS resulting from DP is investigated. For every different subject, other models are needed. An overview of these models is given in this section.

The models that are used in the Section 5.3 to investigate the influence of the components on the fuel consumption and the strategy, are specified in Table 5.1. The models of Chapter 2 and the constraints defined in Section 4.2 are implemented. Furthermore, all hybrid modes (E, M, MA, CH, BER and IS) defined in Section 1.3 are allowed to be used by DP. It is assumed that the motor is warm and the costs to start the engine are nihil. When the vehicle is in motor only or regeneration mode, the engine is assumed to idle.

INFLUENCE COMPONENTS

Model		η_{ice}	η_{em}	η_{batt}	P_{aux}	P_{drag}
I	Basic	$\eta_{ice}(T_{ice}, \omega_{ice})$	100 %	100 %	-	-
II	Battery	$\eta_{ice}(T_{ice}, \omega_{ice})$	100 %	$\eta_{batt}(P_{batt})$	-	-
III	EM	$\eta_{ice}(T_{ice}, \omega_{ice})$	$\eta_{em}(T_{em}, \omega_{em})$	100 %	-	-
IV	Battery+EM	$\eta_{ice}(T_{ice}, \omega_{ice})$	$\eta_{em}(T_{em}, \omega_{em})$	$\eta_{batt}(P_{batt})$	-	-
V	IMA	$\eta_{ice}(T_{ice}, \omega_{ice})$	$\eta_{em}(T_{em}, \omega_{em})$	$\eta_{batt}(P_{batt})$	300 W	$P_{drag}(\omega_{ice})$

Table 5.1: The models used to investigate the influence of the components on the fuel consumption and the power split strategy in Chapter 5.3.

Model VI has been used in Section 5.4 to investigate the influence of the mean efficiency of system S, $\overline{\eta}_s$, on the fuel consumption and strategy (system S = battery + EM). Nine simulations have been done with constant values between 0 and 1. To draw conclusions from these simulations, the results are compared to the outcomings of model II, III and IV.

INFLUENCE MEAN EFFICIENCY η_s

Model	η_{ice}	$\overline{\eta}_s = \eta_{em} \cdot \eta_{batt}$	P_{aux}	P_{drag}
VI	$\eta_{ice}(T_{ice}, \omega_{ice})$	$\overline{\eta}_s$ = constant [0 - 1]	-	-

Table 5.2: The models used to investigate the influence of the mean efficiency $\overline{\eta}_s$ on the fuel consumption and the power split strategy in Section 5.4.

In Section 5.5, the models VII until XI are used to investigate the influence of three hybrid modes (Idle Stop (IS), Charge (CH), and Brake Energy Recovery (BER) mode) on the fuel consumption and strategy. In model VII, the three hybrid modes are disabled and step by step, the modes are enabled until in model XI all modes are enabled. Model XI and V are the same models.

INFLUENCE HYBRID MODES : IDLE STOP, BER AND CHARGE

Model		IS	BER	CH
VII	Conventional	-	-	-
VIII	IS	+	-	-
IX	IS + BER	+	+	-
X	IS + CH	+	-	+
XI = V	IMA	+	+	+

Table 5.3: The models used to investigate the influence of the hybrid modes IS, BER and CH on the fuel consumption and the power split strategy in Section 5.5.

5.2 Step size DP

Before the actual optimization is started, the influence of the grid step size on the results is investigated. The basic model I has been simulated with three different control step sizes: 100 J, 500 J and 1000 J. When the step size is reduced from 1000 J to 100 J, the computation time increases explosively ("the curse of dimensionality"). This means that the most optimal step size has to be chosen with respect to calculation time and reduction in fuel consumption.

In Table 5.4, the fuel consumption for the basic model is shown. The difference in fuel consumption between 100 J and 1000 J is 4 %. The reduction from 1000 J to 500 J yields about the same fuel consumption as from 500 J to 100 J. Possibly 1 or 2 % can be saved additionally by reducing the grid even more. The computation time for this option however is too extensive and has not been used.

	1000 J	500 J	100 J	Additional fuel consumption
Basic (I)	4.02	3.94	3.86	4.01 %

Table 5.4: The additional fuel consumptions from 100 J to 1000 J [%] is 4.01 %

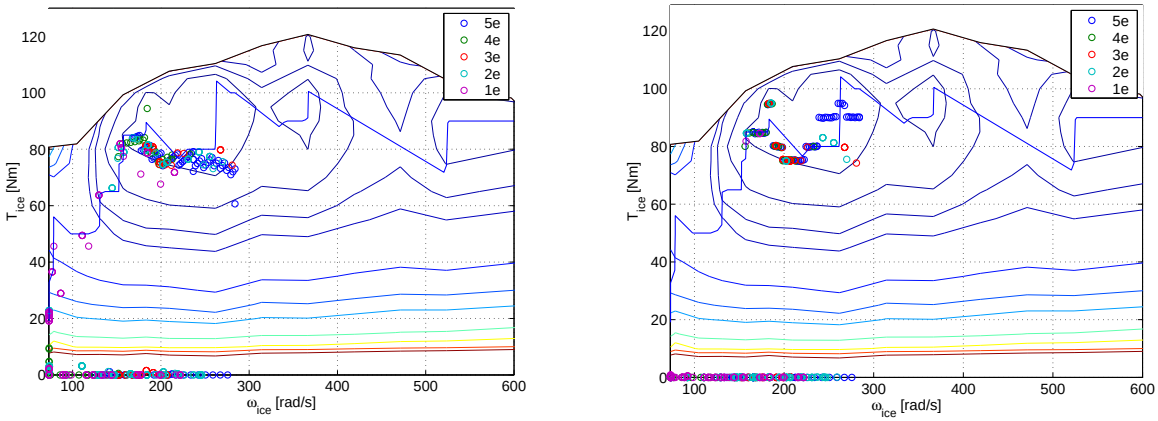

Figure 5.1: The ICE operating points for the two strategies. (Left) 1000 J (Right) 100 J

The difference in resulting strategy can be seen in Figure 5.1. For 1000 J, all operating points are close to the OOL. When the same simulation is done with 100 J, all the operating points are in the sweet spot (the operating point in the efficiency map where the ICE is most efficient) which causes a significant improvement in fuel savings. It can be concluded both fuel consumption and resulting strategy depend on the step size. The step size of 100 J will be used for further calculations.

The conventional Honda Civic (model VII) is simulated in DP to verify the reliability of the results. The possibility of recharging is disabled which means that all power has to be delivered by the ICE. The resulting fuel consumption (5.72 $l/100\ km$) and the operating points of the ICE (see Figure 5.2) are close to the results from the benchmark of the conventional IMA (5.8 $l/100\ km$). From these results can be concluded that DP gives reliable output.

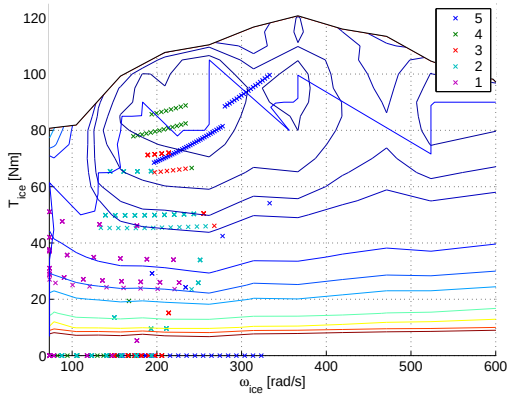

Figure 5.2: The operating points resulting from DP for the conventional Civic. The same results are obtained with the benchmark.

5.3 Influence components

The influence of the components ICE, battery and EM and the influence of the drag torque and auxiliary power on the system operation and fuel consumption are described in this section.

Basic model (model I)

The DP simulation series start with the basic model. This model is a simplified hybrid model in which the efficiency of battery and EM are assumed to be 100 %. Drag and auxiliary losses have not been taken into account.

From the results of the basic model follows that the usage of battery power is high. DP tends to deplete the battery until the SOC constraint is reached. The power is used to drive electrically (M) to avoid part load (between 0 - 10 kW) and to assist the engine (MA, above 15 kW). Due to the M and MA mode, the ICE is able to operate in the sweet spot with a corresponding ICE efficiency of 32%. The electro motor uses the entire region between ω_{em} = 75 and 300 rad/s because the motor and battery efficiency have not yet been taken into account. The regenerative energy is fully recuperated within its constraints. Between -10 kW and -7 kW, not all energy can be restored because of the torque constraint of the EM. The fuel consumption on the NEDC cycle is 3.86 $l/100$ km.

Switching behaviour

Switching behaviour between motor only (M) and charge (CH) mode occur when the SOC constraint is reached, see figure 5.3(left). The area of the SOC where switching occurs has been enlarged in the right figure. When the SOC reaches its constraint and the system is most efficient in a depleting battery mode (M or MA) the switching behaviour occurs. DP would like to deplete the battery more but then the constraint would be violated. Because DP is not allowed to violate the constraint, it now prefers charging the battery to increase the SOC. Subsequently, the electro motor can be used again until the constraint has been reached for the second time. This is repeated until the system comes in a non depleting mode (CH, BER, E) as most efficient mode. When more component efficiencies are added to the system this switching behaviour disappears, because the usage of battery power decreases. The SOC does not reach its constraint anymore and the switching behaviour stops.

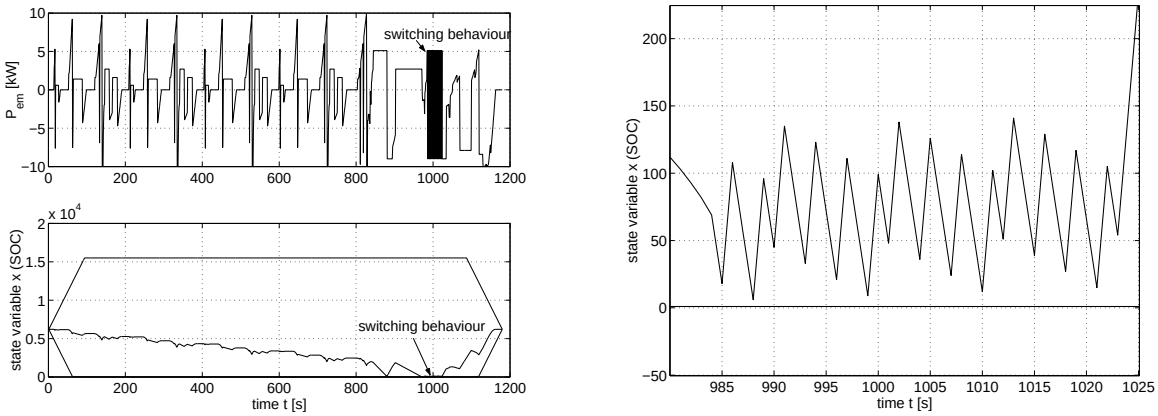

Figure 5.3: *left:* The switching behaviour from motor only (M) to motor assist (MA) mode when the SOC reaches its constraint *right:* Zoom: The switching region at the SOC boundary

Battery Efficiency (model II)

After a successful implementation of the basic model, the battery efficiency is added to this model. This efficiency is assumed not to depend on the SOC (=0.5), see Section 6.4. However, it depends on the internal resistance: the higher the power, the lower the efficiency. The power to the electro motor is between $+10\ kW$ (motoring) and $-10\ kW$ (generating). This means that, taking the efficiency of the battery into account, the battery internal power varies in between $+12.3\ kW$ and $-8.7\ kW$ (Figure 5.4).

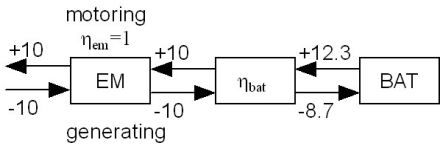

Figure 5.4: The internal battery power flow for max/min power

The results differ substantially from the basic case. Because the efficiency in the high power region of the battery is bad, $P_{em} > 5\ kW$ or $< -5\ kW$ are avoided during driving. The vehicle still drives electrically until $5\ kW$ while electric drive in second gear is not allowed anymore. Consequently, the ICE operating points for this gear move to a less efficient region. The vehicle is now in charging mode between 5 and $15\ kW$. The switching behaviour is disappeared. The mean efficiency of the battery is 0.95. The fuel consumption is increased with 5.0 % with respect to model I.

Electro motor efficiency (model III)

Next, the EM efficiency is added to the basic model (Figure 5.5). The battery efficiency has not been taken into account in this simulation. The results show that electro motor efficiency seems to have

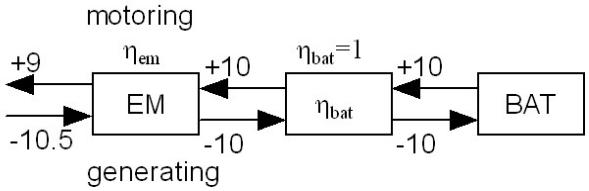

Figure 5.5: The power flow for max/min powers trough the EM and battery

more influence on the power split strategy than the battery efficiency. Only a small area of the EM, in which the efficiency is good, is used for charge and discharge during driving. Speeds lower than $120\ rad/s$ and torques higher than $30\ Nm$ are not allowed. Until $1.5\ kW$, the vehicle always drives electrically (M) to avoid very low ICE efficiency (0-0.2). Between 1.5 and $5\ kW$, the motor only mode occurs when $T_{drive} < 25\ Nm$. The vehicle is in engine only (E) mode when the requested drive torque is higher. The result is that more points in first gear move to less efficient regions in the ICE operating map. The mean efficiency of the EM is 0.89. Because the usage of electrical power has become more "expensive", an engine only region between 15 and $25\ kW$ can be observed. The fuel consumption is increased to $4.12\ l/100\ km$.

Battery and EM efficiency (model IV)

The influence of the combination of the battery and EM efficiency (system S) is investigated with model IV. From this simulation can be seen that the usage of the EM is restricted due to the low

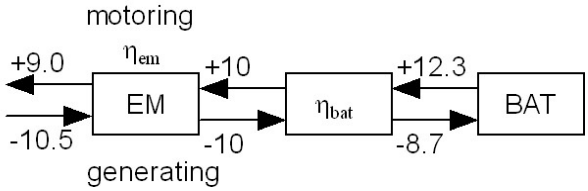

Figure 5.6: The battery + EM power flow

remaining power after charge and discharge. This means that the engine only region is enlarged. The operating points of the ICE in third gear move to less efficient regions as well, because recharging takes place less often and with lower power. This is a result of the combined efficiency region of battery and EM in which the efficiency is still good. The mean efficiencies of battery and EM are still 0.95 and 0.89, although the operating points are changed. The resulting overall efficiency of system S is 0.85. The fuel consumption is increased with 8.7 % compared to model I. The total consumption is now 4.23 $l/100\ km$.

The Honda Civic IMA (model V)

The basic model is completely expanded to the Honda Civic IMA model by adding all component efficiencies, the auxiliary power and the drag torque during regeneration. From the results of this simulation follows that the mean efficiencies of battery and EM remain the same (0.95 and 0.89). The fuel consumption increases a lot, especially due to the use of the auxiliaries. The drag torque of the ICE causes energy loss during recuperation. The remaining regenerative energy is fully recuperated. The charging mode occurs more often to compensate for the energy used by the auxiliaries and the losses due to drag. The vehicle drives still in motor only mode for $T_{drive} < 25\ Nm$. The fuel consumption is 4.57 $l/100\ km$, 15.5 % higher than the basic case.

General conclusions fuel consumption and system operation

The fuel consumption for all cases are in Table 5.5. Adding efficiencies to the DP model leads to an increase in fuel consumption. The EM is used less and therefore the engine has to deliver more power. The influence of efficiencies is investigated further in the next section. The resulting power and torque split are studied in Chapter 6.

		Fuel consumption $[l/100\ km]$	Additional fuel consumption [%]
I	Basic	3.86	-
II	Battery	4.06	5.0 %
III	EM	4.12	6.3 %
IV	Battery+EM	4.23	8.7%
	+ Drag torque	4.34	11.05 %
	+ Auxiliaries	4.45	13.25 %
V	IMA	4.57	15.53%

Table 5.5: The fuel consumption for all cases.

From these results, the following general conclusions with respect to system operation are drawn:

- In model I, all operating points of the ICE are in the sweet spot. When the efficiencies of the battery and EM are added in model II, III and IV, the operating points move to less efficient regions. DP avoids the low efficiency region of the ICE (0 - 0.2).
- Low efficiency regions for battery and EM are avoided during M, MA and CH mode (ω_{em}<120 rad/s, $|T_{em}|$>25 Nm). During BER mode, all energy is recuperated within the constraints, also when the operating points are in a low efficiency region.
- The mean efficiency of battery, EM and battery + EM are respectively 0.95, 0.89 and 0.85.
- If the drive torque T_{drive} < 25 Nm: always motor only mode (M).
- When the battery + EM efficiencies are added in models II-IV, the engine only (E) mode increases. This causes a increase in fuel consumption.
- When the drag losses and auxiliary power are added in model V, the CH mode increases to compensate for the decrease in electrical power.
- The most important component constraints are the minimum torque constraint of the EM (not all regenerative energy can be recuperated) and the SOC constraint ($SOC(t_{end}) = SOC(t_0)$).

5.4 Influence of mean efficiency of S

From the previous section follows that the fuel consumption increases when efficiencies are added to the basic case. To investigate the effect of the efficiency on the fuel consumption and power split strategy, some simulations have been done with constant efficiency for the system S (the battery and EM together) $\overline{\eta}_s$ with model VI. The results are compared to models II, III and IV in which the efficiencies depending on the operating point are used.

In Figure 5.7(left), the resulting fuel consumption as a function of the mean efficiency of S is shown. The difference between constant efficiencies and the mean efficiencies of models II - IV is minimal. The increase in fuel consumption is very sensitive in the high efficiency region of S. That is why DP keeps the EM and battery in good efficiency regions. In Appendix J, the power split strategies for $\overline{\eta}_s$ = 1 (resembling the Basic model I), 0.95 (Battery efficiency II), 0.9 (EM efficiency III) and 0.85 (S: Battery + EM efficiency IV) are shown. The similarity in power split strategy with the efficiencies depending on the operating point can clearly be observed (compare with Appendix I). Due to this resemblance can be concluded that the mean efficiency of S during the cycle defines the power split. When the efficiency is higher, more energy remains after charge and discharge. Therefore the EM can be used more often, which results in a change in the power split and better fuel consumption. DP aims at the highest mean efficiency of S because the biggest fuel consumption savings can be achieved in that region. Little improvement of the efficiency of system S can lead to significant fuel consumption reduction.

The decision for mode choice is a trade off between the electric costs to assist the ICE and the benefits for the fuel consumption. The mean efficiency of S is 0.85 which means that the remaining efficiency after charge and discharge is only 0.72. Therefore the fuel savings during M or MA mode have to countervail the costs made to charge the battery. In Figure 5.7 (right) a schematic representation of the power flow in the system with the corresponding mean efficiencies for the different modes are shown.

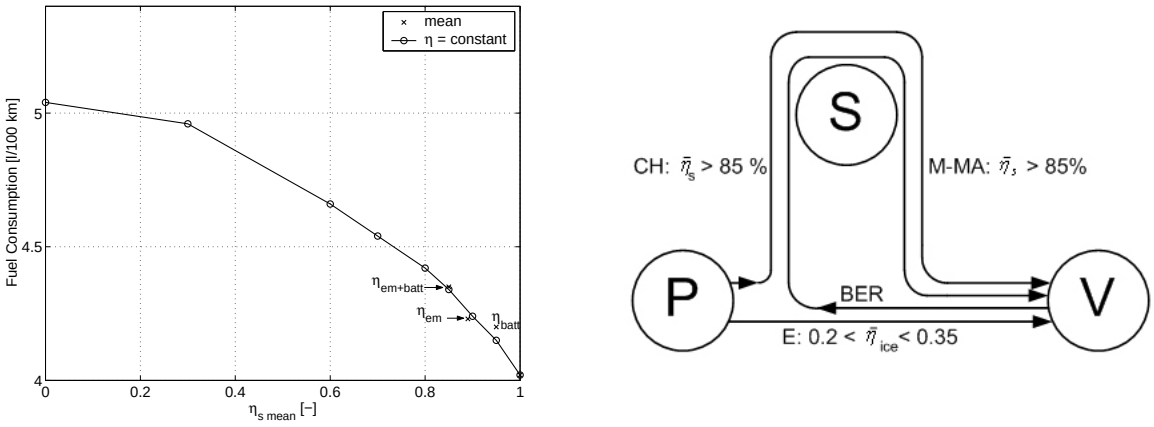

Figure 5.7: *left:* The curve for the fuel consumption as a function of the efficiency of S *right:* A schematic representation of the power flow in the system with the corresponding mean efficiencies for the different modes. P = Primary power source, S = Secondary power source, V = Vehicle

5.5 Influence of idle stop, BER and charge mode

To get an idea of the effect of hybridizing and the profits that it brings along, the effect of idle stop and BER and the charge mode have been investigated separately. The influence of these three modes in fuel consumption is shown in Table 5.6. The models VII - X are used for this investigation.

Model		Fuel cons. $[l/100\ km]$	Fuel savings $[l/100\ km]$	Fuel savings [%]
VII	Conventional	5.72	-	-
VIII	IS	5.40	0.32	5.6%
IV	IS, BER	4.72	1.00 = 0.68 (BER)+ 0.32 (IS)	11.9 + 5.6 = 17.5%
X	IS, CH	5.24	0.48 = 0.16 (CH) + 0.32 (IS)	2.8 + 5.6 = 8.4 %
XI	IS, CH, BER	4.57	1.15 = 0.16 + 0.32 + 0.68	2.8 + 5.6 + 11.9 = 20.3 %

Table 5.6: The fuel consumption and the fuel savings for idle stop (IS), Brake Energy Recovery (BER) and charge mode (CH) with respect to the conventional vehicle

Idle stop causes a fuel saving of 5.6 % with respect to a conventional vehicle. The saving in grams is exactly the same as the idle consumption × idle time (0.076 g/s × 293 s = 22 g). BER causes the greatest amount of fuel consumption with 11.9 %. The possibility to charge during propulsion yields only 2.8 %.

The strategy defined by DP can be depicted by a power split figurein which the electro motor power (P_{em}) and the engine power (P_{ice}) are plotted against the drive power (P_{drive}). The power split figures for BER and CH differ substantially (Figure 5.8).

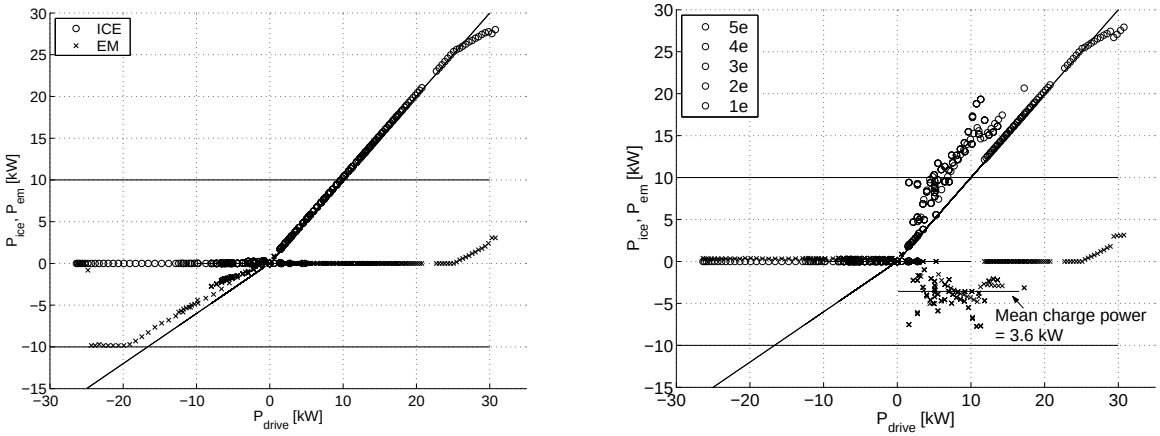

Figure 5.8: The power split for BER (left) and CH (right) only. The maximum/minimum power line of the EM (+ and - 10 kW), a line of 60% of the drive power for regeneration and 100% of the drive power for driving are depicted as well.

The energy recovered with BER (model IX) is used to reduce fuel consumption at low (<5 kW) power request with motor only (M) mode and high (>25 kW) power request with motor assist (MA) mode. Although it can not be seen very clearly in the power split figure, most of the energy is used in the low power region. In Figure 5.9 the histograms for the motor assist and motor only mode are depicted. From these figures can clearly be seen that the major part of the electric energy is used for the motor only mode.

Although the EM in model X (investigation CH mode) shows much activity, it does not save much fuel. The engine comes in more efficient regions due to the charge mode. However, the fuel consumption in $[g/s]$ increases because extra power is needed to charge the battery. The decrease in fuel consumption for charge mode is small because the extra fuel used to charge the battery and the fuel saved by the motor only mode are almost in balance. Recharging the battery happens on average at 3.6 kW. The major part of the recharged energy is used in motor only (M) mode as well.

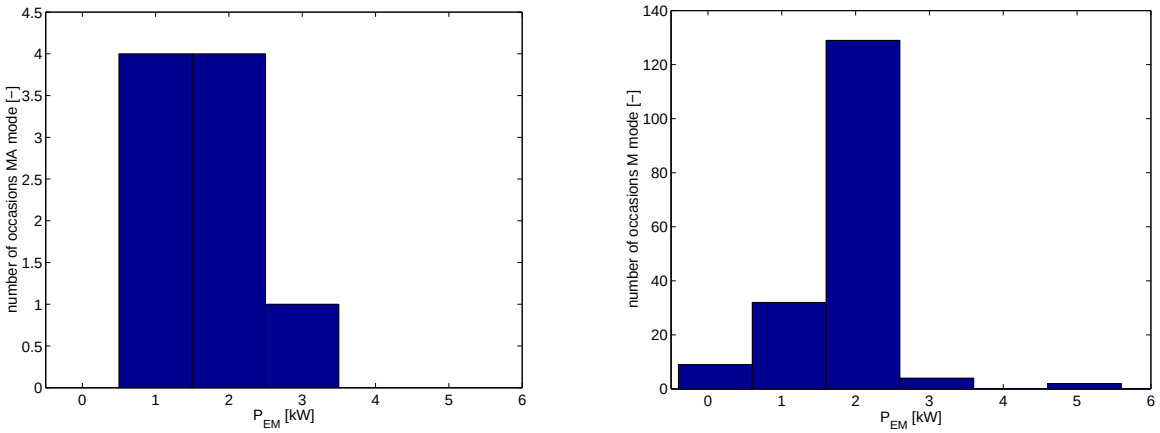

Figure 5.9: *left:* The histogram for the motor assist mode (MA) *right:* The histogram for the motor only mode (M)

5.6 Influence of the drive cycle

To investigate the influence of the drive cycle on the power split strategy, the FTP cycle (See Figure 3.2) has been used to simulate the Honda Civic IMA (V) as well. The fuel consumption is $4.8\ l/100\ km$ which is higher than the usage on the NEDC cycle. The FTP is a more aggressive cycle with more accelerations and decelerations. The total positive energy needed in the FTP cycle is $6750\ kJ$ while the negative energy is only $-990\ kJ$. For the NEDC cycle these values are respectively 3990 and -720 kJ. The ratio between negative and positive energy is lower for the FTP cycle which explains the extra fuel usage. The resulting power and torque split are plotted in red and green in Figure 5.10. The results of NEDC cycle have been plotted in black to compare the results.

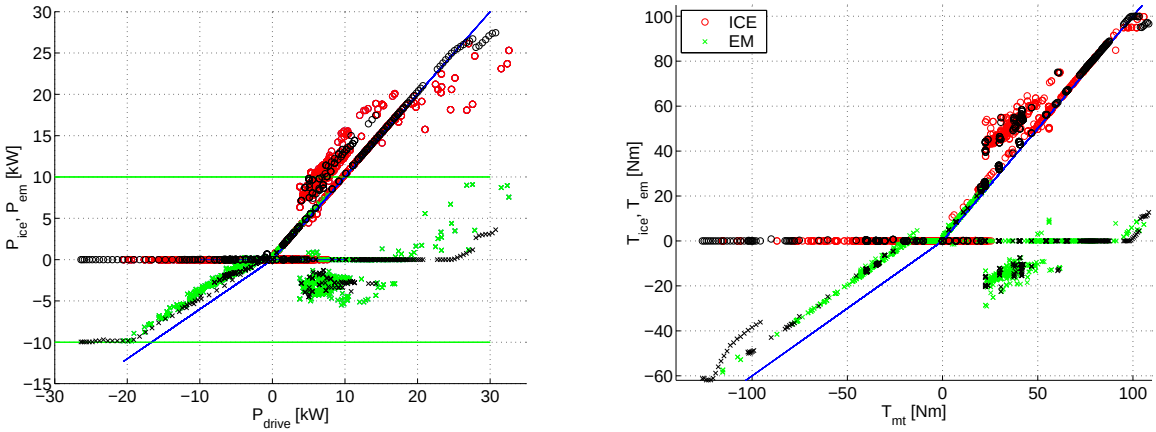

Figure 5.10: The power split (left) and torque split (right) for the FTP cycle (red+green) and the NEDC cycle (black)

From these figures can be concluded that the torque split is less sensitive for different drive cycles than the power split. The main difference in the power split is seen in the motor assist mode (MA until $10\ kW$ instead of $5\ kW$ for requested drive powers above $17\ kW$ instead of $25\ kW$). The two torque split figures very correspond well. A little difference is seen in the regeneration mode: the vehicle can regenerate all power for the FTP cycle while during the NEDC, the maximum torque constraint is reached.

Chapter 6

Rule Based Controller

The results for the Honda Civic IMA (model V) from Chapter 5 have been analyzed and translated to rules for a Rule Based (RB) controller. In this chapter two RB controllers are derived for the Honda Civic IMA when driving over the NEDC. The first one is defined by a power split, the second one by torque split. A charge sustaining strategy is implemented to avoid battery damage. The FTP cycle is used to check the robustness of both controllers.

6.1 Power split rule based controller

The power split figure from the Honda Civic IMA can be divided into a couple of regions. Each region represents a mode, see Figure 6.1.

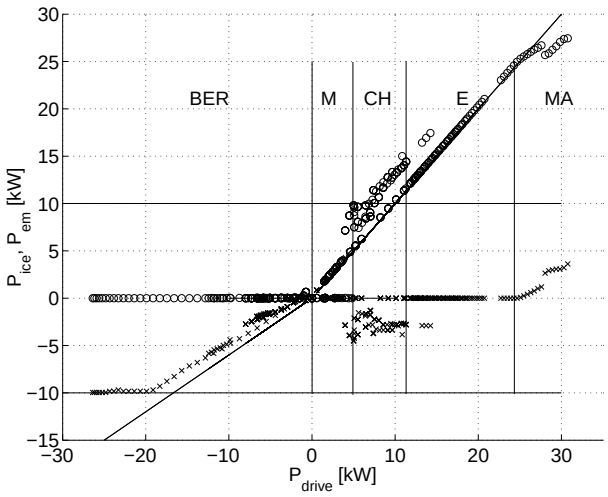

Figure 6.1: The power split divided into mode regions

The regions can clearly be seen but the mode between 0 and 5 kW is difficult to define. Engine and motor only mode occur alternately in this region. A histogram has been made to find out which mode dominates (Figure 6.2). From this figure can be concluded that the system is mostly in motor only mode.

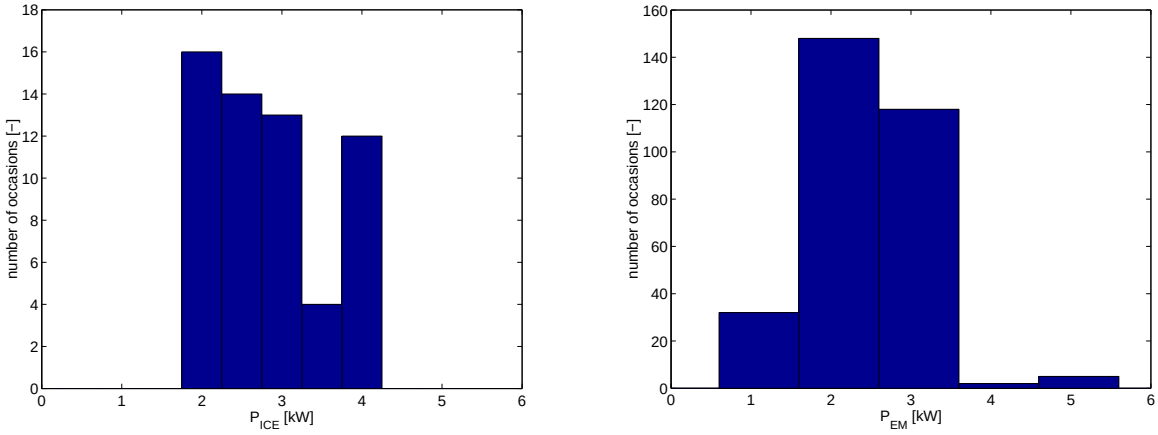

Figure 6.2: The histogram for the ICE (left) and for the EM (right) in the region $0 < P_{drive} < 5\ kW$. The motor only mode is dominant in this region.

Now, a very simple rule based controller can be derived

If		P_v	$< 0\ kW$	BER $\Rightarrow$	$P_{em} = P_v$ - P_{drag}	$P_{ice} = 0$,
If	$0 \leq$	P_v	$< 5.2\ kW$	M $\Rightarrow$	$P_{em} = P_v$	$P_{ice} = 0$,
If	$5.2 \leq$	P_v	$< 12\ kW$	CH $\Rightarrow$	$P_{em} = -0.4\ (P_v - 1000)$	$P_{ice} = P_v - P_{em}$,
If	$12 \leq$	P_v	$< 25\ kW$	E $\Rightarrow$	$P_{em} = 0$	$P_{ice} = P_v$,
If		P_v	$> 25\ kW$	MA $\Rightarrow$	$P_{em} = 0.66\ (P_v - 25000)$	$P_{ice} = P_v - P_{em}$.

6.1.1 NEDC

This rule based controller is implemented and the resulting power and torque split for the NEDC are plotted in black in Figure 6.3. To compare these results, the DP results are plotted in color as well. The results from the rule based controller are almost similar to the results of DP.

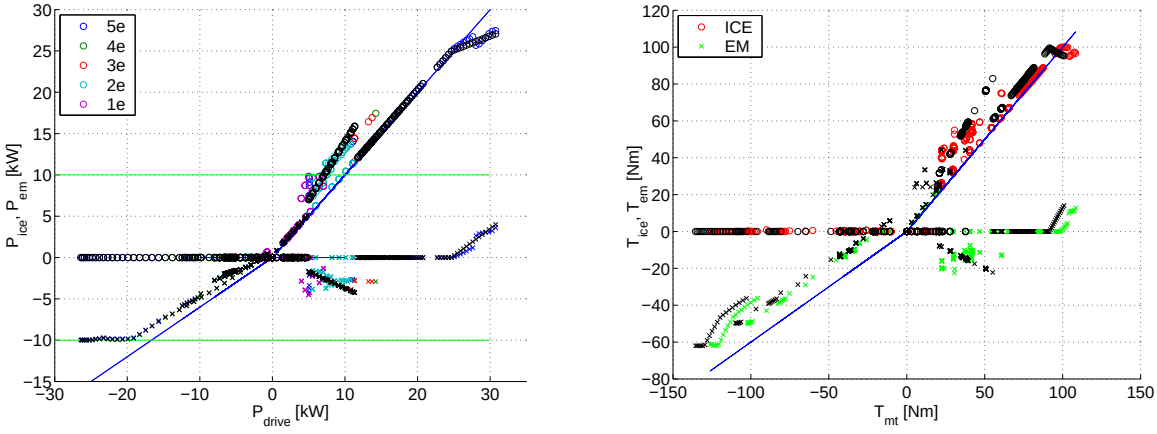

Figure 6.3: Power split (left) and Torque split (right) of the rule based controller in black and DP in color

Fuel consumption calculation

The resulting fuel consumption is $4.42\ l/100\ km$, which is $0.15\ l/100\ km$ lower than the result of DP. A difference in SOC (Figure 6.5 left) causes this lower fuel consumption. This SOC difference can be taken into account with an additional fuel consumption. It is assumed that the energy deficiency is supplied by the ICE. The overall charge efficiency η_{charge} (= $\eta_{ICE+EM+battery}$) for P_{charge} (= P_{ice}) between 0 and $10\ kW$ is calculated to define the most optimal charge power. The efficiencies are depicted in Figure 6.4. From this figure can be concluded that charging the battery at $10\ kW$ is most efficient. The fuel consumption at $10\ kW$ is $0.737\ g/s$. The difference in SOC is $216\ kJ$. When $21.6\ s$ is generated at $10\ kW$, which means an extra fuel consumption of $15.9\ g$, the corrected fuel consumption is $4.62\ l/100\ km$.

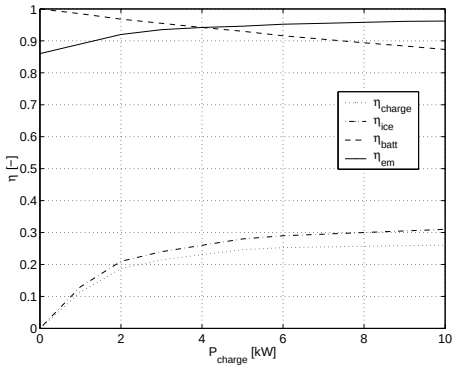

Figure 6.4: The efficiency for charging the battery, η_{charge} as a function of P_{charge}. The efficiency of EM, ICE and battery are depicted as well.

6.1.2 Charge sustaining strategy

When this rule based controller is implemented into a vehicle, a charge sustaining strategy has to be developed. When the battery reaches its lower constraint, corrective measures must be taken to avoid complete discharge of the battery. An extra rule is implemented: When the SOC level exceeds the constraint SOC = 0.3, the M and MA mode ($P_{em} \not> 0$) are not allowed to be used until SOC = 0.35 is reached. When one of these modes occur, the SOC controller overrules these modes: the EM has to charge with $3.6\ kW$. This value has been chosen because the mean power during charging in the CH only model (X) in Section 5.5 was $3.6\ kW$. The modes E, BER, CH and IS are still allowed to take place. In the rule based controller, a boolean *a* is set *true* when the SOC constraint of 0.3 is reached. The battery has to be charged until the constraint of 0.35 is reached. Then the boolean is set to *false* again which enables the normal RB controller. The frequency of the recharge mode (*a = true*) depends on the setpoint constraint (SOC = 0.35), the charge power ($3.6\ kW$) and the drive power (P_{drive}). When the SOC reaches the upper constraint, SOC = 0.8, the EM is not allowed to charge.

If 0.3 < SOC	$\vee\ P_{em} > 0$	$\Rightarrow P_{em}$ = -3.6 kW, $P_{ice} = P_v - P_{em}$,	a = true
If 0.3 < SOC < 0.35 $\vee$ a = true	$\vee\ P_{em} > 0$	$\Rightarrow P_{em}$ = -3.6 kW, $P_{ice} = P_v - P_{em}$,	a = true
If 0.3 < SOC < 0.35 $\vee$ a = false	RB		a=false
If 0.35 < SOC < 0.8	RB		a=false
If SOC > 0.8	No CH + BER		a=false

This rule costs only 0.05 $l/100\ km$. In Figure 6.5 (right), the SOC development for 3 cycles over the NEDC is shown. The final power rule based controller has a fuel consumption of $4.67\ l/100\ km$.

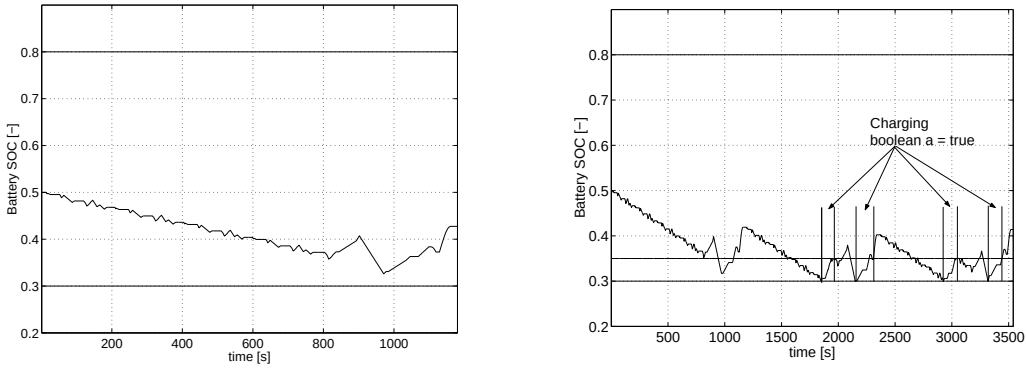

Figure 6.5: *left:* The begin and end value of the state of charge are different *right:* The SOC development for 3 NEDC cycles with charge sustaining strategy to avoid complete discharge. When the SOC reaches the constraint SOC = 0.3, the battery has to be charged until the SOC has reached the level of 0.35.

6.1.3 FTP cycle

The FTP cycle has been used to investigate the robustness of the rule based controller with respect to other cycles. The results are in Figure 6.6. Many points, especially at high driving power, can not be covered by the power split strategy. The torque split seems to be less sensitive to the difference in cycle. The fuel consumption is 5.09 $l/100km$, which is higher than the result obtained with DP (4.8 $l/100km$). During the cycle the SOC constraints are not reached (see Figure 6.7) while at the end of the cycle, a small SOC deviation is observed.

Due to the increase in fuel consumption and the difference in power split, it is concluded that the power split rule based controller not robust enough for other drive cycles.

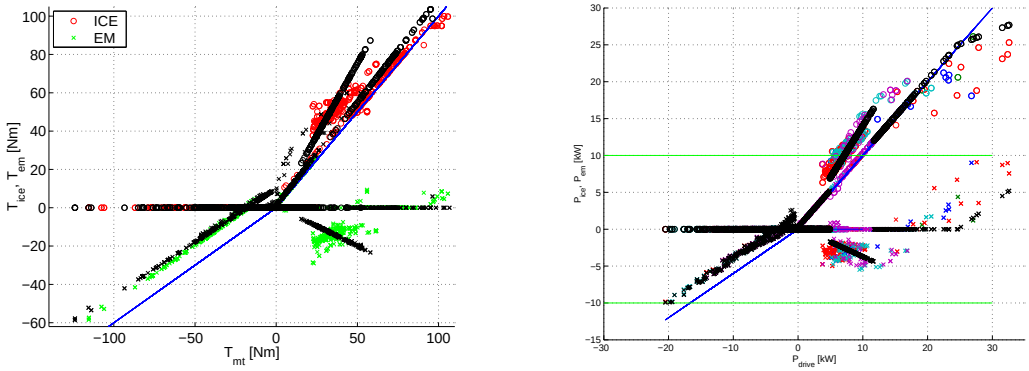

Figure 6.6: (left) The resulting torque split for the FTP cycle when power split is defined. (right) Many points at higher power are not covered by the power split rule based controller

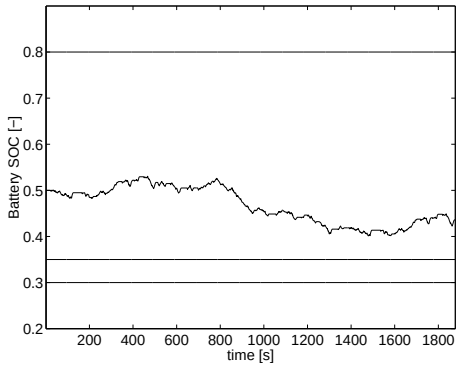

Figure 6.7: The the SOC does not reach its constraints during the FTP cycle

6.2 Torque split rule based controller

6.2.1 NEDC

Because the torque split in Section 5.6 and 6.1.3 seemed to be robuster than the power split, a torque split controller is designed as well. The rules are derived from the torque split of the IMA (model V), see Figure 6.8.

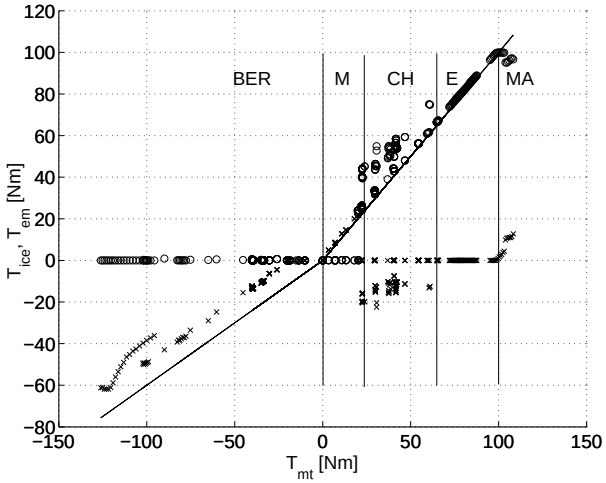

Figure 6.8: The regions for defining the torque split

In this case there is some uncertainty about the mode choice between 25 < T_{mt}< 65 Nm. The histogram method has been applied again. The charge mode occurs 200 times while engine only mode occurs only 70 times. Therefore the charge mode is chosen for this region. The rules for the torque rule based controller can now be defined as

If		T_v	$< 0\ Nm$	BER $\Rightarrow$	$T_{em} = T_v$ - T_{drag}	$T_{ice} = 0$,
If	0	$\leq T_v$	$< 25\ Nm$	M $\Rightarrow$	$T_{em} = T_v$	$T_{ice} = 0$,
If	25	$\leq T_v$	$< 65\ Nm$	CH $\Rightarrow$	$T_{em} = -15$	$T_{ice} = T_v - T_{em}$,
If	65	$\leq T_v$	$< 100\ Nm$	E $\Rightarrow$	$T_{em} = 0$	$T_{ice} = T_v$,
If		T_v	$> 100\ Nm$	MA $\Rightarrow$	$T_{em} = 1.7(T_v - 100)$	$T_{ice} = T_v - T_{em}$.

The torque split and the resulting power split are depicted in Figure 6.9. By defining the torque split, the power split figure resembles the outcomings of DP better than by defining the power split itself. The fuel consumption is $4.62\ l/100\ km$. In this case, the end SOC is a little too high. The fuel consumption is $4.61\ l/100\ km$ when the difference in SOC is taken into account. This result is almost as good as the result obtained with DP.

In contrast with the power split RB, the torque split RB controller sustains the SOC very well over the NEDC. Even when five cycles are driven successively, the battery energy does not reach its constraints (Figure 6.10). Measures have been taken to avoid constraint violation but are not necessary. The operating points of the ICE are all above $40\ Nm$ in a relatively good efficiency region.

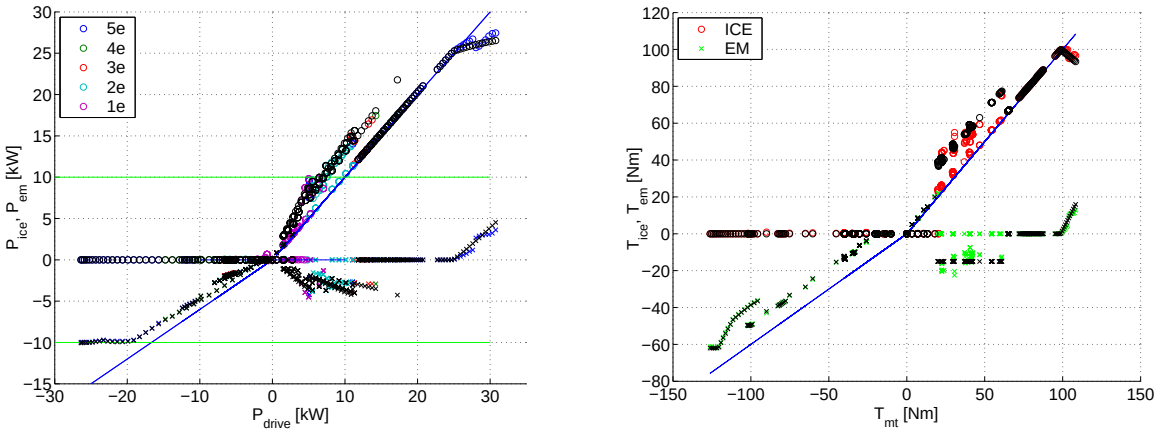

Figure 6.9: *left:* Power split resulting of the torque rule based in black and of DP in color *right:* The defined torque split of the rule based(black) and DP (color)

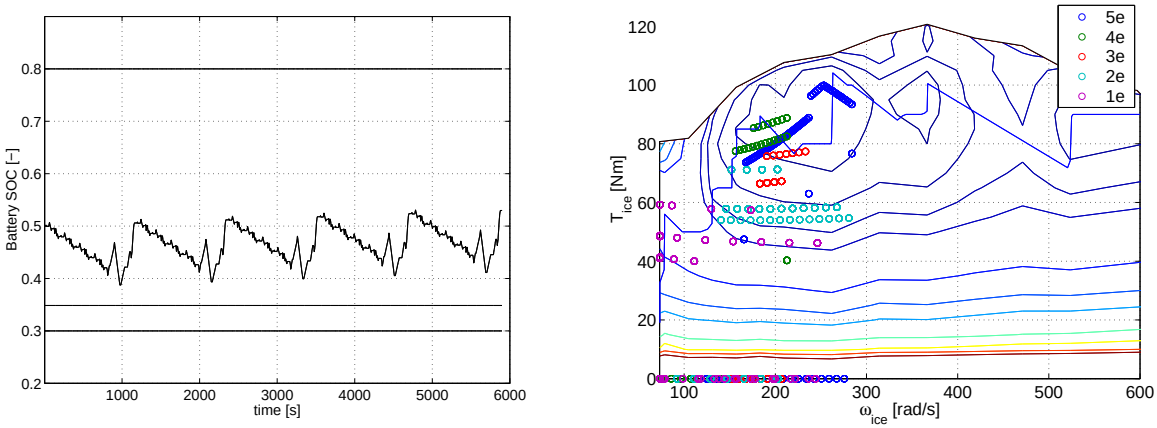

Figure 6.10: (left) Even when the NEDC is driven five times, the SOC does not reach its constraints. (right) The operating points of the ICE for the torque rule based controller

6.2.2 FTP cycle

The FTP cycle has also been used for the torque split rule based controller to test the robustness. The results are in Figure 6.11. The power split figure resembles the results of DP very well. The motor assist behaviour at high power that could not be seen with power split rule based, can now be observed. The fuel consumption is 4.8 $l/100$, which is the same as the result of DP. Furthermore, the strategy is almost charge sustaining (Figure 6.12).

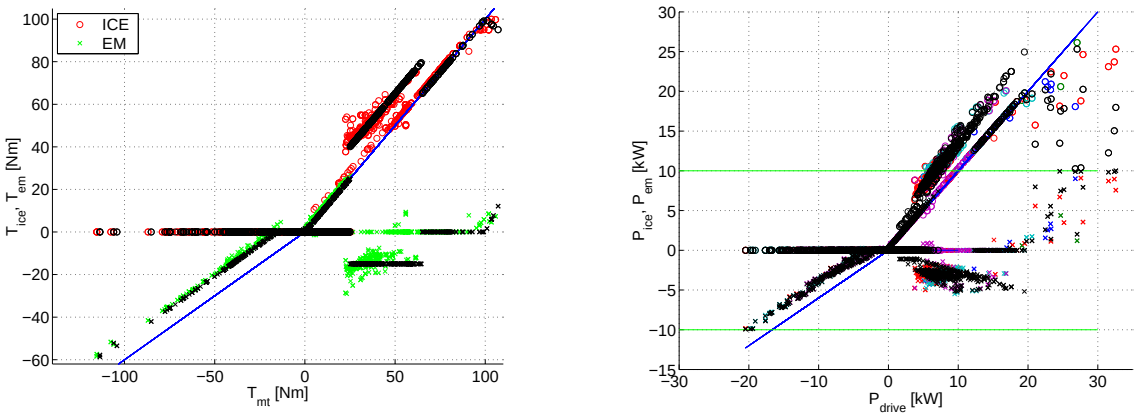

Figure 6.11: (left) The torque split for DP (color) and RB (black) of the FTP cycle (right) The resulting power split

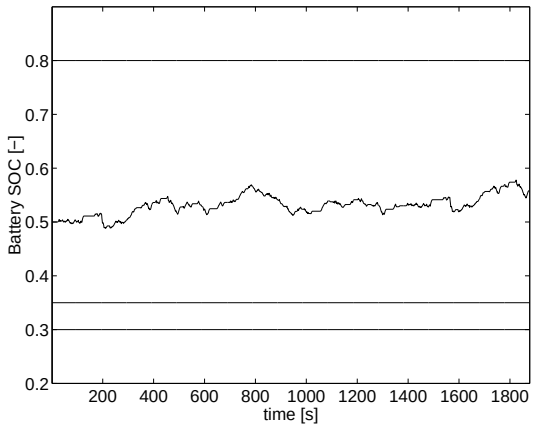

Figure 6.12: The battery SOC does not reach its constraint during the FTP cycle.

The torque rule based controller is very robust and results in the best fuel consumption. When the torque split is defined, the power split figure resembles the results of DP more. By defining a torque split instead of a power split, a difference can be made for acceleration and driving with constant speed. For example, when a power split is defined, there is no difference between driving at a constant speed at 5 kW or accelerating with 5 kW. When a torque split is used, this difference can be made which finally results in a better power split.

6.3 Overall fuel consumption reduction

The Honda Civic IMA has a fuel consumption of $4.9\ l/100km$ tested on the NEDC. In order to improve this fuel consumption, DP has been used to calculate the most optimal energy management strategy. The fuel consumption resulting from DP is $4.57\ l/100km$ and the torque rule based controller derived from DP uses $4.61\ l/100km$. Taking into account that the model used consumes 3.4% less on the NEDC cycle due to the warm motor effect (see Section 3.2), the fuel consumption for the final rule based EMS is $4.77\ l/100km$. This is an improvement of only 2.5 % with respect to the Honda Civic IMA. For this thesis was assumed that during the BER mode and motor only mode, the ICE was idling. When the motor is shut off during these phases, the fuel consumption improves significantly. The system is $173\ s$ BER mode and $312\ s$ motor only mode, which saves $36.8\ g$. The fuel consumption over the cycle is then $4.1\ l/100km$ and this is an significant improvement of 16.3 % with respect to the fuel consumption of the Honda Civic IMA. Because the engine is shut off for a long time ($1/4$ of the cycle), a study has to be made to the extra fuel consumption and emissions due to starting with a colder engine and catalytic converter.

In Figure 6.13, the fuel reduction in [%] for each hybrid function is given. The percentage of engine downscaling is given with respect to the benchmark of the $1.6\ l$ Civic while the effect of idle stop, BER and charge mode are given with respect to the $1.3\ l$ Civic. The total improvement (from $1.6\ l$ Civic to Civic IMA $1.3\ l$ rule based) is 29.4 %, which is a significant difference. Compared to the fuel improvement of the already existing hybrids, which achieve a fuel consumption improvement of $\pm\ 25$ % already, it is not a significant improvement. Especially when the goal of the research programme "Impulse Drive" is to improve the fuel consumption with 50 - 75 %, another method has to used to achieve this goal. Investigation to more frequent or longer usage of the idle stop mode can result in a significant fuel consumption. Furthermore, the system efficiency (so the fuel savings as well) can be increased by the design of new components or the usage of existing components in new system configurations. The choice for the component size is relevant in this design as well. DP is a helpful tool to get more insights in the optimal EMS for these new configurations.

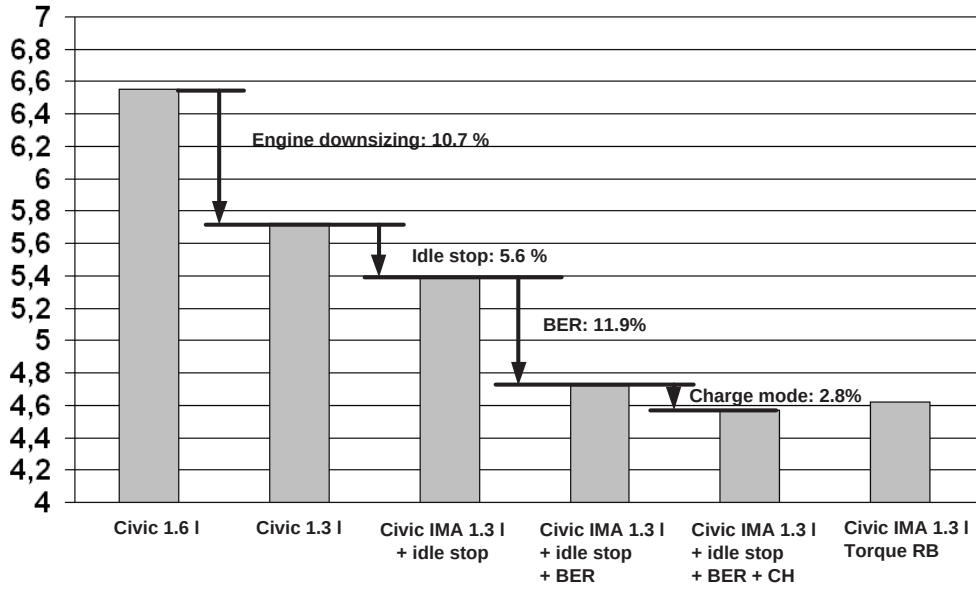

Figure 6.13: The fuel consumption reduction of all hybrid functions and the final fuel consumption with the torque split rule based controller. The reduction due to engine downsizing in [%] is with respect to the $1.6\ l$ Civic, the other reductions are with respect to the $1.3\ l$ Civic.

Chapter 7

Conclusions

A Quasi Static model to describe the power flow in the vehicle and dynamic model to describe the vehicle dynamics have been made for the Honda Civic IMA. The efficiencies and constraints of all components (Internal Combustion Engine (ICE), Electro Motor (EM), Battery, Manual Transmission, Final Drive), the drag torque and the clutch losses have been taken into account. The models are validated by comparing the fuel consumption over the NEDC drive cycle to the catalogue values for a conventional vehicle. This fuel consumption is used as a benchmark later on.

The energy management problem for the Honda Civic IMA is implemented in DP. The method to calculate the cost matrix, the grid choice for control and state variables and the DP algorithm are explained. A test with the conventional IMA modelled in DP is performed to check the reliability of the outcomes of DP. The resulting fuel consumption and the operating points of the ICE are close to the results from the benchmark of the conventional IMA.

The influence of three different subjects (components, mean efficiency and hybrid modes) on the fuel consumption and the EMS resulting from DP are investigated. For every different subject, other models are needed. The DP simulation series started with a simplified model of the Honda Civic IMA. Step by step, all component efficiencies were implemented and the effect of each component on the resulting strategy and fuel consumption could clearly be observed. The resulting fuel consumption for the Honda Civic IMA is $4.57\ l/100km$ over the NEDC cycle. From these simulations, the following conclusions can be made:

- All operating points of the ICE are in the sweet spot when no efficiencies for battery and EM are taken into account. When adding the efficiencies, the operating points move to less efficient regions. DP avoids the low efficiency region of the ICE (0 - 0.2).
- Low efficiency regions for battery and EM are avoided during M, MA and CH mode. During BER mode, all energy is recuperated within the constraints, also when the operating points are in a low efficiency region.
- The mean efficiency of battery, EM and battery + EM are respectively 0.95, 0.89 and 0.85.
- If the drive torque $T_{drive} < 25\ Nm$: always motor only mode (M).
- When the battery + EM efficiencies are added, the engine only (E) mode increases. This causes a increase in fuel consumption.
- When the drag losses and auxiliary power are added, the CH mode increases to compensate for the decrease in electrical power.
- The most important component constraints are the minimum torque constraint of the EM (not all regenerative energy can be recuperated) and the SOC constraint ($SOC(t_{end}) = SOC(t_0)$).

To investigate the effect of the mean efficiency on the fuel consumption and power split strategy, some simulations have been done with constant efficiency for the battery and EM (system S). When these results for the power split strategy are compared to the simulations with the efficiency depending on the operating points, the similarity can clearly be observed. The fuel consumption remains more or less the same. Due to this resemblance can be concluded that the mean efficiency of S defines the power split. Furthermore, when the mean efficiency increases, the fuel savings increase even more (high sensitivity in high mean efficiency region). Little improvement of component efficiencies can lead to significant lower fuel consumption.

The effect of the hybrid functions such as Brake Energy Recovery (BER), idle stop and charge mode on fuel consumption has been investigated as well. Idle stop causes a large fuel consumption decrease (5.6%). BER is plays an important role in fuel consumption improvement (11.9 %). The major part of the power regenerated in the BER mode is used later in the motor only mode when T_{drive}<25 Nm. The possibility to charge during driving does not yield much fuel consumption improvement (2.8 %).

When the NEDC is replaced by the FTP cycle, a higher fuel consumption (4.8 $l/100km$) and other power split results can be seen. The torque split seems to be less sensitive for different drive cycles. The increased fuel consumption is a result of more accelerations during the cycle.

Two rule based controllers are derived from the results of DP. The first one is a power split controller. A charge sustaining strategy is implemented to avoid battery damage. The resulting power and torque split strategy resemble the results from DP for the NEDC cycle. The fuel consumption is slightly higher (4.67 $l/100km$). When the FTP cycle is used, the fuel consumption increases (5.09 $l/100km$) and another power split is obtained. This controller is not robust for different cycles.

The torque rule based controller is very robust and results in the best fuel consumption (4.61 $l/100km$). When the torque split is defined, the power split figure resembles the results of DP very well. The fuel consumption is only 1 % higher than the result of DP. Even for the FTP cycle, the results remain good. A charge sustaining rule has been implemented but is not necessary because the SOC does not reach its constraints during both drive cycles.

With respect to the conventional Honda Civic 1.6 l, the torque rule based controller improves the fuel consumption with 29.4 %. When the fuel consumption is compared to the catalogue value of the Honda Civic IMA, only 2.5 % is saved additionally. Further EMS optimization seems to be useless to obtain better fuel consumption. In the recommendations, other methods to save extra fuel are proposed.

Chapter 8

Recommendations

There is little flexibility left in the fuel consumption improvement due to optimizing the energy management strategy. Other methods have to be used to achieve to goal of the research project "Impulse Drive" of 50 - 75 % fuel consumption improvement. Two other methods for additional fuel savings presented in this thesis are promising:

- Optimization of the component efficiencies. Due to the higher efficiencies, the fuel consumption increases. Especially in the high efficiency region (0.85-1) much fuel consumption savings can be achieved.
- A higher frequent usage of idle stop during motor only and BER mode. When the idle stop is used for these two modes as well, the engine can be shut off 1/4 of the cycle which improves the fuel consumption significantly.

These methods have to be investigated further to define the exact improvement and the (dis)advantages which are involved by these methods. A third interesting research object has not been investigated in this thesis: The influence of new components or existing components in new system configurations on the fuel consumption. The usage of DP is a helpful tool to investigate the best energy management strategy for the new configurations.

Furthermore, it is interesting to finish the results for the optimal energy management strategy for the CVT in DP. Many insights for the usage of CVT's in hybrid vehicles can be obtained from this study which can be used further on in the study of other system configurations and components.

Bibliography

[1] http://www.honda.com.

[2] http://www.insightcentral.net.

[3] http://www.new-cars.com/2003/honda/honda-civic-hybrid-specs.html.

[4] M. Amano. Practical optimization of energy management for parallel hybrid electric vehicles. *The 20th international electric vehicle symposium and exposition*, November 2003.

[5] R.E. Bellman. *Dynamic programming*. Princeton : Princeton University Press, 1962.

[6] R. van Druten. *Transmission Design of The Zero Inertia Powertrain*. Technische Universiteit Eindhoven, 2001.

[7] L. Guzzella. *Fahrzeugantriebssysteme*. ETH Zurich, 2002/2003.

[8] L. Guzzella and A. Sciarretta. *Vehicle Propulsion Systems*. Springer Berlin Heidelberg New York, 2005.

[9] T. Hofman and R. van Druten. Reasearch overview design specifications for hybrid vehicles. *European ELE-DRIVE Transportation, Lissabon*, 2004.

[10] T. Hofman, R. van Druten, M. Steinbuch, and A. Serrarens. Design specifications for hybrid vehicles. *7th International Symposium on Advanced Vehicle Control*, 2004.

[11] T. Hofman, R.v. Druten, A. Serrarens, and J.v. Baalen. A fundamental case study on the Prius and IMA drivetrain concepts. *EVS 21, Monaco*, 2005.

[12] K.J. Kelly, M. Mihalic, and M. Zolot. Battery usage and thermal performance of the Toyota Prius and the Honda Insight for various chassis dynamometer test procedures. In *17th Annual Batery Conference on Applications and Advances, Long Beach, California*, January 2002.

[13] K.J. Kelly and A. Rajagopalan. Benchmarking of OEM hybrid electric vehicles at NREL, Milestone report. August 2001.

[14] K.J. Kelly, M. Zolot, G. Glinsky, and A. Hieronumus. Battery usage and thermal performance of the Toyota Prius and the Honda Insight for various chassis dynamometer test procedures. November 2001.

[15] M. Koot, J.T.B.A. Kessels, B. de Jager, P.P.J. van den Bosch, and M. Steinbuch. Energy manangement strategies for vehicular electric power systems. *IEEE Transactions on Vehicular Technolohy*, 54(3), May 2005.

[16] C. Lin, Z. Filipi, Y. Wang, L. Louca, H. Peng, D. Assanis, and J. Stein. Integrated, feed-forward hybrid electric vehicle simulation in Simulink and its use for power management studies. *SAE paper No. 2001-01-1334*, March 2001.

[17] C. Lin, J. Kang, J.W. Grizzle, and H. Peng. Energy management strategy for a parallel hybrid electric truck. *Proceedings of the 2001 Amarican Control Conference, Arlington, VA*, pages 2878–2883, 2001.

[18] C. Lin, J. Kang, J.W. Grizzle, and H. Peng. Power management strategy for a parallel hybrid electric truck. *SAE Technical Papers*, 2001.

[19] C. Lin, H. Peng, and J.W. Grizzle. A stochastic control strategy for hybrid electric vehicles. *in Proc.of the ACC, Boston, MI*, June 2004.

[20] C. Lin, H. Peng, J.W. Grizzle, and J. Kang. Power managment strategy for a parallel hybrid electric truck. *IEEE Transactions on Control Systems Technology*, 2003.

[21] C. Lin, H. Peng, J.W. Grizzle, J. Liu, and M. Busdiecker. Control system development for an advanced-technology medium-duty hybrid electric truck. *SAE Paper*, 01, 2003.

[22] M. Matsuki, Y. Hirano, and A. Matsubara. Development of a power train for the hybrid automobile - the Civic IMA. *EVS 21, Monaco*, 2005.

[23] I. Matsuo, S. Nakazawa, H. Maeda, and E. Inada. Development of a hybrid propulsion system with CVT. *Aachener Kolloquium Fahrzeug- und Motorentechnik*, pages 1299–1999, 1999.

[24] National Renewable Energy Laboratory (NREL). http://www.ctts.nrel.gov/analysis/advisor.html, 2002.

[25] Hans B. Pacejka. *Tyre and vehicle dynamics*. Oxford : Butterworth-Heinemann, 2002.

[26] P. Pisu and G. Rizzoni. H infinity control for hybrid electric vehicles. *43rd IEEE Conference on Decision and Control, Atlantis, Paradise Island, Bahamas*, December 2004.

[27] N.J. Schouten, M.A. Salman, and N.A. Kheir. Fuzzy logic control for parallel hybrid vehicles. *IEEE Transactions on Control Systems Technology*, 10(3):460–468, May 2002.

[28] A. Sciarretta, M. Back, and L. Guzzella. Optimal control of parallel hybrid electric vehicles. *IEEE Transactions on Control Systems Technology*, 12(3), May 2004.

[29] A. Sciarretta and L. Guzzella. Rule based and optimal control strategies for energy management in parallel hybrid vehicles. *6th International Conference on Engines for Automobile(ICE 2003), Capri, 14-19 September*, 2003.

[30] A. Sciarretta, L. Guzzella, and M. Back. A real-time optimal control strategy for parallel hybrid vehicles with on-board estimation of the control parameters. *IFAC*, 2004.

[31] A. Sciarretta, L. Guzzella, and C.H. Onder. On the power split control of parallel hybrid vehicles: from global optimization towards real-time control. *Automatiserungstechnik*, (51):195–203, 2003.

[32] R. Seaks, J.J. Cox, J. Neidhoefer, P.R. Mays, and J.J Murray. Adaptive control of a hybrid electric vehicle. *IEEE Transctions on Intelligent Transportation Systems*, 3(4):213–233, December 2002.

[33] B. Vroemen. *The component control for the zero inertia powertrain*. Technische Universiteit Eindhoven, 2001.

[34] Y. Zhu, Y. Chen, and Q. Chen. Analysis and design of an optimal energy management and control system for hybrid electric vehicles. *in Proc. of EVS 19, Busan, Korea*, 2002.

[35] Y. Zhu, Y. Chen, G. Tian, H. Wu, and Q. Chen. A four-step method to design an energy management strategy for hybrid vehicles. *in Proc. of the ACC, Boston*, June 2004.

[36] Y. Zhu, Z. Han, G. Tian, H. Wu, and Q. Chen. Optimal energy management strategy for hybrid electric vehicles. *SAE Technical Papers*, 2004-01-0576.

Appendix A

List of Abbreviations

ADVISOR	Advanced Vehicle Simulator
BSFC	Brake Specific Fuel Consumption
CIS	Cilinder Idling System
DP	Dynamic Programming
EMS	Energy Management Strategy
FTP	Federal Test Procedure
HEV	Hybrid Electric Vehicle
IMA	Integrated Motor Assist
NEDC	European Drive Cycle
NREL	National Renewable Energy Laboratory
OOL	Optimal Operating Line
SOC	State of Charge
RB	Rule Based
WOT	Wide Open Throttle
BATT	Battery
CVT	Continuous Variable Transmission
EM	Electro Motor
FD	Final Drive
G	Generator
GM	Motor-Generator
ICE	Internal Combustion Engine
MT	Manual Transmission
PA	Power Amplification
W	Wheels
C	Control strategy
P	Primary power source
S	Secondary Power Source
T	Transmission
V	Vehicle
BER	Brake Energy Recovery
CH	Charge mode
E	Engine only mode
IS	Idle Stop mode
M	Motor only mode
MA	Motor assist mode

Appendix B

List of Symbols

General

η	Efficiency	$[-]$
P	Power	$[W]$
F	Force	$[N]$
T	Torque	$[Nm]$
ω	rotational speed	$[rad/s]$
P_{fuel}	Fuel power	$[W]$
P_v	Vehicle drive power	$[W]$
P_{drive}	Vehicle drive power	$[W]$
$P_{c,loss}$	Power loss at the clutch	$[W]$
P_{aux}	Auxiliaries power	$[W]$
ΔH	Lower heating value	$[J/g]$
$\dot{m}_{fuel}$	Mass flow fuel consumption	$[g/s]$
m	consumed mass	$[g]$

Battery

I_{batt}	Battery current	$[A]$
I_{chg}	Charge current	$[A]$
I_{dis}	Discharge current	$[A]$
V_{batt}	Battery voltage	$[V]$
V_{oc}	Open circuit voltage	$[V]$
R_i	Internal resistance	$[\Omega]$
P_{loss}	Battery losses	$[W]$
P_{batt}	Battery power	$[W]$
P_s	Internal battery power	$[W]$
t_f	Discharge time until cut voltage	$[s]$
C	Peukert constant	$[-]$
n	Peukert coefficient	$[-]$

Vehicle dynamics

F_t	Tracking force	$[N]$
F_g	Grade resistance Force	$[N]$
F_a	Aerodynamic drag force	$[N]$
F_d	Disturbance force	$[N]$
F_r	Rolling resistance force	$[N]$
F_{load}	Load force	$[N]$
A_f	Frontal service area	$[m^2]$
c_d	Air drag coefficient	$[-]$
c_r	Rolling resistance coefficient	$[-]$
g	Gravitational constant	$[m/s^2]$
ρ_{air}	Air density constant	$[kg/m^2]$
a	Acceleration	$[m/s^2]$
v	Speed	$[m/s]$
ω	Rotational speed	$[rad/s]$
$\dot{\omega}$	Rotational acceleration $[rad/s^2]$	
J_{tot}	Inertia all components	$[kgm^2]$
J	Inertia	$[kgm^2]$
m_v	Vehicle mass	$[kg]$
m_{rot}	Additional vehicle mass due to rotational inertia	$[kg]$
m	m_v+m_{rot}	$[kg]$
r_w	Wheel radius	$[m]$
i_{fd}	Final drive ratio	$[-]$
i_{mt}	Manual transmission ratio	$[-]$

Dynamic Programming

x_k	State variable
u_k	Control variable
t	Time
S_k	State space
C_k	Control space
U_k	Constrained control space
J	Cost criterium
L	Cost-to-go matrix
C	Cost matrix
N	Node matrix

$\overline{P}_{em}$	EM power vector	[W]
$\overline{P}_{drive}$	Drive power vector	[W]
$\overline{P}_{ice}$	ICE power vector	[W]
$\overline{P}_{mt,in}$	Input MT power vector	[W]
P_{step}	Step size control grid	[W]
n_x	Number of steps state space	[-]
n_u	Number of steps control space	[-]
n_t	Number of steps time grid	[-]
E_{batt}	Battery energy	$[J]$
E_{max}	Maximum battery energy level	$[J]$
E_{min}	Minimum battery energy level	$[J]$
$E(0)$	Energy level $t = 0$	$[J]$

Appendix C

Control Strategy for the Honda Insight

The precursor from the Honda Civic IMA was the Honda Insight. To get an idea how the energy management control strategy has been implemented in practice, the Insight has completely been measured by the National Renewable Energy Laboratory (NREL, Colorado) [13], [12], [14] and the Milestone report containing all the results is written. The most important conclusions about SOC control, torque assist/regenerative braking, idle stop and the impact of airconditioning on the fuel consumption are summarized in this chapter.

C.1 SOC control

The Insight's SOC control tries to maintain the initial SOC during a cycle. This can be seen in figure C.1. The upper and lower bound of the SOC in which the battery is allowed to operate are respectively 20 % and 80 %.
When the battery is depleted by a uphill driving test, the SOC reaches the lower limit. At that moment, the engine starts operating at a higher power level than required. The resuming energy is used to charge the battery. When the battery is charged by a downhill test, it reaches its upper limit. The current is then cut off to avoid system damage.

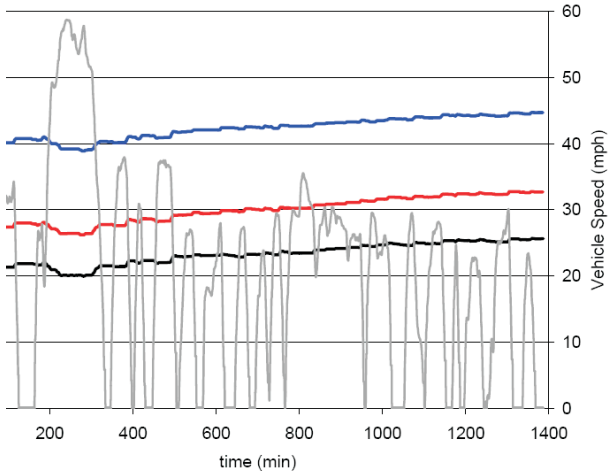

Figure C.1: SOC evaluation during a test cycle

C.2 Auxiliaries

The auxiliaries are powered from the electro motor which acts as an alternator, regenerating a small current to supply the accessory loads. When the electro motor is used for torque assist, the auxiliaries are powered by the battery. When the airconditioning is used, the total fuel consumption increases with 34 %. The power needed for the auxiliaries increases then from 288 W to 745 W.

C.3 Torque assist and regenerative braking

The electro motor is used to assist in conditions of high load. The measurements indicate that the electro motor kicks in when the drive line torque exceeds 20 Nm and that it provides a relatively constant torque of 10 Nm, see figure C.2. When the vehicle drives in the first gear or at very low speed, no torque assist is provided and no regeneration takes place. This is due to the fact that regenerative braking may provide lack of control and unwanted decelerations at very low speeds.
The amount of regenerative braking depends on the braking pedal angle. When the brakes are depressed, 50-60% of the braking energy goes into the drive line and is captured by the electro motor.

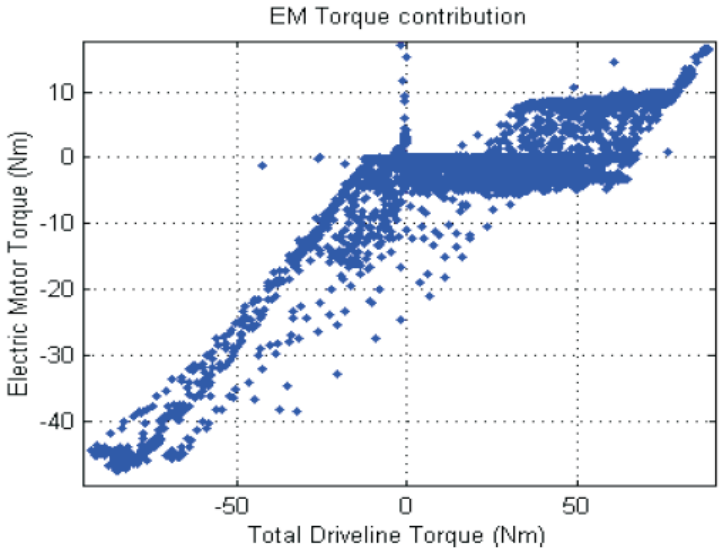

Figure C.2: Electric motor contribution

C.4 Idle stop

When the engine is warm, idle stop can be used to save fuel. When the vehicle is stopped or when the vehicle speed comes below 9 m/s, the gear is in the neutral position and the SOC is above the minimum SOC, the engine is allowed to stop and eliminates idle fuel consumption.

Appendix D

Data Honda Civic IMA

Vehicle			
m	Mass	1189	$[kg]$
c_d	Coefficient of drag	0.28	[-]
A_f	Frontal Area	1.9	$[m^2]$
r_{fd}	Ratio Final Drive	5.77	$[-]$
ρ_{air}	Density air	1.22	$[kg/m^m]$
ICE			
V	Volume	1.339	$[l]$
P_{max}	Maximum Power	61@5700 rpm	$[kW]$
T_{max}	Maximum Torque	119@3300 rpm	$[Nm]$
J_{ice}	Inertia Ice	0.14	$[kgm^2]$
Elektro Motor			
Type	Permanent Magnet(PM)		
m	Mass	60	$[kg]$
P_{max}	Maximum Power	10@3000 rpm	$[kW]$
T_{max}	Maximum Torque	62@1000 rpm	$[Nm]$
J_{em}	Inertia Elektro motor	0.01	$[kgm^2]$
V	Voltage	144	$[V]$
Battery			
Type	Panasonic EV Energy		
Material	Nickel Metal Hydride (NiMH)		
n	Number of cells	120($6x20$)	-
V	Voltage	144	V
C	Published capacity	6.5	Ah
C_n	Nominal Pack capacity	6.0	Ah
C_s	Storage Capacity	0.936	kWh
m	Weight of cells	0.183	kg x 120 cells
m_p	Weight Pack	28.9	kg
Wheels			
Type	195/60R15		
r_w	Wheel radius	0.31	$[m]$
c_r	Rolling resistance coefficient	0.009	[-]
m_w	Mass Wheel	20.4	$[kg]$
J_w	Inertia wheel	3.88	$[kgm^2]$
MT			
1^{st} gear	3.461		
2^{nd} gear	1.896		
3^{rd} gear	1.241		
4^{th} gear	0.911		
5^{st} gear	0.756		
Final gear	3.6		
CVT			
Type	Van Doorne CVT Type 920		
r_{ud}	Under Drive Ratio CVT	2.367	$[-]$
r_{od}	Over Drive Ratio CVT	0.407	$[-]$
J_{cvtp}	Inertia CVT Primary Puly	0.01	$[kgm^2]$
J_{cvts}	Inertia CVT Primary Puly	0.014	$[kgm^2]$

D.1 Data sheet ICE

Engine Specifications

Engine code	LDA
Cylinder Configuration	In-line 4 cylincer
Bore x Stroke	73 x 80 mm
Displacement	1 339 cm^3
Compression Ratio	10.8:1
Valve train	SOHC, Cylinder Idling System (CIS)
Number of valves	2 per cylinder
Valve diameter	Inlet: 32 mm, Exhaust: 28 mm
Ignition System	Dual and Sequential Ignition (DSI)
Exhaust Manifold	Stainless Steel
Catalytic Converter	Under floor:TWC
Maximum Power	61 kW @ 5700 rpm
Maximum Torque	119 Nm @ 3300 rpm

Appendix E

Data Honda Jazz

HONDA

Technische gegevens: Jazz - 1.4 LS

Prijs	**EURO 18.170,00***
Motor	
Cilinderinhoud cm³	1339
Boring x slag mm	73 X 80
Aantal cilinders	4
Kleppen per cilinder	2
Ontsteking / Klepbediening	i-DSi / 8 V SOHC
Vermogen (kw/pk - tpm)	61 (83) - 5.700
Maximum koppel (Nm - tpm)	119 / 2.800
Brandstofbehoefte	95 RON
Emissieuitstoot	2005-norm
Automaat versie	Continu Variabele Transmissie
Prestaties en brandstofverbruik (1999/100/EC-norm)	
Handgeschakeld / CVT	
Zuinigheids categorie	B
Stadsrit (l/100km)	6.9 / 7.2
Buitenweg (l/100km)	4.9 / 5.0
Combinatierit (l/100km)	5.7 / 5.8
CO2 uitstoot (gr/km)	134 / 137
Topsnelheid (km/u)	170 / 160
Wielophanging	
Wielophanging voor	McPherson
achter, semi-onafhankelijk met torsiebuis	S
Stuurinrichting	
electrisch bekrachtigd/ snelheidsafhankelijk	S
Draaicirkel spoor/koets (mtr)	9.4 / 10.0
Wielen en banden	
Banden	175/65 R14 82T
Velgmaat / ET-waarde	14x5,5J / 45
Remmen	
Remmen achter	Schijven
Maten (mm)	
Lengte	3830
Breedte	1675
Hoogte	1525
Wielbasis	2450
Spoorbreedte voor / achter	1460 / 1445
Inhoud bagageruimte Min./Max. (VDA-norm) (ltr)	380 / 1323
Inhoud brandstoftank (ltr)	42
Gewichten (kg) (MT / CVT)	

***De vermelde prijzen zijn de aanbevolen verkoopprijzen, incl. 19% BTW**

HONDA

Technische gegevens: Jazz - 1.4 LS

Kentekengewicht	971 / 1002
Maximaal toelaatbaar totaalgewicht	1470 / 1490
Maximum aanhanggewicht geremd	1000 / 800
Maximum aanhanggewicht ongeremd	450 / 450
Maximum kogeldruk	70
Maximum daklast	37
Transmissie	
Overbrengingsverhoudingen	5MT / CVT
1e versnelling	3.142 / 2.367~0.407
2e versnelling	1.750 / 2.367~0.407
3e versnelling	1.241 / 2.367~0.407
4e versnelling	0.969 / 2.367~0.407
5e versnelling	0.805 / 2.367~0.407
Achteruit	3.230 / 4.227~2.367
Totale eindreductie	4.111 / 4.333

Appendix F

Paper

A fundamental case study on the Prius and IMA drivetrain concepts

A fundamental case study on the Prius and IMA drivetrain concepts

Theo Hofman[1,2)], Roell van Druten[1,2)], Alex Serrarens[2)], Janneke van Baalen[1)]
[1)] Technische Universiteit Eindhoven
Faculty of Mechanical Engineering, Control Systems Technology
[2)] Drivetrain Innovations BV
The Netherlands

Abstract

In this paper the drivetrain concepts of the IMA and the Prius are analyzed and evaluated in order (i) to disclose potential limitations in fuel economy and performance and (ii) to quantify the design and cost trade-offs involved in achieving this (limited) fuel economy and performance. The final objective of the underlying research is to determine the minimum specifications of the Primary power source (P), the Secondary power source (S) and the Transmission technology (T) achieving a pre-defined fuel economy and performance, with constraints on cost and lifetime. Once these are determined new technologies for P, S and T can be selected and designed.

Keywords: modeling, planetary gear, regenerative braking, transmission, vehicle performance

1 Introduction

A hybrid drivetrain improves the driving functions, such as fuel economy, emissions, driveability (dynamic performance), comfort and safety. The hybrid driving functions are mainly determined by the drivetrain topology, system component technology and vehicle system Control (C). Drivetrain hybridization implies adding a Secondary power source (S) to a Primary power source (P), i.e., internal combustion engine. Generally, S consists of bi-directional energy conversion components and an energy storage system, e.g., flywheel, battery. S allows downsizing of P, performing brake energy recuperation and optimization of the overall drivetrain efficiency.
The drivetrain topology defines the possible power paths and transmission ratios between the P, S and the wheels of the Vehicle (V). The transmission technology adds kinematic constraints, which restricts the achievable transmission ratios. Therefore, the topology and transmission technology restrict the required torque-speed combinations that can be obtained between P, S and V. To obtain a good acceleration performance as well as good fuel consumption, the main requirements of a transmission are sufficient ratio coverage and smooth operation. For conventional drivetrains, the demand for higher efficiency and dynamic performance has led to an increase of ratio coverage for transmissions (automatic and manual). In addition shifting without torque interruption (smooth operation) thereby increasing the dynamic performance is the latest development in the field of transmissions (DCT- Dual Clutch Transmission, CVT- Continuously Variable Transmission, [1]). However, the maximum gain in efficiency with a conventional drivetrain is limited by the actual driving power demand being matched by P as good as possible. This is different for hybrids where the production of power by P does not necessarily have to match with the actual driving power demand. This implies a higher potential for efficiency improvement.
Nowadays, the passenger car market offers two hybrid vehicles: Honda Civic equipped with Integrated Motor Assist system (IMA) and Toyota Prius equipped with Toyota Hybrid System (THS), see Figure 1. Both vehicles fulfill almost identical driving functions, see Table 1. However, the drivetrain topology and component technology differ greatly. One of the main differences is that the IMA uses a mechanical Continuously Variable Transmission (CVT) and the Prius uses a CVT with Electromechanical power splitting, referred to as E-CVT. The E-CVT comprises an epicyclic gearset with electric machines (EM1 and EM2) to control power split of a mechanical and electrical path.

THS – Toyota Hybrid System *IMA – Integrated Motor Assist*

Figure 1: Toyota Prius with THS and Honda Civic with IMA

Specification	*Prius-THS*	*Civic-IMA*
Fuel consumption (combined, EG-norm)	4.3 [l/100km]	4.9 [l/100km]
CO_2 - emission	104 [g/km]	116 [g/km]
Acceleration performance 0 – 100 [km/h]	10.9 [s]	12.9 [s]
Top speed	170 [km/h]	177 [km/h]

Table 1: Fuel economy, emissions and dynamic performance of Prius and IMA

Transferring a majority of the engine power directly through the epicyclic gear to the vehicle wheels minimizes the losses of the electrical path. The maximum torque of EM1 reduces the limitless range of torque-speed combinations transmitted through the epicyclic gear ([2]).
The actual CVT ratio in the IMA depends on the engine speed envelope and the vehicle speed and is limited to the underdrive and overdrive value. The IMA requires a clutch in order to overcome the engine-vehicle speed difference during vehicle launch. At low vehicle speed and power demand the Prius only uses EM2 and as such it drives purely electrically.
The aim of the research presented in this paper is to investigate the influence of the drivetrain topology and technology on fuel economy and dynamic performance. The final goal of the underlying research project is to design the drivetrain topology, component technology and system control for future cost-effective hybrids.

1.1 Outline of paper

The remainder of this paper is divided in three more chapters. Chapter 2 describes the modeling of the components and the two drivetrains under consideration. Chapter 3 describes the results of fuel economy and dynamic performance simulations. Finally, in Chapter 4 the paper is concluded and recommendations for future research are given. The fuel economy study shows the differences in fuel consumption when alternately choosing for another transmission, combustion cycle, vehicle or secondary energy source. Two transmission types are used, the CVT of the IMA and E-CVT of the Prius. Three combustion cycles are compared: Otto, Diesel and Atkinson cycle. Three vehicle bodies are compared, the Toyota Prius, Honda Civic and an average of the two vehicles. In comparing these cross-technologies, the batteries (secondary power source) are omitted. In the final comparison the influence of adding the batteries of the IMA on the fuel economy is computed using Dynamic Programming (DP) ([3]). In Chapter 3 motivations for the approach in the fuel economy study are described. Regarding the dynamic performance, the acceleration from 0 – 100 [km/h] with and without power assisting of the battery will be investigated for the IMA and the Prius. In both cases, the engine is assumed being operated at maximum combustion torque.

2 Drivetrain modeling

In this section the models used for the system components are described as a static function of several state variables. Some of these state variables may also be control inputs, e.g., gear ratio speed change CVT and power flow out of the battery. This section starts with describing the integrated models of the Prius and the Civic in which the static component maps and the drivetrain dynamics are combined.

2.1 Prius and Civic Drivetrains

In this section the equations describing the drivetrain dynamics of the THS and IMA concepts will be given. In Figure 2, the outline of the drivetrain in the Prius and the block diagram showing the power flow paths are depicted.

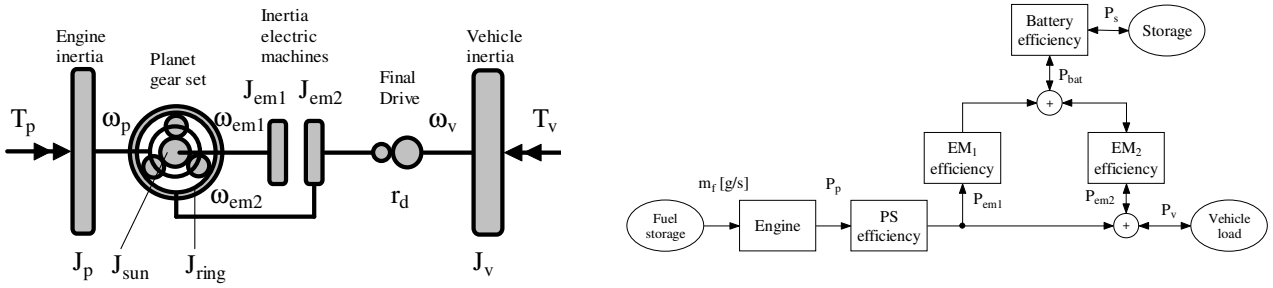

Figure 2: Toyota Prius Drivetrain model: (*l*) Model structure; (*r*) Block diagram including the battery.

The curb vehicle mass M and the final drive is lumped within the wheels with the wheel radius R_w into a total vehicle inertia J_v

$$J_v = M \cdot R_w^2 \,. \tag{2.1}$$

The external resistance torque acting on the vehicle is

$$T_v(t) = \underbrace{M \cdot g \cdot f_r \cdot R_w}_{roll\ resis\tan ce} + \underbrace{\tfrac{1}{2} \cdot \rho \cdot C_d \cdot A_d \cdot v(t)^2 \cdot R_w}_{air\ drag\ resis\tan ce}, \tag{2.2}$$

which consists of the sum of the roll resistance torque and the air drag resistance torque. The dynamic torque balance at the input (carrier) and output gears (sun and ring) is given by the equations of motion:

$$T_p - \left(J_{carrier} + J_p\right) \cdot \dot{} _p = \left(T_{sun} + T_{ring}\right) / \ _{ps} \,, \tag{2.3}$$

$$T_{sun} - \left(J_{sun} + J_{em1}\right) \cdot \dot{} _{em1} = T_{em1} \,, \tag{2.4}$$

$$T_{ring} - \left(J_{ring} + J_{em2}\right) \cdot \dot{} _{em2} = \left(T_v + J_v \cdot \dot{} _v\right) \cdot r_d - T_{em2} \,. \tag{2.5}$$

The efficiency of the Planetary gear Set (PS) η_{ps} is assumed to be constant. The carrier inertia $J_{carrier}$ includes the inertia of the planet wheels. The kinematics of the planetary gear set results in the following angular speed relations:

$$_p = \ _{em1} \cdot 1/(1+z) + \ _{em2} \cdot z/(1+z), \ z = 78/36, \tag{2.6}$$

$$_v = \ _{em2} \cdot r_d = v_v / R_w \,. \tag{2.7}$$

In Figure 3, the drivetrain of the IMA and the block diagram with the power flows are depicted.

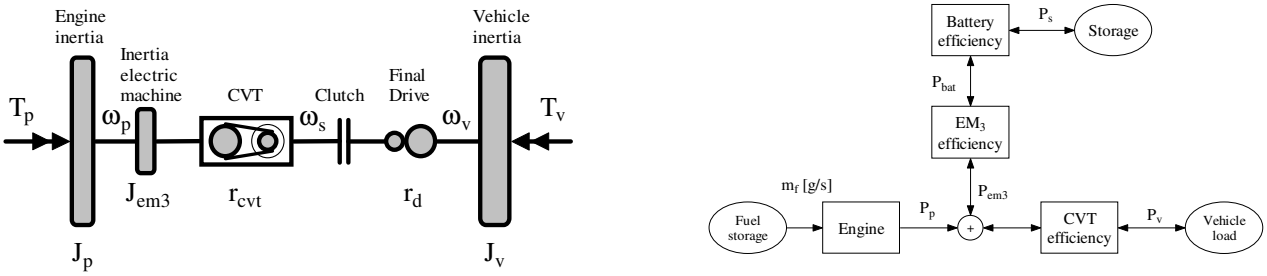

Figure 3: Honda IMA Drivetrain model: (*l*) Model structure; (*r*) Block diagram including battery.

The torque balance for this drivetrain results in

$$\left(T_p - \left(J_p + J_{em3}\right)\cdot \dot{\omega}_p\right)\cdot \eta_{cvt}\left(T_p, \omega_p, r_{cvt}\right) = r_{cvt}\cdot r_d \cdot T_v + r_{cvt}\cdot r_d^2 \cdot J_v \cdot \dot{\omega}_s \,. \qquad (2.8)$$

Only the torque transmitted through the CVT, and not the shaft speeds, influences the CVT efficiency. The shaft speed and the time derivative of the shaft speed are,

$$\omega_s = r_{cvt}\cdot \omega_p \,, \;\Rightarrow\; \dot{\omega}_s = \dot{r}_{cvt}\cdot \omega_p + r_{cvt}\cdot \dot{\omega}_p \,. \qquad (2.9)$$

In order to obtain positive vehicle acceleration, the gear ratio speed change rate needs to be

$$\dot{r}_{cvt} > -\frac{T_p - r_{cvt}\cdot r_d \cdot T_v}{\left(J_p + J_{em3}\right)\cdot \omega_s}\cdot r_{cvt}^2 \,. \qquad (2.10)$$

The CVT efficiency is neglected in this equation. This result may be obtained after substitution of equation (2.10) into equation (2.8). The derivation is discussed in more detail in [4]. If the constraint in (2.10) is violated then the vehicle will decelerate even though the engine is accelerated and produces more power. The parameters values used for the simulated models are shown in Table 2. In the next paragraphs the static efficiency maps of the engine, CVT, batteries and electric machines are discussed.

Quantity	*Symbol*	*IMA*	*Prius*	*Average V**	*Unit*
Mass	M	1189	1243	1216	[kg]
Frontal area	A_d	1.9	1.746	1.832	[m^2]
Air friction coefficient	C_d	0.28	0.26	0.27	[-]
Rolling resistance	f_r	0.0054	0.009	0.0072	[-]
Air density	ρ	1.19	1.19	1.19	[kg/m^3]
Gravity	g	9.81	9.81	9.81	[m/s^2]
Wheel radius	R_w	0.31	0.31	0.31	[m]
Inertia engine	J_e	0.14	0.18	-	[kgm^2]
Inertia EM3 EM2 EM1	J_{em3}	0.01	-	-	[kgm^2]
	J_{em2}	-	0.05	-	
	J_{em1}	-	0.02	-	
Inertia primary pulley	$J_{cvt,p}$	0.01	-	-	[kgm^2]
Inertia secondary pulley	$J_{cvt,s}$	0.014	-	-	[kgm^2]
Inertia ring gear	J_{ring}	-	0.01	-	[kgm^2]
Final drive ratio	r_d	1/5.77	1/3.93	-	[-]
Gear ratio	r_i	2.46 – 0.42	-	-	[-]

Table 2: Parameter values for the simulation models

2.2 Engine

The engine is assumed to be operated quasi-static, i.e., the cyclic fluctuation of the engine torque is neglected. Instead, the mean value torque is applied and requested torque transients occur instantly even though the vehicle and all drivetrain parts are still in a transient condition (accelerating or decelerating). The vehicle is assumed to be stationary if the vehicle and all drivetrain parts exhibit no change of speed.

Temperature effects on fuel consumption and emissions are left out of consideration. In Figure 4, the static efficiency maps for the Toyota Prius (Atkinson) engine and the Honda IMA (Otto) engine are shown [5]. Also indicated are the maximum engine torque line at Wide-Open Throttle (WOT), and the Optimal Operation Line (OOL). The engine torque-speed combinations for all engine powers with minimum brake specific fuel consumption (bsfc) are defined as 'optimal operation points'. The line connecting these points is the OOL releasing a quite erratic curve.

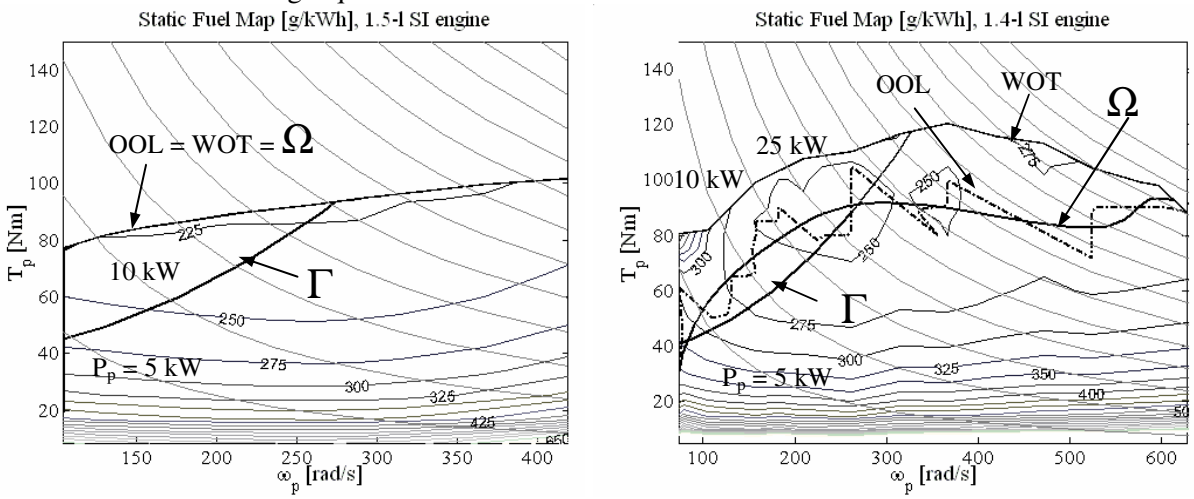

Figure 4: Static map of a 1.5l-SI engine (Atkinson) and a conventional engine map, i.e., 1.4l-SI engine (Otto). Indicated curves are iso-power curves (light gray), OOL (optimal operation line, dashed line), WOT (Wide-Open Throttle, thick black line), Γ (maximum gear ratio driving resistance curve for IMA transmission), Ω (smooth optimal operation line).

A 6th-order polynomial function fitted through the OOL results in a much smoother curve Ω. This approximate curve also ensures monotonous increase of the engine speed at increasing power request. In both maps, also the driving resistance curve Γ for the overdrive ratio is drawn. The overdrive ratio constraint causes that not all stationary optimal operation points can be reached. This results in Γ lying under Ω for a substantial part of the operating range. Using the bsfc-maps, the momentous mass fuel flow rate can be computed as:

$$\dot{m}_f = bsfc(T_p, \quad _p) \cdot P_p = bsfc(T_p, \quad _p) \cdot T_p \cdot \quad _p . \tag{2.11}$$

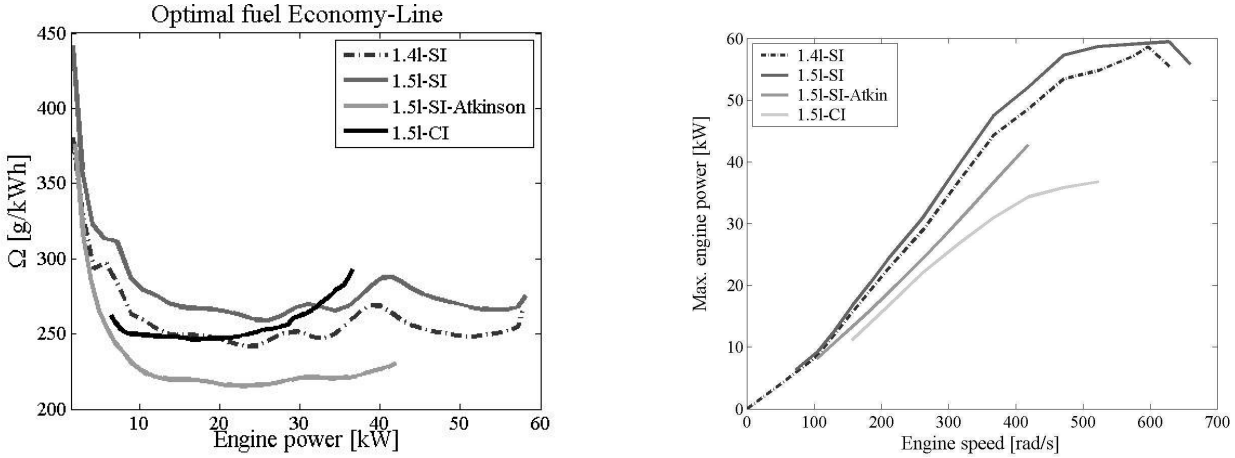

Figure 5: (*left*) Brake-specific fuel consumption at OOL for the different engines; (*right*) Maximum output power for the different engines.

In figure 5, the bsfc (brake specific fuel consumption) obtained for the different engines at their respective Ω-curves is plotted as function of the engine output power. In the same figure on the right, the maximum engine output power as function of the engine speed is shown.

2.3 CVT

The IMA has a mechanical V-belt CVT. The losses of such a CVT consist of friction losses and hydraulic pump losses. The overall CVT efficiency including the pump losses and the losses of the final gear as a function of three input variables: (i) input torque, (ii) input speed and (iii) CVT gear ratio. The efficiency can be written as a non-linear static function of the form $\eta_{cvt} = \eta_{cvt}(T_p, \omega_p, r_{cvt})$. The input torque and speed are equally to that of the engine, because the input shaft of the CVT is directly connected to output shaft of the engine. The overall efficiency data is obtained from measurements performed on a high dynamic CVT test bench at the Technische Universiteit of Eindhoven. The subject transmission is the Jatco CK2. The CVT efficiency is assumed to be independent of the gear ratio change rate of the CVT, simulations with detailed models and measurements under dynamic conditions show that this is valid (see also [4]).

2.4 E-CVT and Electric Machines

The Toyota Hybrid System (THS) is equipped with two electric machines EM1 and EM2 (see Figure 2). The first machine EM1 is connected to the sun gear of the planetary set and can generate 22 [kW] of mechanical power. The second machine EM2 is connected to the ring gear of the planetary gearset, which is also connected via a chain drive to the final reduction with differential. The EM2 machine can produce 50 [kW] of mechanical power. In Figure 6, the torque-speed maps of EM1 and EM2 are shown, along with their iso-efficiency lines [5]. The electric machine EM3 in the IMA can produce/generate 10 [kW] of mechanical power. For reasons of space the characteristics of EM3 are not shown here.

2.5 Battery

The batteries in the THS and IMA systems are both of the NiMh type. The net battery output power is

$$P_{bat}(t) = P_s(t) - P_{loss}(t) = V_{oc}\left(SoC(t), P_{bat}(t), T\right)I(t) - I(t)^2 R_{\text{int}}(SoC(t), T), \qquad (2.12)$$

with V_{oc} the open circuit voltage and R_{int} the internal battery resistance, both are dependent on State-of-Charge (SoC) of the battery (see battery model in Figure 7). The net output power of the secondary power source P_{em} is dependent on the efficiency of the electrical machine η_{em},

$$P_{em}(t) = I(t) \cdot V_{oc}\left(SoC(t), P_{bat}(t)\right) \cdot \eta_{bat}\left(SoC(t), P_{bat}(t), T\right) \cdot \eta_{em}\left(T_{em}(t), \omega_{em}(t)\right), \qquad (2.13)$$

and the machine efficiency depends on the operation point of the electric machine. Since, the absolute internal storage capacity of the battery is very high and SoC fluctuation is within a relative narrow band, for simplicity the battery efficiency has assumed to be independent on the SoC level and temperature (T). The battery output power can be written as a function of the storage power for different SoC levels.

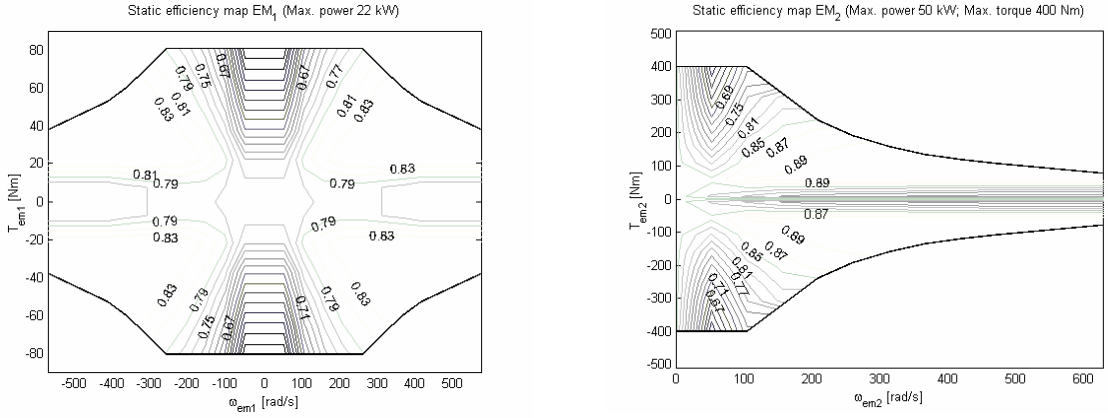

Figure 6: Static efficiency maps electric machines (including power electronic efficiency) for THS. Also indicated are maximum torque curves (thick lines).

In the graph of Figure 7, this is shown for the battery pack of the IMA (type NiMh Spiral Wound, [5]). Since the influence of SoC on the battery efficiency is rather low, only the average power characteristic is used here.

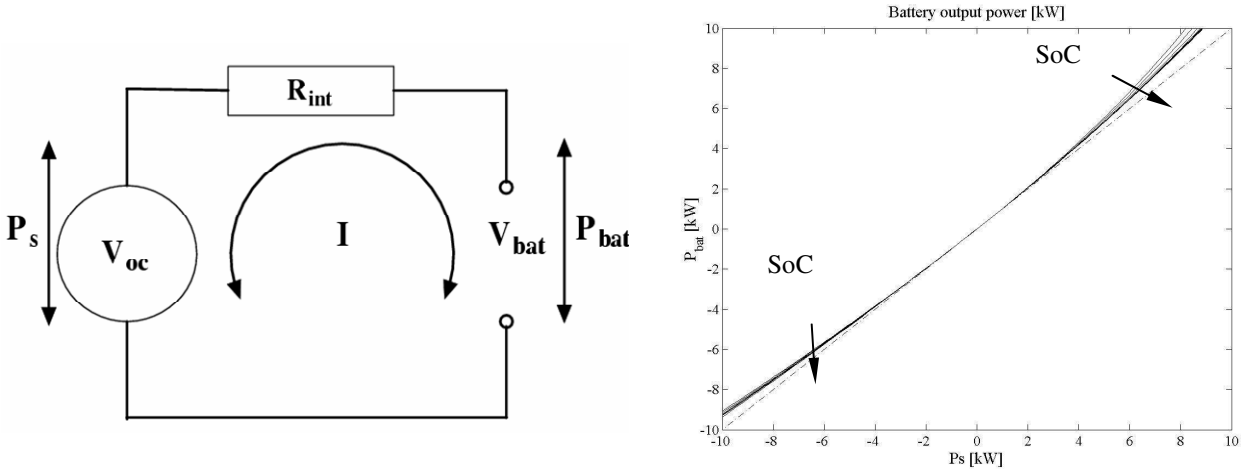

Figure 7: (*left*) Battery model; (*right*) Battery efficiency

For the IMA the nominal cell voltage is 1.2 [V] and the total number of cells is 120 (6 cells x 20 modules) with a nominal voltage of 144 [V]. The test data obtained from NREL are valid for 25 degrees Celsius ambient [5]. This data has been used for calculating the battery efficiencies used in the IMA and the THS. The battery pack of the Toyota Prius (1998) is reported to be the same technology as for the IMA with 28 modules instead of 20. The output voltage for the THS battery pack is 201.6 [V] (6 cells x 28 modules = 168 cells x 1.2 [V]). Maximum battery output power is 20.9 [kW] and the system voltage is 500 [V] maximum.

2.6 Simulation approach

Both THS and IMA experience drivetrain losses. Regarding the THS, the losses of the generator, the motor and the inverter are considered to be the largest contributors. The efficiency of the planetary gear

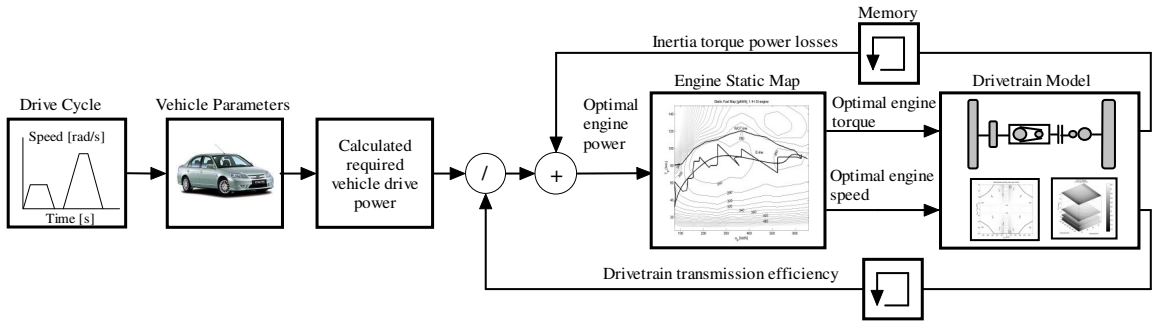

Figure 8: Simulation block diagram

set is assumed to be 95%. The efficiencies of both drivetrains depend on engine torque and speed. However, the required engine torque and speed are determined by the drivetrain efficiencies and required vehicle drive power. Due to this causality conflict, it is impossible to determine the optimal engine torque and speed exactly. In this study, the losses in the IMA and THS are estimated in the following procedure.
Given the requested drive power, the optimal engine torque, speed and required CVT ratio (IMA) or generator torque (Prius) are determined without any drivetrain losses at time t=0. Using these values the efficiencies of the CVT and the Motor/Generator can be calculated. This is done in the "Drivetrain Model"

of Figure 8. At later time steps the required engine power can be calculated using the known values for the efficiencies at the previous time-step. Thereto, the requested vehicle drive power is divided by the computed drivetrain efficiency. A similar approach is taken when incorporating the drivetrain inertias. These are taken into account by adding/subtracting the inertial power computed from numerical differentiation of the drivetrain component speeds. A similar procedure has been used and explained in [6] for integrated engine-CVT control considering drivetrain loss and CVT response lag.

2.7 Influence of hybridization on fuel economy

Adding a secondary energy storage with bi-directional energy conversion components allows for Brake Energy Recuperation (BER) and re-use of that energy for further reduction of fuel consumption. Basically, we choose the same control input variables as in the battery-less drivetrains, however now an additional degree of freedom is added, i.e. battery power flow. For determining minimal fuel consumption Dynamic Programming (DP) is used (see also [3], [7]-[9]). The elegance of this method is that the minimal fuel consumption can be found while still complying with SoC constraints (e.g. SoC-neutral) at the beginning and end of the drive cycle. The model of Figure 3 will be used. The objective is to optimize the power flow between the power sources over a defined drive cycle in order to minimize (i) the fuel consumption and emissions, (ii) Maintain SoC of the accumulator within a certain range, (iii) Accomplish any drive power demand P_v. Therefore, the problem can be described as an optimization problem.

$$\min_{\bar{x}} J(\bar{x}) \text{ subject to } h(\bar{x}) = 0;\ g(\bar{x}) \le 0\,, \tag{2.14}$$

with $h(\bar{x})$ equality and $g(\bar{x})$ inequality constraints. The cost function J is the total fuel consumption over the drive cycle as function of the battery power flow P_s, which is the only control design variable. The engine is assumed to be operated at the Ω.

$$J = \int_{t_0}^{t_f} \dot{m}_f \left(P_v(t),\, P_s(t),\, \_\_\_{p}(t)\right) dt\,. \tag{2.15}$$

However, the operation range of the system components is limited, the boundaries are:

$$P_{s,\min} \le P_s \le P_{s,\max}$$

$$E_{s,\min} \le E_s \le E_{s,\max} \qquad \max\left(\_\_\_{v} / r_{d\ \_\_\_{p,\min}}, r_{ud}\right) \le r_{cvt} \le \min\left(\_\_\_{v} / r_{d\ \_\_\_{p,\min}}, r_{od}\right)$$

$$P_{bat,\min} \le P_{bat} \le P_{bat,\max} \qquad \_\_\_{p,\min} \le \_\_\_{p} \le \_\_\_{p,\max} \qquad T_{p,\min} \le T_p \le T_{p,\max}$$

$$P_{em3,\min} \le P_{em3} \le P_{em3,\max} \qquad \_\_\_{em3,\min} \le \_\_\_{em3} \le \_\_\_{em3,\max} \qquad T_{em3,\min} \le T_{em3} \le T_{em3,\max}$$

Furthermore, the optimization problem is subjected to an integral constraint, i.e. state-of-charge balance of accumulator, which leads to

$$E_s(t)\Big|_{t_0}^{t_f} = \int_{t_0}^{t_f} P_s(t)dt = 0\,. \tag{2.16}$$

The optimization problem can be described as a multi-step decision problem in discrete-time format. The DP problem is solved by numerical discretization and interpolation of the state and control design values.

3 Simulation results

In this section the influence of the drivetrain topologies, the system component technologies and hybridization (allowing Brake Energy Recovery (BER) and Idle-Stop) on the fuel economy and dynamic performance are discussed.

3.1 Fuel economy and Dynamic Performance

In the Table 3, the different system component configurations are shown for the comparison study.

Comparison	*T*	*P*	*V*	*S*	*C*	*Influence*
			Fuel economy (section 3.1)			
1) T – ad. 3.1.1	$T_2 \leftrightarrow T_1$	P*	V*	S*	$\Omega(T_p,\omega_p)$	Ratio range CVT
2) P – ad. 3.1.2	T_2	$P^* \leftrightarrow P_1$	V*	S*	$\Omega(T_p,\omega_p)$	Engine displacement
3) P – ad. 3.1.2	T_2	$P^* \leftrightarrow P_3$	V*	S*	$\Omega(T_p,\omega_p)$	Diesel combustion
4) P – ad. 3.1.2	T_2	$P^* \leftrightarrow P_2$	V*	S*	$\Omega(T_p,\omega_p)$	Atkinson combustion
5) S – ad. 3.1.3	T_2	P_2	V_2	S*	$\Omega(T_p,\omega_p)$	Vehicle parameters THS
6) S – ad. 3.1.4	T_1	P_1	V_1	$S^* \leftrightarrow S_1$	$\Omega(T_p,\omega_p)$– DP	Energy Storage IMA
			Dynamic Performance (section 3.1)			
7) S – ad. 3.1.5	T_1	P_2	V_2	$S^* \leftrightarrow S_2$	Max. torque	Energy Storage THS
8) S – ad. 3.1.5	T_2	$P_2 \leftrightarrow P_5$	V_2	S*	Max. torque	Engine displacement
9) S – ad. 3.1.5	T_1	P_1	V_1	$S^* \leftrightarrow S_1$	Max. torque	Energy Storage IMA
10) S – ad. 3.1.5	T_1	$P_1 \leftrightarrow P_4$	V_1	S*	Max. torque	Engine displacement

Table 3: Research steps for fuel economy and dynamic performance, T_1 = CVT, T_2 = E-CVT, P* = scaled 1.5L OTTO engine, P_1 = 1.4L OTTO engine (IMA), P_2 = 1.5L ATKINSON engine (THS), P_3= 1.5L DIESEL engine, P_4 = 1.6L OTTO engine, P_5 = 2.0L OTTO engine, V* = averaged vehicle, V_1 = Honda Civic, V_2 = Toyota Prius, S* = no batteries, S_1 = 144 [V], 6 [Ah] NiMh batteries (IMA), S_2 = 202 [V], 6.5 [Ah] NiMh batteries (THS).

The fuel economy and dynamic performance results corresponding with the cross-technology comparison as shown in Table 3 are shown in Figure 9. The results are compared to a reference vehicle with index 1, which is equipped with E-CVT, P*, V* (average vehicle parameters) and S* (no battery power).

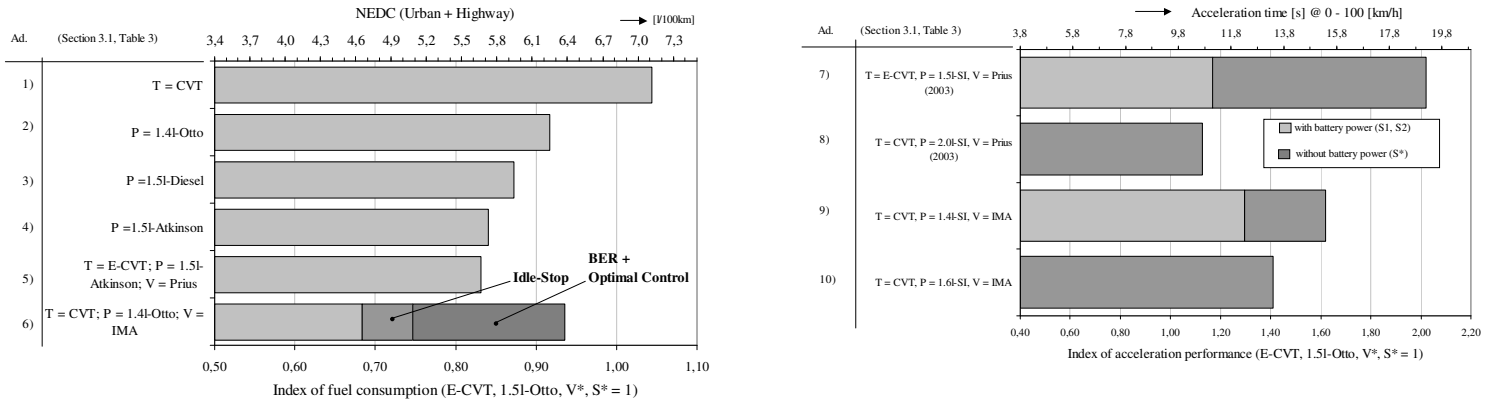

Figure 9: Simulation results: (*left*) Fuel economy; (*right*) Dynamic performance

3.1.1 Influence of Transmission – T (comparison 1)

In the first research step, the influence of the T has been investigated. During this analysis no hybrid functionality is considered, that is no battery power flow is possible (S*). To make a fair comparison, an average engine (P*) and average vehicle parameters ($V^* \cong (V_1 + V_2)/2$) for both vehicles are assumed. P* is the Honda engine linearly up-scaled from 1.4l to 1.5l displacement, which is equal to the Atkinson engine displacement in the Prius. The fuel economy will be calculated based on a defined drive cycle (NEDC). The reference vehicle is equipped with an E-CVT, 1.5l-SI-Otto engine and the vehicle parameters are the average vehicle parameters V*. Since, there is no battery flow possible all generated

power by EM1 is transmitted to EM2, and if EM2 is not able to consume this power it is assumed that the generated power by EM1 is not used. In Figure 9 can be seen that the V-belt CVT of the IMA increases the fuel consumption with approximately 4% compared to the reference vehicle with index 1.

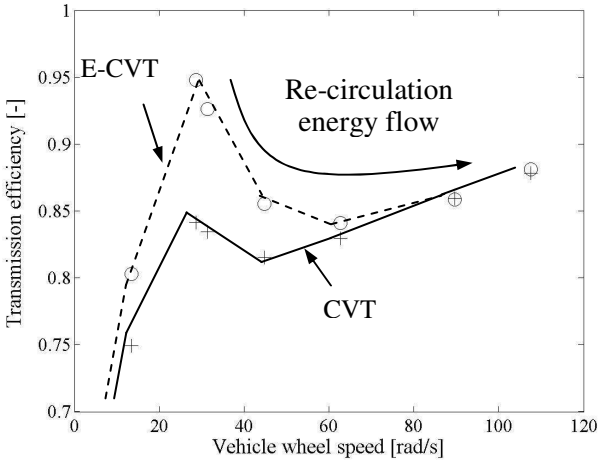

Figure 10: Transmission efficiencies of the E-CVT and CVT as function of the stationary vehicle speeds, while the engine speeds tracks OOL.

In figure 10, the transmission efficiencies of the E-CVT and the CVT as function of the stationary vehicle speeds, while the engine speeds tracks the Ω are shown. During simulations it was found that at certain stationary vehicle speeds, the angular speed of the generator EM1 and the torque of EM2 changes sign. At these conditions, the engine torque directly transmitted over the planetary set to the vehicle wheels is too large causing a generative braking torque at EM2. The generative energy in turn is used to drive the EM1 that supports the engine torque. The function of EM1 and EM2 is reversed. This causes additional transmission losses. By increase of stationary vehicle speed the E-CVT efficiency is deteriorated. The lowest efficiency in this mode is at a stationary vehicle wheel speed of 63 [rad/s].

Only at very low vehicle wheel speeds (<13.4 [rad/s]) no transmission energy circulation occurs. However, then more power is transferred via the electrical path and the electric machines with power electronics mainly determine the energy losses. In practice, at low vehicle speeds the vehicle is fully driven by the EM2 while the engine is off or idling. To avoid re-circulation of energy flow, the engine speed has to be increased for the same required engine power. This causes also an increase in fuel consumption. Toyota optimized the vehicle system control such that at re-circulation conditions, the system optimal operation point is chosen as set-point for the engine, which is a trade-off between minimization of the re-circulation transmission losses and not operating the engine at the OOL [2]. The mean efficiency of the E-CVT of Toyota is approximately 5% higher than for the IMA CVT, even with additional energy losses due to re-circulation of power flow. Since the largest amount of energy flow is transmitted over the ring to the vehicle wheels, the transmission efficiency of the E-CVT is typically larger than the absolute efficiencies of the electric machines.

3.1.2 Influence of Combustion cycle - P (comparison 2, 3, 4)

During this part of the study, P* is replaced by P_2 (Atkinson) and P_3 (Diesel) respectively. Still, no batteries are used in these simulations (S*). By replacing the engine, the influence of the type of combustion cycle on the fuel economy can be investigated. Since, the Ω of the Atkinson engine shows the lowest bsfc (225 [g/kWh]), the 1.5l-Diesel and 1.4l-Petrol have the second - and third lowest bsfc, the largest fuel saving is obtained with Atkinson engine. Furthermore, the performance of the Prius engine is improved by reducing the engine friction during deceleration. Although, with E-CVT it is possible to stop the revolution of the engine crankshaft (no drag losses), stopping the engine causes problems in achieving proper re-acceleration responses ([2]). The IMA reduces pumping losses by stopping three engine cylinders during deceleration. Both engines of the Prius and IMA use variable valve timing, i.e., VVT or VTEC in order to reduce the pumping and friction losses ([2]).

3.1.3 Influence of Vehicle parameters – V (comparison 4, 5)

In this stage the influence of the actual vehicle parameters for the IMA and the Prius on the fuel economy is investigated. The transmission is still T_2, the engine is P* and still no batteries are installed or S*. It can be seen that the vehicle parameters almost don't have any influence on the fuel consumption by comparing the results of 4 and 5.

3.1.4 Influence of energy Storage (hybridization) – S (comparison 6)

During this study the influence of energy exchange of the battery with the engine and the vehicle on the fuel economy for the Honda IMA has been investigated. Since the electric machine is directly coupled to the crankshaft of the engine, engine friction losses play an important role in the BER. Honda reported that the regenerative braking energy is increased from 37% to 57% by reduction of engine friction losses (VTEC). The resulting optimal control strategy and energy recovery during braking gives a fuel saving of approximately 18% and idle-stop strategy gives an additional fuel saving of approximately 6%. The simulated fuel consumption on the NEDC for IMA with CVT is 4.53 [l/100km], which is lower than the fuel consumption for the IMA with manual transmission (catalogue value 4.9 [l/100km]).

3.1.5 Influence of battery power & engine size on dyn. perf. (7 with 8 and 9 with 10)

From the results shown in Figure 9 can be seen that the battery power decreases the acceleration time significantly. Compared to a conventional drivetrain equipped with a V-belt CVT and a 1.6l-Otto engine, the IMA performs even better. The Prius achieves performance almost equivalent to a conventional drivetrain with a CVT and 2.0l-Otto engine. In the following figures, the relationship between the vehicle drive shaft output power P_v and the vehicle wheel speed for the Prius and the IMA are shown.

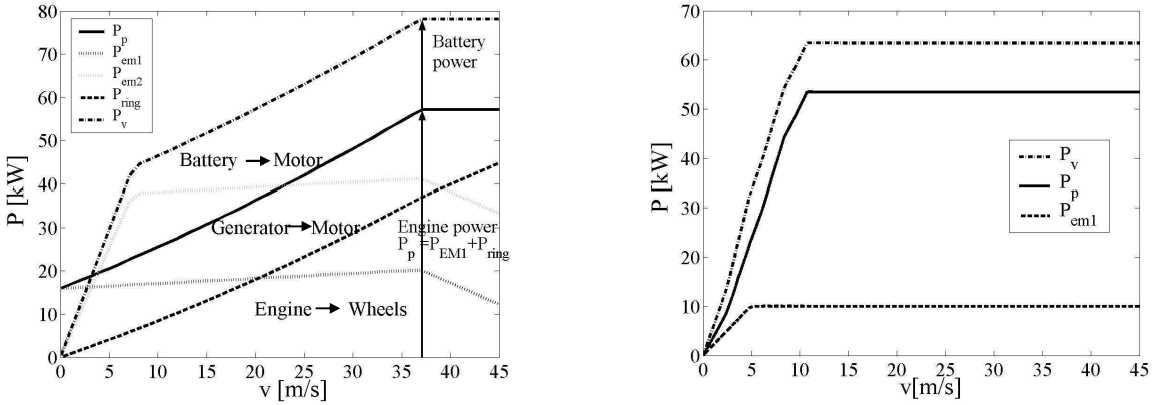

Figure 11: Power distribution for the Prius (*l*) and
(*r*) IMA drivetrain during acceleration vehicle wheels 0 – 45 [m/s]

The maximum output power for the Prius is constrained by the maximum torques of the electric machines and the speed of the generator. To obtain the required dynamic performance the battery supplies the additional required power to EM2 for the Prius and EM3 for the IMA. During maximum acceleration from 0 up to 45 [m/s] or 162 [km/h] no re-circulation of power through the E-CVT occurs, because the engine speed prescribed by the WOT is higher than the vehicle wheel speed.

4 Conclusions and future work

In this paper the drivetrain concepts of the IMA and the Prius are analyzed and evaluated regarding fuel economy and dynamic performance by performing a cross-technology exchange study. The V-belt CVT with respect to the E-CVT results in an approximately 4% higher fuel consumption. Regarding the engine displacement and combustion cycle, the following can be concluded, downsizing the engine from 1.5l-SI-Otto to 1.4l-SI-Otto results in an 8% improvement in fuel economy. Changing the combustion cycle from Otto to Diesel and from Otto to Atkinson saves about 13% and 16% respectively. The Honda IMA and the Toyota Prius have set their acceleration performance target 0 – 100 [km/h] to that of a conventional vehicle equipped with 1.6l-SI-Otto and a 2.0l-SI-Otto engine respectively. Thereto, the IMA requires in combination with a 1.4l-Otto engine 10 [kW] and the Prius requires in combination with a 1.5l-Atkinson engine 20 [kW] of additional battery power assist. Applying hybrid functions for the IMA, such as BER, with an off-line optimal engine control strategy and Idle-Stop results in an additional fuel saving of respectively 18% and 6%. In future work, the drivetrains of the IMA and Prius will be further analysed, by determining the optimal control strategy independent of the pre-scribed OOL condition for the engine with help of the DP. The engine operation point is then determined by ratios of the E-CVT, CVT, the wheel

speed, the battery power flow and required vehicle drive power. The goal is to determine the influence of the system component (P, S and T) efficiencies on the overall vehicle performance (fuel economy, emissions and dynamic performance). The final objective of the underlying research is to determine the minimum specifications of P, S and T achieving a pre-defined fuel economy and performance, with constraints on cost and lifetime. Once these are determined new technologies for P, S and T can be selected and designed.

References

[1] R.G. Herbst, *Dual Clutch Transmission – Two clutch technologies and their possible market segments*. ZF Sachs AG, Schweinfurt. In: Proc. of Acchener Kolloquium Fahrzeug- und Motorentechnik. Aachen, 2003.

[2] Toshifumi Takaoka, Takeshi Kotani, Shinichi Abe, and Tatehito Ueda, *Study of the optimization between engine and hybrid system*. Toyota Motor Comp., Japan. In: Proc. of Acchener Kolloquium Fahrzeug- und Motorentechnik. Aachen, 2003.

[3] Bellman, R.E., *Dynamic programming*, Princeton University Press, 1962.

[4] R. Pfiffner. *Optimal Operation of CVT-Based Powertrains*. PhD.-thesis, ETH, 2001.

[5] Advanced Vehicle Simulator, ADVISOR of the National Renewable Energy Laboratory (NREL) of U.S. Department of Energy, 2002.

[6] T. Kim and H. Kim. *Performance of an Integrated Engine-CVT Control, Considering Powertrain Loss and CVT Response Lag, Integrated Powertrains and their Control.* Editor: N.D. Vaughan, Prof. Engineering Publishing Ltd., London, UK, 2000.

[7] M. Koot, J.T.B.A. Kessels, B. de Jager, and P.P.J. van den Bosch. *Energy Management for vehicle power nets: A performance analysis.* In: Proc. of the American Control Conf. Boston, 2004

[8] A. Sciarretta, M. Back, and L. Guzella. *Optimal control of parallel hybrid electric vehicles.* In IEEE Transactions on control systems technology, vol. 12(**3**), 2004.

[9] C. Lin, et.al., *Integrated, Feed-Forward HEV Simulation in SIMULINK and its Use for Power Management Studies.* SAE 2001 World Congress, Detroit, Michigan, SAE 2001-01-1334, 2001, 13 pages.

Authors

Theo Hofman was born on the September 5th, 1976 in Utrecht, the Netherlands. He studied Mech. Eng. at the Technische Universiteit Eindhoven (TU/e). Since August 2003, he is a Ph.D. candidate with the Control Systems Technology group. The research programme, named 'ImpulseDrive' focusses on the design methodologies for a hybrid vehicle drivetrain with significant reduction of fuel consumption and emissions. TU/e; *Dept. of Mech.Eng.* (WH –1.118); Section Control Systems Technology; PO Box 513; 5600 MB Eindhoven; The Netherlands. Tel: +31 40 247 4132; Fax: +31 40 247 5904; E-mail: t.hofman@tue.nl.

Alex Serrarens was born 6 september 1973 in Hulst, The Netherlands. He received his MSc-degree MechEng in april 1997 at the Technische Universiteit Eindhoven. In 2001 he received his PhD degree from the same university in the field of powertrain control of passenger cars with CVT. Currently he is business partner within Drivetrain Innovations (DTI) which is a licensing and contract-research center on automotive powertrains, transmissions and components.
Drivetrain Innovations: MMP 1.42, Horsten 1, 5612 AX Eindhoven , The Netherlands.
Tel +31 40 247 5812; Fax: +31 40 247 5904;
E-mail: serrarens@dtinnovations.nl.

Roell van Druten finished his Masters in June 1996 and his Ph.D. in October 2001, both at the Technische Universiteit Eindhoven. Currently he is a CEO of Drivetrain Innovations (DTI), which is a licensing and contract-research center on automotive powertrains, transmissions and components.
1) Drivetrain Innovations: MMP 1.42; Horsten 1; 5612 AX Eindhoven; The Netherlands. Tel +31 40 247 5812; Fax: +31 40 247 5904; E-mail: druten@dtinnovations.nl; URL: www.dtinnovations.nl.
2) TU/e; *Dept. of Mech. Eng.* (WH -1.125); Section Control Systems Technology; Technische Universiteit Eindhoven; PO Box 513, 5600 MB Eindhoven, The Netherlands,
Tel: +31 40 247 4828; Fax: +31 40 246 1418;
E-mail: r.m.v.druten@tue.nl;
URL: www.wtb.tue.nl.

Janneke van Baalen was born in Papendrecht, the Netherlands in 1980. She received the Bachelor degree in Mechanical Engineering in 2002 from the Technische Universiteit Eindhoven. In 2003 she worked on the fuel optimization of a fuel cell powered vehicle at the Swiss Federal Institute, Zurich. At the moment she is doing her Master degree in automotive engineering. Her research interests are modeling and fuel optimization of vehicle systems.
TU/e; *Dept. of Mech.Eng.* (WH –1.113); Section Control Systems Technology; PO Box 513; 5600 MB Eindhoven; The Netherlands.
Tel: +31 40 247 4132; Fax: +31 40 246 1418;
E-mail: J.v.Baalen@student.tue.nl.

Acknowledgment

This study is part of ``Impulse Drive" which is a research project at the Technische Universiteit Eindhoven in The Netherlands within the section Control Systems Technology of the Department of Mechanical Engineering. The project is financially supported by the NWO Technology Foundation within the Innovational Research Incentives Scheme 2000/2001.

Appendix G

IMA with CVT

The Honda Civic IMA is available with a Continue Variable Transmission (CVT) as well. The advantage of the CVT above a manual transmission is that the ICE can be used over the OOL for the greater part. Rather than having a fixed set of gear combinations, the CVT transmission allows an almost limitless number of engine speed and torque combinations. This provides significant benefits over a traditional manual transmission. Although the efficiency of the CVT is significantly lower than a manual transmission, the overall efficiency is higher because the ICE can operate at its most efficient points. In figure G.1, a schematic picture of a CVT can be seen. The CVT transmission consists of an oil-pressure variable input (aka "primary'") and output (aka "secondary") pulley, and a metal belt that connects the two. The two pulley widths react to the position of throttle, speed, and other conditions.

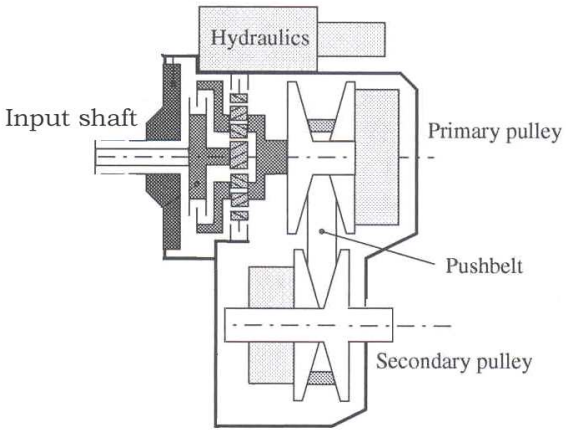

Figure G.1: A schematic representation of a Pushbelt CVT

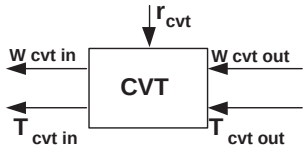

Figure G.2: The quasi static representation of the CVT

The formulas that give the relations between torque and speed for 100% efficiency are given in Equation. G.1 to G.3. $r_{p,cvt}$ and $r_{s,cvt}$ refer to the radius of respectively the primary pulley and the secondary pulley. The quasi static model in which the input and output variables of the CVT have been modeled, is depicted in Figure G.2. The CVT has an under drive ratio of 2.36 and overdrive ratio of 0.4. These ratios constrain the minimum and maximum torque and speed that can be transmitted.

$$\omega_{in} = \frac{r_{p,cvt}}{r_{s,cvt}}\,\omega_{out} \tag{G.1}$$

$$T_{in} = \frac{r_{s,cvt}}{r_{p,cvt}}\,T_{out} \tag{G.2}$$

$$i_{cvt} = \frac{\omega_{out}}{\omega_{in}} = \frac{r_{s,cvt}}{r_{p,cvt}} \tag{G.3}$$

G.1 Vehicle dynamics with CVT

In Figure G.3, the free body diagram for the Honda Civic IMA drive train is depicted in which all forces and torques acting on the system are shown. The efficiency of all transmission components has been set to 100 % for this dynamic evaluation. The driving axles are assumed to be rigid and the ratio speed change of the CVT $\frac{di_{cvt}}{dt}$ has not been taken into account.

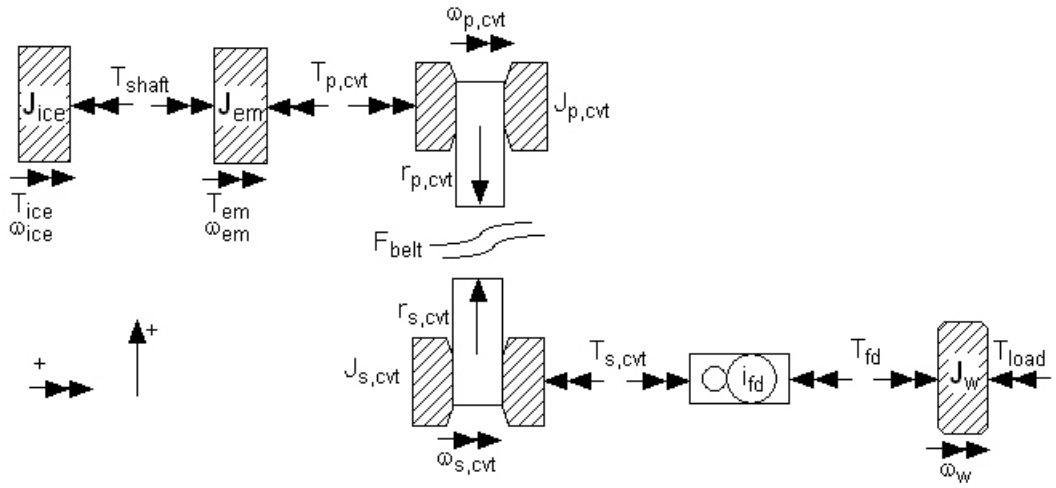

Figure G.3: The fores and torques working on the entire system

The following equations express the moments of equilibria of the different subsystems

$$T_{ice} - T_{shaft} = J_{ice}\,\dot{\omega}_{ice}, \tag{G.4}$$

$$T_{shaft} + T_{em} - T_{p,cvt} = J_{em}\,\dot{\omega}_{em}, \tag{G.5}$$

$$T_{p,cvt} - F_{belt}\,r_{p,cvt} = J_{p,cvt}\,\dot{\omega}_{p,cvt}, \tag{G.6}$$

$$-T_{s,cvt} + F_{belt}\,r_{s,cvt} = J_{s,cvt}\,\dot{\omega}_{s,cvt}, \tag{G.7}$$

$$T_{fd} - T_{load} = J_w \cdot \omega_w, \tag{G.8}$$

$$T_{s,cvt} \cdot i_{fd} = T_{fd}, \tag{G.9}$$

$$i_{cvt} = \frac{\omega_{p,cvt}}{\omega_{s,cvt}}, \tag{G.10}$$

$$T_{load} = F_t\,r_w. \tag{G.11}$$

When all the linking variables are eliminated, the relation between the torque of the ICE and EM

and the load forces can be derived(Eqation G.12)

$$T_{ice} + T_{em} - J_{tot} \cdot \dot{\omega}_{ice} - \frac{1}{i_{cvt} \cdot i_{fd}} \cdot F_{load} \cdot r_w = 0 \tag{G.12}$$

in which

$$J_{tot} = J_{ice} + J_{em} + J_{p,cvt} + J_{s,cvt} \cdot \frac{1}{i_{cvt}^2} + J_w \cdot \frac{1}{i_{cvt}^2 \cdot i_{fd}^2} \tag{G.13}$$

$$\dot{\omega}_{ice} = i_{cvt} \cdot i_{fd} \cdot \frac{a}{r_w} \tag{G.14}$$

$$F_{load} = F_a + F_r + m \cdot a \tag{G.15}$$

When Eqn G.12 is multiplied by $\frac{i_{cvt} \cdot i_{fd}}{r_w}$ and the equations above are substituted into this equation, the next equation follows

$$(T_{ice} + T_{em}) \cdot \frac{i_{cvt} \cdot i_{fd}}{r_w} - J_{tot}^* \frac{a}{r_w^2} - (F_a + F_r + m \cdot a) = 0, \tag{G.16}$$

in which

$$J_{tot}^* = (J_{ice} + J_{p,cvt} + J_{em}) \cdot (i_{cvt}^2 \cdot i_{fd}^2) + J_{s,cvt} \cdot i_{fd}^2 + J_w. \tag{G.17}$$

Subtract a from Eqn G.16 leads to

$$a = \frac{(T_{ice} + T_{em}) \cdot \frac{i_{cvt} \cdot i_{fd}}{r_w} - (F_a + F_r)}{\frac{J_{tot}^*}{r_w^2} + m} \tag{G.18}$$

in which the additional mass factor can be described by the term $\frac{J_{tot}}{r_w^2}$.

With this model for the vehicle dynamics some acceleration performance simulations have been made. The results are incorporated in a paper which can be found in Appendix F.

The Simulink file, used to compute the driving power, is shown in Figure G.4. Equation 2.20 has been implemented in the block "vehicle dynamics". Some initial values at $t = 0$ have to be defined to close the loop and start the computation. The initial values for the CVT ratio, CVT efficiency and additional mass due to rotation are respectively 0.46 (under drive ratio), 0.6 and $0\ kg$. The power of the ICE is computed using these values and the speed of the ICE can be looked up (OOL tracking is assumed). Together with the wheel speed, the ratio of the CVT is calculated. The CVT efficiency and the additional mass due to rotational inertia can now be computed as well.

G.2 CVT efficiency model

The power loss for a CVT is the difference between input power ($P_{in} = T_{in} \cdot w_{in}$) and output power ($P_{out} = T_{out} \cdot w_{out}$) due to pumping and mechanical losses. The power loss can be divided into torque and speed loss. For implementation it is preferred to lump the speed into the torque losses.

$$T_{loss}(T_{s,cvt}, w_{s,cvt}, i_{cvt}) = T_{pump} + T_{mech} \tag{G.19}$$

This means that

$$w_{s,cvt} = w_{p,cvt} \cdot i_{cvt}, \tag{G.20}$$

$$T_{s,cvt} = \frac{T_{p,cvt} - T_{loss}}{i_{cvt}} = \frac{T_p}{i_{cvt}} \cdot \eta_{cvt}(T_{s,cvt}, w_{s,cvt}, i_{cvt}), \tag{G.21}$$

in which the subscripts p and s represent the primary and secondary pully of the CVT. The efficiency depends on the sign[1] of the torque. When regeneration takes place, the torque on the primary side

[1] $\text{sign}(x) = \frac{x}{|x|}$

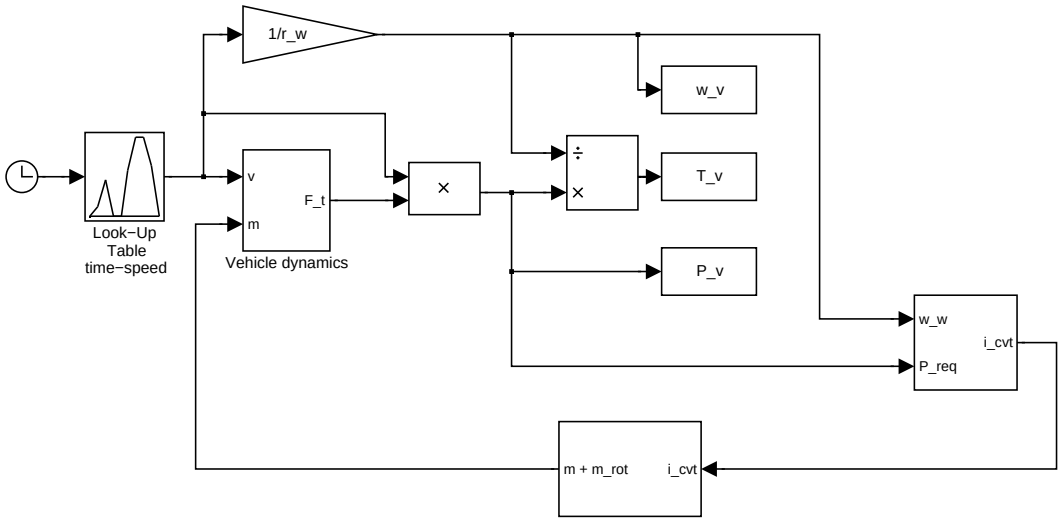

Figure G.4: The Simulink File to compute the driving power.

is lower than on the secondary and therefore the efficiency is higher than 1. Equation G.21 can be represented better by

$$T_s = \frac{T_p}{i_{cvt}} \cdot \eta_{cvt}^{sign(T_p)}(T_{s,cvt}, w_{s,cvt}, i_{cvt}). \tag{G.22}$$

The values for the efficiency are shown in Figure G.5 [33]. The used CVT is a Van Doorne CVT Type 920, a hydraulically actuated metal pushbelt CVT. As can be seen, the efficiency is very sensitive for low torques.

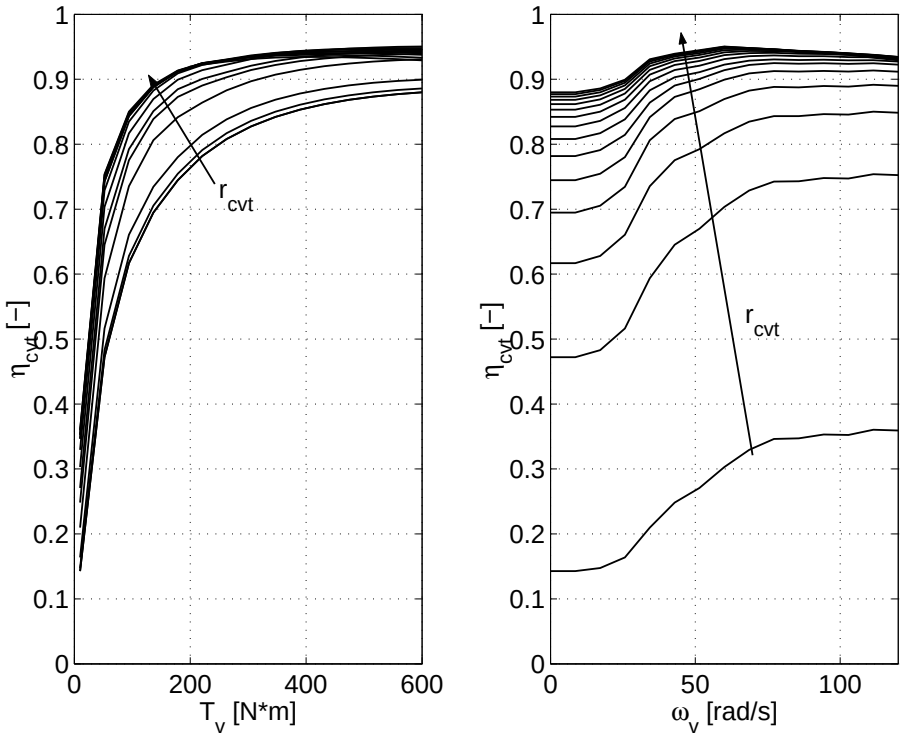

Figure G.5: The efficiency as a function of vehicle torque and speed for the CVT

Validation CVT model

The Honda Jazz is a conventional vehicle available with the same CVT as the Honda Civic IMA. To validate the CVT model, the vehicle parameters of the Honda Civic IMA are replaced by the parameters of the Jazz. The simulated values for the fuel consumption are in Table G.1. These results differ +/- 9% from the catalogue values. Up to 4% of this difference can be declared by the cold-warm engine phenomenon (See Chapter 3.2). The resting 5% is probably caused by the difference in CVT control and other model uncertainties. During the simulation, OOL tracking has been assumed. In reality the control strategy for a CVT is not controlled over the OOL to obtain a better dynamic performance. This causes an increase in fuel consumption. The CVT model is implemented in the conventional IMA too. The slightly higher fuel consumption is caused by the extra mass.

model	City $[l/100\ km]$	Highway $[l/100\ km]$	Combi $[l/100\ km]$
CVT Jazz	6.46 (7.2)	4.72 (5.1)	5.38 (5.9)
CVT IMA	6.69	4.92	5.59

Table G.1: Fuel consumption for the conventional Jazz and IMA with CVT. The catalogue values are between brackets.

G.3 Results DP

The results from DP with the CVT model are presented in this section. The entire problem has been implemented with the same steps as the MT (see Chapter 5). During the simuations, OOL tracking is assumed. The control of the CVT is based on this assumption. Due to lack of time, three important aspects have not been taken into account: the CVT efficiency is the most important aspect. The battery and EM efficiency are better than the CVT efficiency. This will probably cause a change in Energy Management Strategy. Furthermore, the auxiliaries power and the engine drag losses are not taken into account.

Basic problem

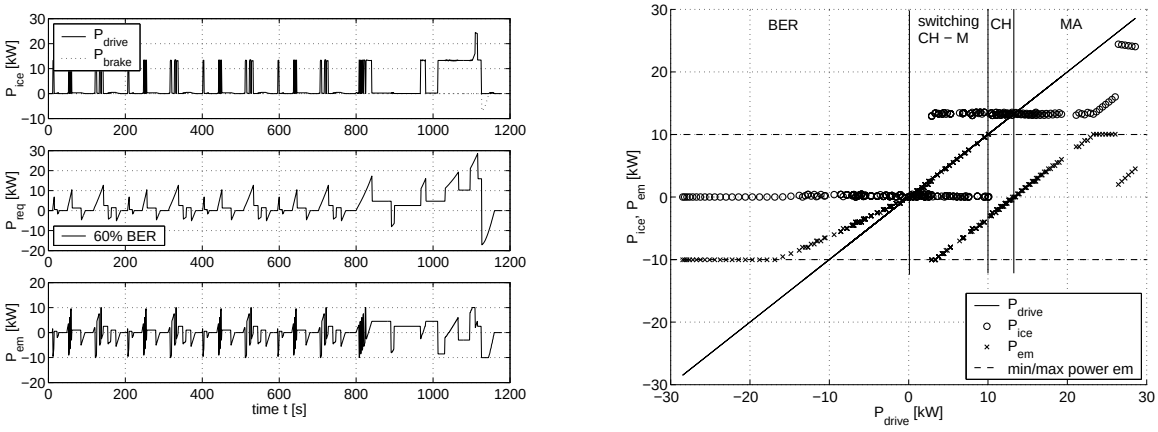

Figure G.6: *left:* The strategy resulting from DP for the basic problem as a function of time *right:* The power split for the basic problem. BER = Brake Energy Recovery mode, M = Motoring mode, MA = Motor assist mode, CH = Charging mode

In Figure G.6 the results for the basic case are shown. TheICE is used in two optima: 13 kW and 24 kW. The switching behaviour described in Chapter 5 can be seen again. Until 10 kW, it drives purely electrical and switches to charge mode. Between 10 kW and 13 kW, the system is in charging mode while above 13 kW the motor assist mode occurs. Until 23 kW, the ICE delivers a constant power of 13 kW. At this point, the maximum power of the EM has been reached which means that the ICE has to operate at higher power to maintain the power equilibrium. When the drive power exceeds 26 kW, the power of the ICE is 24 kW.

Efficiency battery

As can be seen in Figure G.7 the strategy changes drastically due to the implementation of the battery efficiency. Until 2 kW, the vehicle drives electrically. Above 2 kW, the motor assist mode and charging mode alternately occur. The points of 13 kW and 24 kW found in the basic problem and a new point of 9 kW are the mode change points between charge and motor assist. DP tries to keep the battery efficiency above 95% (see Figure G.8, right). Only for recharge, the battery is allowed to have lower efficiencies because the braking energy is "for free" and therefore it is always generated.

When $P_{drive} < 0$, the efficiency of the ICE is up to 10%. This is a result of the grid choice. When the vehicle is decelerating, the ICE has an power in between 0 - dPa (dPa = 1000), which results in efficiencies between 0 - 0.1.

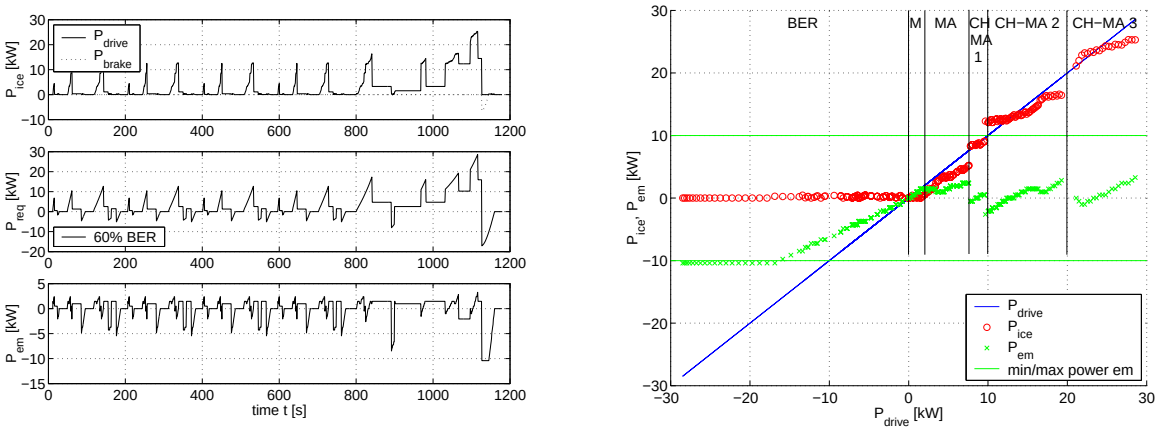

Figure G.7: *left:* The strategy resulting from DP for the battery problem as a function of time *right:* The power split for the battery problem.

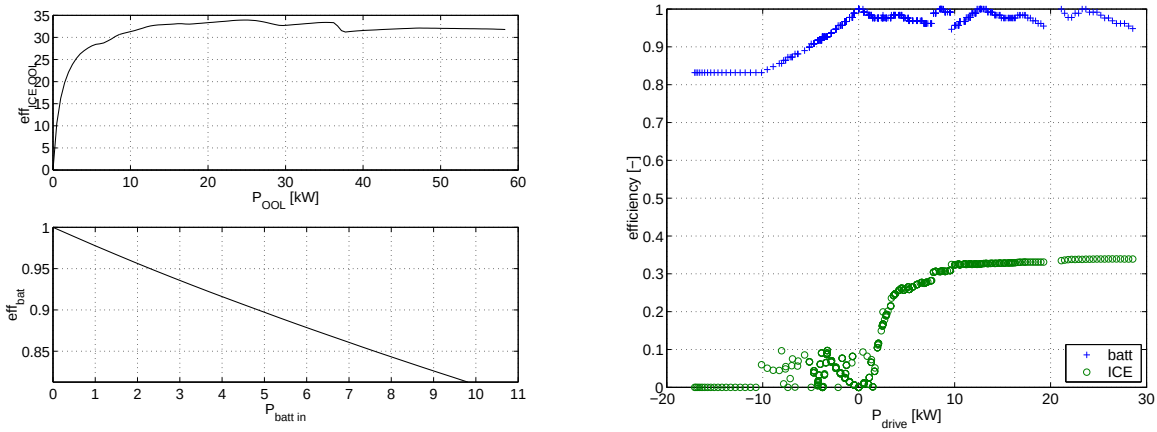

Figure G.8: *left:* The efficiency of ICE over the OOL and battery efficiency as a function of requested power. *right:* The efficiencies following from DP

Efficiency EM

A sequence of engine only and the motor only mode for powers < 15 kW can be seen in Figure G.9. When the power is higher, the motor only mode is replaced by the motor assist mode but the sequence of modes still occurs. At 9 kW, the third engine only region starts. The 13 kW and 24 kW operating points (both switching points E-MA), and the 9 kW and 16 kW points (switching M-MA) can be seen again. Another new remarkable point is 6 kW.

It can be concluded that DP keeps the mean EM efficiency above 87%. The ICE is not used in the regions with high EM efficiency. When the required power is higher than 15 kW, the electro motor is used to let the ICE operate at more efficient operating points. It is remarkable that the charging mode does not occur anymore. The extra amount of fuel needed to charge the battery is too high with respect to the fuel savings during motor assist mode.

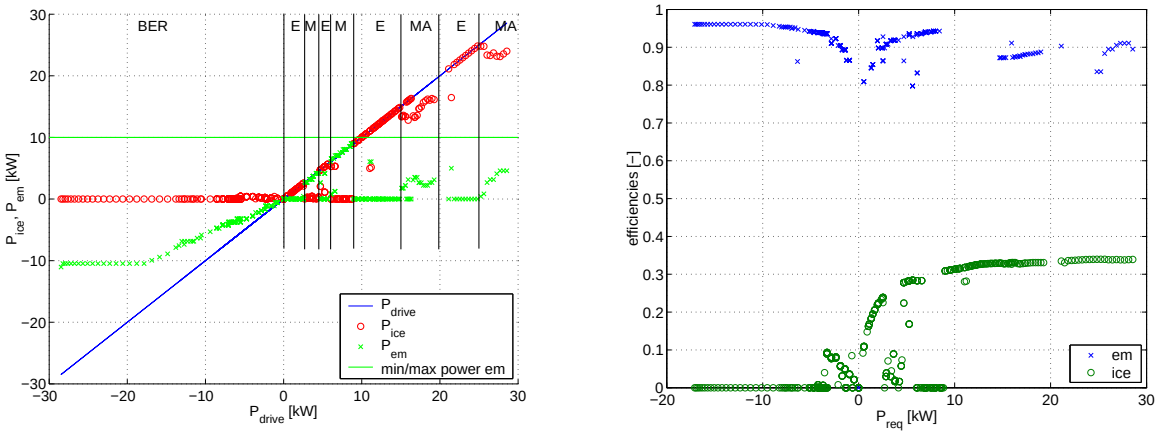

Figure G.9: *left:* The power split strategy resulting from DP for the EM problem *right:* The efficiencies of EM and belonging to the optimal strategy.

Efficiency battery + EM

The optimal power split for the battery + EM case is depicted in Figure G.10 (right). It can be seen that the motor only mode occurs only in the region between 2 and 4 kW (Figure G.11 right). To give an explanation for this phenomenon, the efficiencies of the battery, the electro motor and the system S (battery + EM) have been plotted in Figure G.11 left. The battery efficiency decreases while the electro motor efficiency increases when the requested power is increased. The most optimal region of efficiency S is between 2 and 4 kW and therefor the EM is intensively used in this region.

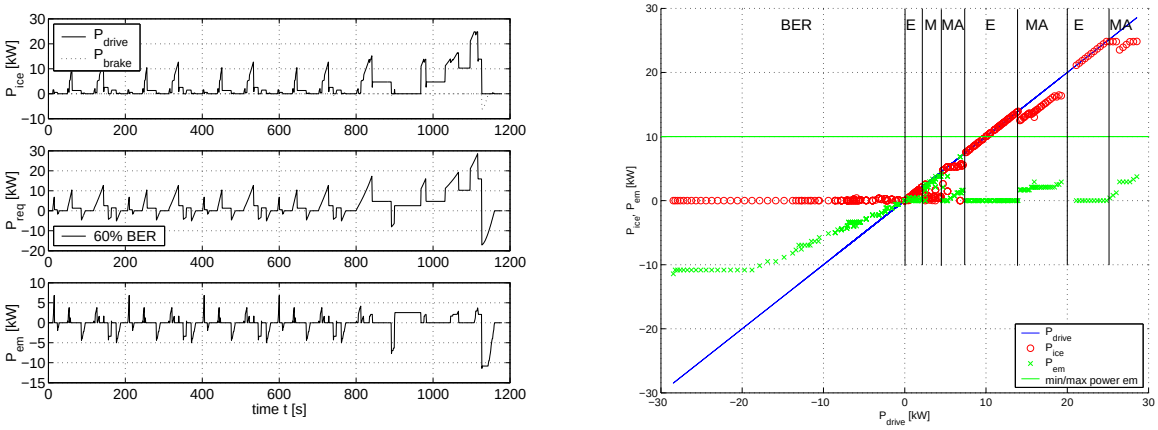

Figure G.10: The power split strategy resulting from DP for the battery + EM problem

After the motor only mode, the mode changes to motor assist at 6 kW. Subsequently, a sequence of engine only and motor assist mode takes place. 13 kW, 16 kW and 24 kW are the mode changing points.

In Figure G.12, the efficiencies of the electro motor, engine and battery for every required driving power is plotted. The different modes can be distinguished in this figure as well. A remarkable area for the engine efficiency during the motor only mode can be seen. The points between 0 and 0.1 are caused by the grid step. The other points in between 0.1 and 0.24 are coming from a few points that are not in the motor only mode. These points can be seen in G.10 as well.
In Table G.2, the fuel consumption rate in grams are give for the four cases. The electro motor causes

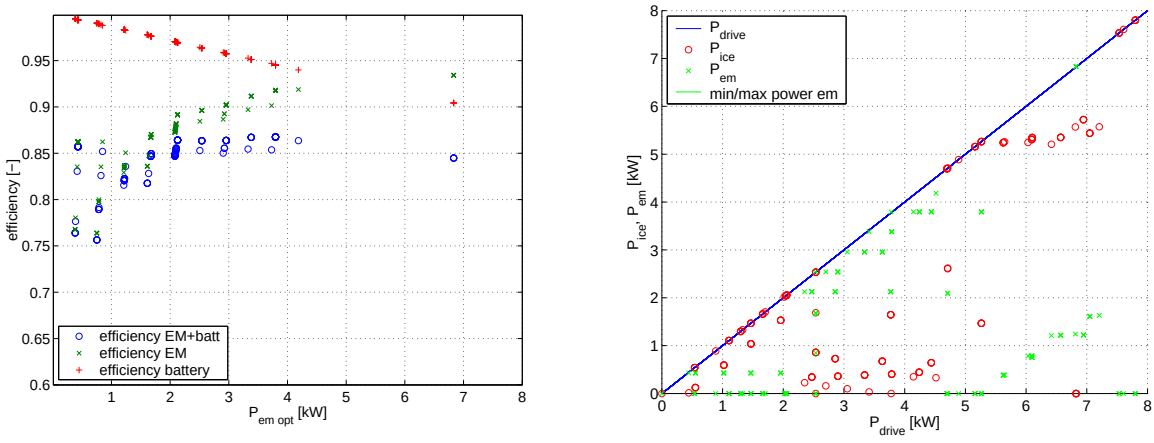

Figure G.11: The power split strategy resulting from DP problem in which battery efficiency has been taken into account

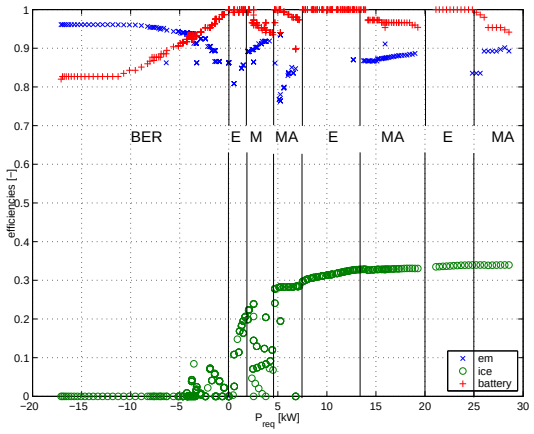

Figure G.12: The battery power

the biggest loss in fuel efficiency.

G.4 Operating points ICE

The mode change points are probably the optima of the OOL efficiency curve. To prove this, the optima have to be exactly defined. The criterium for an optimum are

$$\eta_{OOL}(P_{OOL})' = 0, \tag{G.23}$$
$$\eta_{OOL}(P_{OOL})'' < 0. \tag{G.24}$$

The points which satisfy this criteria are 16.1 (local optimum) and 24.5 (global optimum) kW, see Figure G.13. These points were found in the DP routine as well. The other mode change points occur when no optimum available in de direct region of the requested power. These points seem to be points of inflection(b). For points of inflection , the following criteria are valid:

$$\eta_{OOL}(b-)'' < 0, \tag{G.25}$$
$$\eta_{OOL}(b+)'' > 0. \tag{G.26}$$

	Fuel consumption [g]	Additional fuel consumption [%]
basic	278 g	-
battery	285.3 g	2.6 %
EM	289.7 g	4.2 %
batterij+EM	295.7 g	6.3 %

Table G.2: The fuel consumption for the four cases

The only satisfying points are 5.5, 9.3 and 13.8 kW. These three values were indeed found in the optimization of DP as the mode change points. From these results can be concluded that DP is very sensitive for the derivative of the efficiency.

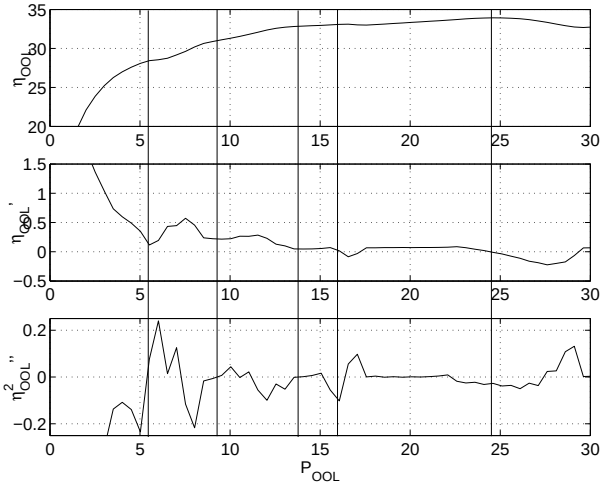

Figure G.13: The OOL efficiency curve (upper figure), the derivative (middle) and second derivative (lower).

G.5 EMS without BER

To investigate the relation between the available breaking power and the power split strategy, a test has been done without Brake Energy Recovery. The results are depicted in the Figures below for the basic (left) and battery+EM (right) cases.
The power split figures for the basic case with and without BER look exactly the same. The histogram method is applied to get more insight in this figure. The frequency for the charge mode without BER (ICE at 13 kW and the EM -9 kW) is 60 times higher than during the case with BER. This means that 60 x 13 = 780 kW is extra generated to make motor assist possible. The situation is completely different for the battery+em case. Motor assist and charge mode do almost not occur. Only around P_{drive} = 9 kW, the ICE delivers 1 or 2 kW more to charge the battery. This power is used for motor assist at 24 kW and higher. This means that power assist at high power is more efficient than power assist at low power.

When the fuel consumption in Table G.3 is studied, it can be concluded that in both cases 10% fuel can be saved by BER.

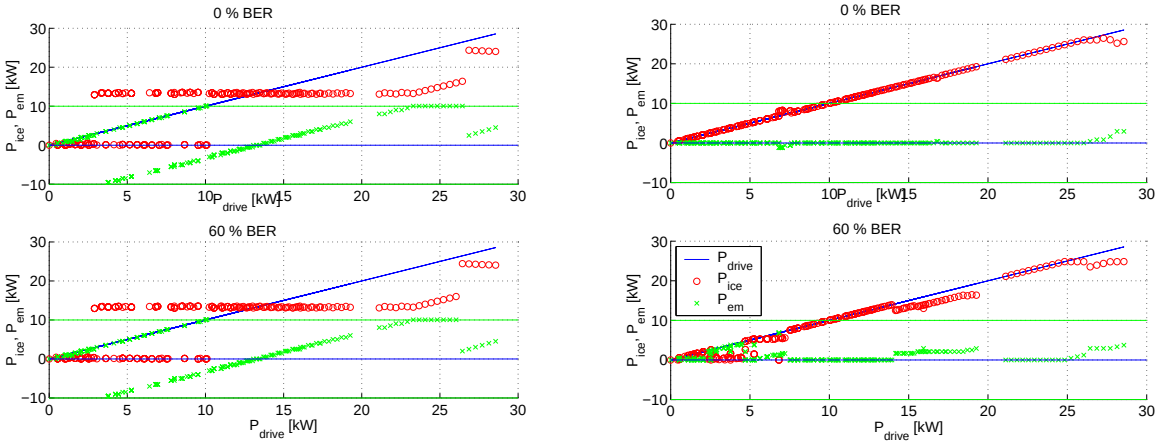

Figure G.14: *Left:* The power split with and without BER for the basic case. *Right:* The battery+EM case.

	0 % BER [g]	60 % BER [g]	Fuel savings [%]
basic	309.1 g	277.9 g	10.1 %
batterij+EM	327.7 g	295.7 g	10.8 %

Table G.3:

G.6 Conclusions DP

A couple of conclusions can be drawn from these simulations:

- When no efficiencies for battery and EM are taken into account, the ICE is operated in two optima: 13 kW and 24 kW. The usage of the EM is only limited by the maximum power and torque constraints. The EM is used for charge and motor only mostly.
- When the battery efficiency is added, a sequence of charge and motor assist mode is observed. The mode change points are optima of the OOL.
- When the EM efficiency is added, two sequences can be observed: E-M and E-MA. Less power remains after charge and discharge due to the efficiency of the EM. For this reason, the engine is used more an no charging takes place anymore.
- After implementing both battery and EM efficiency, the motor only mode is decreased and the engine only mode increased. The mode change points are still the optima of the OOL. The EM is only used in its most optimal region (2 < P_{em} <4 kW).
- BER is an important method for fuel saving. A 10 % decrease in fuel consumption can be seen when the BER mode is disabled.

Recommendations

This study has not yet been finished. To get the complete picture of the EMS for the Honda Civic IMA with CVT, the drag losses, the auxiliaries power and the CVT efficiency has to be implemented. This will probably cause big differences in the EMS.

Appendix H

Matlab Script DP

H.1 Definition grids

```
%%%%%%%%%%%%%%%%%%%%%%%%%%%%%%%%%%%% GRIDS %%%%%%%%%%%%%%%%%%%%%%%%%%%%%%%%%%%%
% define time grid t
t       =   t_v;            % time vector
n_t     =   length(t);      % length time vector
dt      =   t(2)-t(1);      % length time step (=1)

% define energy grid E (state space)
Ecap    =   3.1e6;          % total energy battery
Emin    =   0.3*Ecap;       % minimum constraint
Emax    =   0.8*Ecap;       % maximum constrain
E0      =   0.5*Ecap;       % start/end value
dPa     =   100;            % step in power grid
dEa     =   dPa*dt ;        % stap in energy grid
n_x     =   ceil((Emax-Emin)/dEa)       % number of steps state space
E       =   linspace(Emin,Emax,n_x);    % state space

% define control variabele u
P_s     =   P10.*eff_batt;      % [-10 10] : P_batt
Pmax    =   P_s(end);           % Max internal battery (P_s) power chg battery (8736 W)
Pmin    =   P_s(1);             % Min internal battery (P_s) power dis battery (-12351 W)
umax    =   ceil(Pmax/dPa);     % maximal control step
umin    =   floor(Pmin/dPa);    % maximal control step
u       =   umin:umax;          % control vector u
n_u     =   length(u);          % length control vector
P_s_grid    =   u.*dPa;         % definition grid P_s
P_em_grid   =   interp1(P_s,P10,P_s_grid,'linear','extrap') % defenition grid P_batt

% define constraints state grid x
x0 = 1 + ceil((E0-Emin)/dEa);           % intial state value of energy accumulator [-]
xmin    =   [x0 ones(1,n_t-2) x0];      % initialize min constraint
xmax    =   [x0 n_x*ones(1,n_t-2) x0];  % initialize max constraint

umax1   =   floor((n_x-x0)/umax);   % time until upper constraint is reached from x0
umax2   =   floor((x0-n_x)/umin);   % time from upper constraint to x0
umin1   =   floor((1-x0)/umin);     % time until lower constraint is reached from x0
umin2   =   floor((x0-1)/umax);     % time from lower constraint to x0

% max charge until upper constraint
for i = 1:umax1
 xmax(i+1)  =   umax*i + x0;
end
% max discharge from upper constraint to x0
for i = 1:umax2,
 xmax(n_t-i) =  n_x + umin*(umax2-i);
end
% max discharge from x0 to lower constraint
for i = 1:umin1,
 xmin(i+1)  =   x0+umin*i;
end
% max charge from lower constraint to x0
for i = 1:umin2,
 xmin(n_t-i) =  1 - umax*(i-umin2);
end
```

H.2 Calculation cost matrix

```
load grids
load power_EUDC

% Control input is P_em_grid: the power between battery and EM
% P_mt is the power at the input shaft of the MT

%%% CALCULATION COST MATRIX %%%

for time = 1:n_t
    %%% 60 % BER %%%
    if P_v(time)<0
        P_mt(time,:)   =   0.6*ones(1,n_u).*P_mt(time);
    else
        P_mt(time,:)   =   ones(1,n_u).*P_mt(time);
    end

    %%% DRAG LOSSES %%%
    if  P_v(time)>=0
        P_drag  =   zeros(1,n_u);
    else
        P_drag_reg(time,:)  =   ones(size(P_em_grid)).*interp1(w_drag,P_drag,w_mt(time),'linear','extrap');%calculate P_drag
    end

        P_mt(time,:)       =    P_mt(time,:)+P_drag_reg(time,:);% P_mt = P_mt + P_drag (less recuperation possible)
        P_em(time,:)        =   P_em_grid.*eff_em(time,:);  % calculation P_em at input shaft MT
        P_ice(time,:)       =   P_mt(time,:)+P_em(time,:);  % equilibrium of power at input shaft MT
        ind                 =   find(P_ice(time,:)<0);      % if P_ice<0: index P_brake (negative engine powers not allowed)
        P_brake(time,:)     =   zeros(1,n_u);               % initiate P_brake
        P_brake(time,ind)   =   P_ice(time,ind);            % P_brake
        P_ice(time,ind)     =   0;                          % Negative powers ICE not allowed: idle
        w_ice(time,:)       =   interp1(P_eline,w_eline,P_ice(time,:),'linear','extrap');   % calculate w_ice
        T_ice(time,:)       =   P_ice(time,:)./w_ice(time,:);       % calculate T_ice
        w_em_grid(time,:)   =   w_ice(time,:);                      % calculate w_em
        T_em_grid(time,:)   =   P_em(time,:)./w_em_grid(time,:);    % calculate T_em

        % CALCULATION FUEL CONSUMPTION FOR EACH CONTROL INPUT
        C(time,:)           =   interp2(fc_map_spd,fc_map_trq,fc_fuel_map_gps,w_ice(time,:),T_ice(time,:),'linear');

            % torque constraint: indexing when constraint violated
            % !!! T_em_grid = neg: motor:
            T_max(time,:)               =   -interp1(w_em,T_em_max,w_em_grid(time,:));
            ind_T_max                   =   find(T_em_grid(time,:)< T_max(time,:));
            T_em_grid(time,ind_T_max)   =   T_max(time,ind_T_max);
            % minimum torque line: indexing when constraint violated
            % !!! T_em_grid = pos: generate
            T_min(time,:)               =   -interp1(w_em,T_em_min,w_em_grid(time,:));
            ind_T_min                   =   find(T_min(time,:)<T_em_grid(time,:));
            T_em_grid(time,ind_T_min)   =   T_min(time,ind_T_min);
         C(time,ind_T_max)       =   Inf;                % infinitive value when max constraint violated
         C(time,ind_T_min)       =   Inf;                % infinitive value when min constraint violated
         % calculate efficiency EM for next time step
         eff_em(time+1,:)   =   1./interp2(T_em,w_em,eff_map_em,-T_em_grid(time,:),w_em_grid(time,:)).^sign(P_em(time,:));

        if P_v == 0 %%% IDLE STOP %%%
        ind             =   find(P_em(time,:)==0);    %  if P_em and P_v = 0: P_ice = 0: idle stop
        C(time,ind)     =   0;                        %  if idle stop: C = 0
    end
end
```

H.3 Routine DP

```
%%%%%%%%%%%%%%%%%%%%%%%%%%%%%%%%%%%%%%%
%%% Calculation cost-to-go Matrix L %%%
%%%%%%%%%%%%%%%%%%%%%%%%%%%%%%%%%%%%%%%

% n_x the is number of state space steps
% u is the control vector
% C is the cost matrix

L               =   inf*ones(n_x,n_t);  % initialization cost-to-go matrix
L(n_x+1-x0,1)   =   0;                  % costs at x0, t=0 are 0

for i=1:n_t-1;          % time step
    xmi    =   xmin(i);         % xmin at time i
    xma    =   xmax(i);         % xmax at time i
    for pos   =   xmi :  xma;       % for state from xmin -> xmax
        for j=1:n_u;                    % control step
            from_pos    =   n_x+1-pos ; % position state space (upside down construction)
            step_u      =   u(j) ;      % control j
            to_pos      =   from_pos-step_u;    % new position
                if to_pos>n_x+1-xmin(i+1)       % if to_pos outside feasible domain
                disp('smaller than xmin')
                elseif to_pos<n_x+1-xmax(i+1)   % if to_pos outside feasible domain
                disp('bigger dan xmax')
                else                            % to_pos binnen grid: berekenen C matrix
                cost_t  =   C(j,i);                 % costs: from C at time i, with control j
                costs   =   L(from_pos,i)+cost_t;   % calculate new costs (costs previous node + cost for this step)
                    if costs < L(to_pos,i+1)        % if the costs are lower at the new node
                    L(to_pos,i+1)   =  costs;       % Replace with lower costs
                    N(to_pos,i+1)   =  from_pos;    % save node matrix N with optimal nodes
                    else
                    disp('costs are higher')
                    end
                end
        end
    end
end
```

Appendix I

DP Results for the MT

The results of DP are represented in figures in this appendix. In all figures, the circles represent the ICE and the crosses the EM.

The electro motor power (P_{em}), the engine power (P_{ice}), the drive power (P_{drive}) and the change in SOC are depicted in the left upper figure. In the right upper figure, the component efficiencies at every drive power are shown. The left and right middle figures are respectively the operation points of the EM and ICE. The strategy defined by DP can be depicted by a power split figure. In such a figure, the electro motor power (P_{em}) and the engine power (P_{ice}) are plotted against the drive power (P_{drive}) at every time step. The maximum/minimum power line of the EM (+ and - 10 kW) is depicted as well as a line of 60% of the drive power for regeneration and 100% of the drive power when $P_{drive} > 0$. The same kind of figure is made for the torque split as well. In the lower two figures, the power and torque split defined by DP are depicted.

I.1 Basic

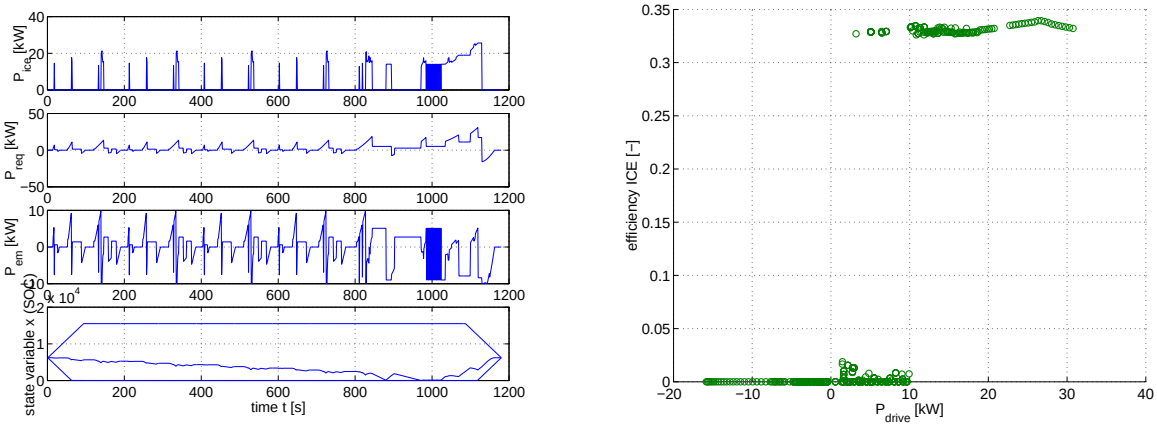

Figure I.1: Basic: (left) The power provided by the ICE and EM and the change in SOC during the cycle. (right) The efficiency of the ICE as a function of the requested drive power.

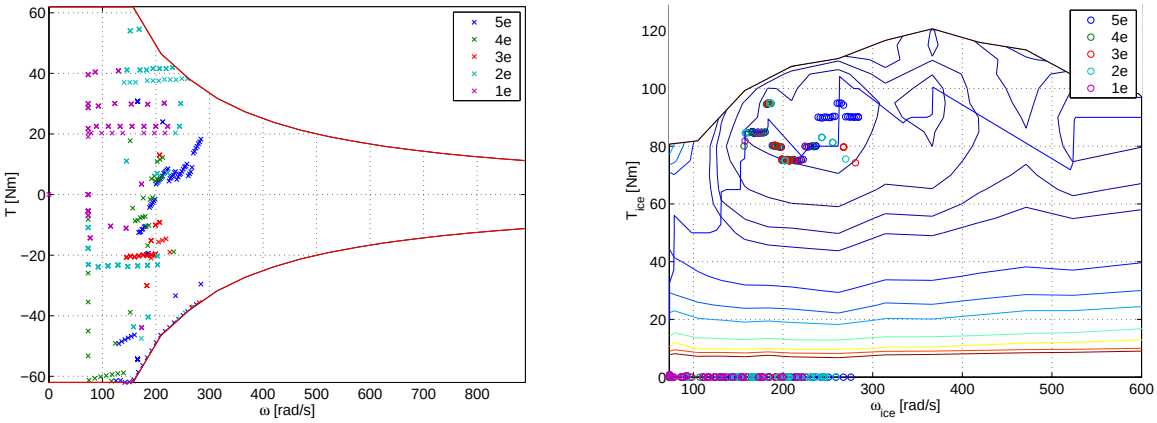

Figure I.2: Basic: (left) The operating points for the EM. The entire area between $\omega_{em} = 75$ and 300 rad/s is used. (right) All operating points of the ICE are close to the sweet spot.

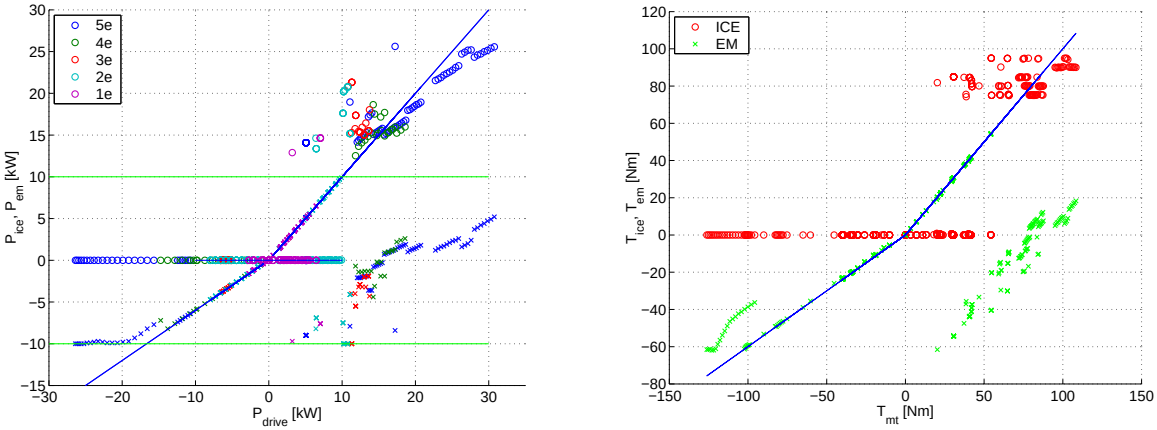

Figure I.3: Basic: (left) Power split: Until 10 kW: Motor Only mode (M) switching with Charge mode (CH). Between 10 - 15 kW: CH. Above 15 kW: Motor assist (MA). (right) The torque split: Electric drive until 60 Nm. Switching from M to CH can be seen as well.

I.2 Battery

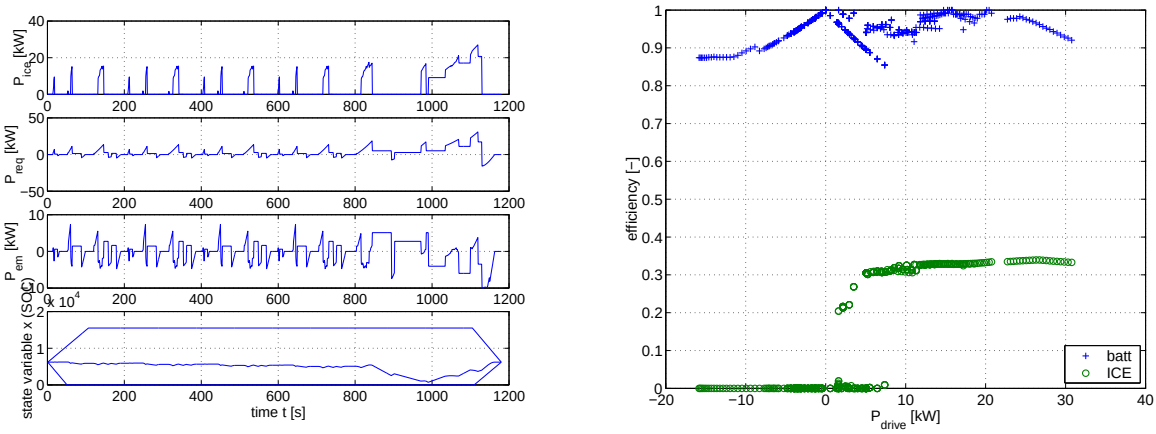

Figure I.4: Battery: (left) The switching behaviour does not occur anymore. (right) The mean efficiency of the battery is 0.95 %. The ICE shows some points with lower efficiency (0.2).

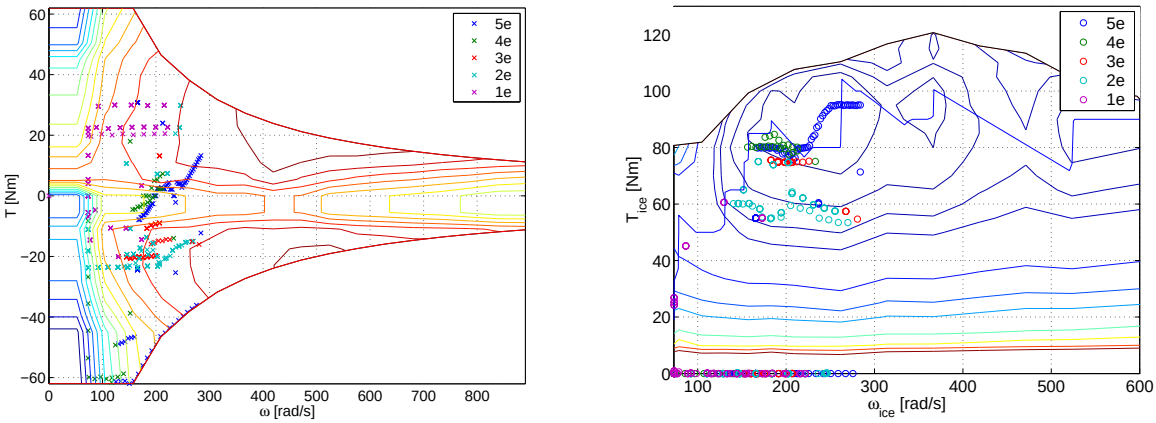

Figure I.5: Battery: (left) The EM is not used above T_{em} = + or - 30 Nm anymore in motoring mode. (right) Mainly the second gear points drop down the sweet spot because the EM does not recharge below -5 kW anymore (in CH mode), see Figure I.6 left.

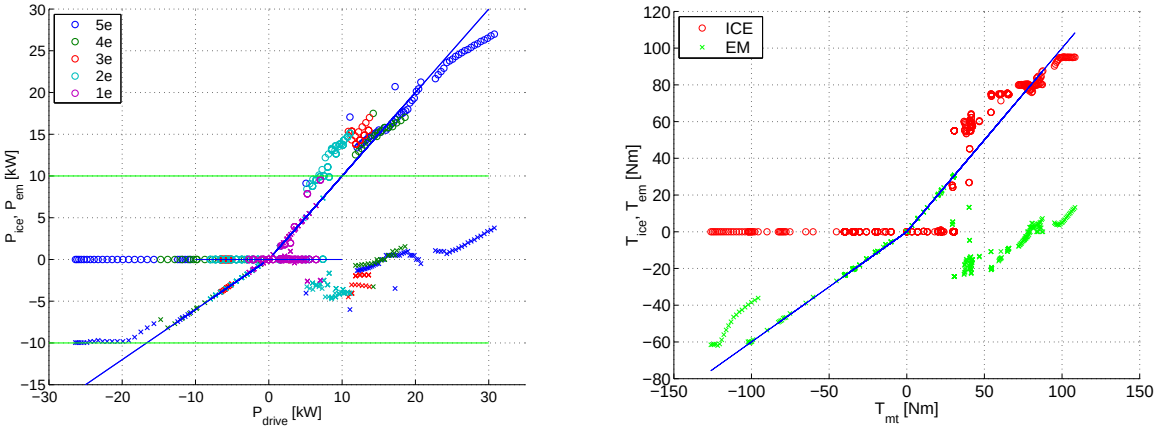

Figure I.6: Battery: (left) Until 5 kW mainly motoring mode (M), between 5 - 15 kW: CH, Above 15 kW: MA (right) Until 20 Nm, M. between 20 - 70 Nm: CH, above 70 Nm: MA

I.3 EM

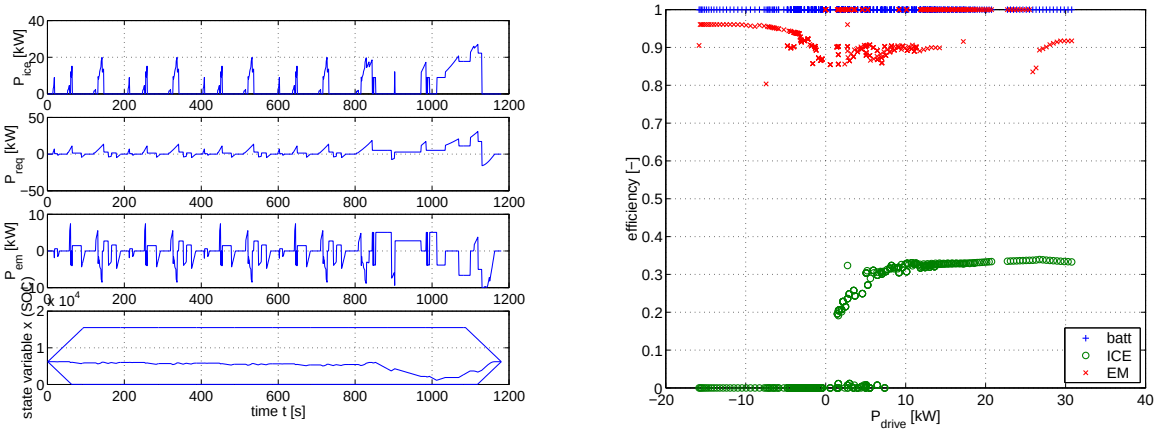

Figure I.7: EM: (left) The power split as function of time (right) Mean efficiency of the EM during motoring is 89 %. ICE does not operate between 0 -1.5 kW: bad efficiency

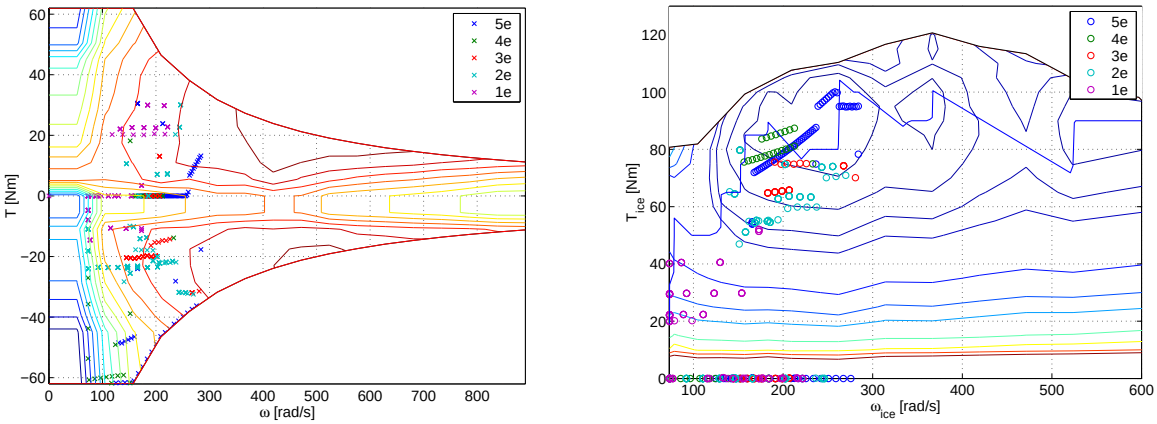

Figure I.8: EM: (left) The operating points for motoring are only in the high efficiency region. (right) Some first gear points are spotted in the low efficiency region of the ICE. The points were covered by the EM in the basic/battery case.

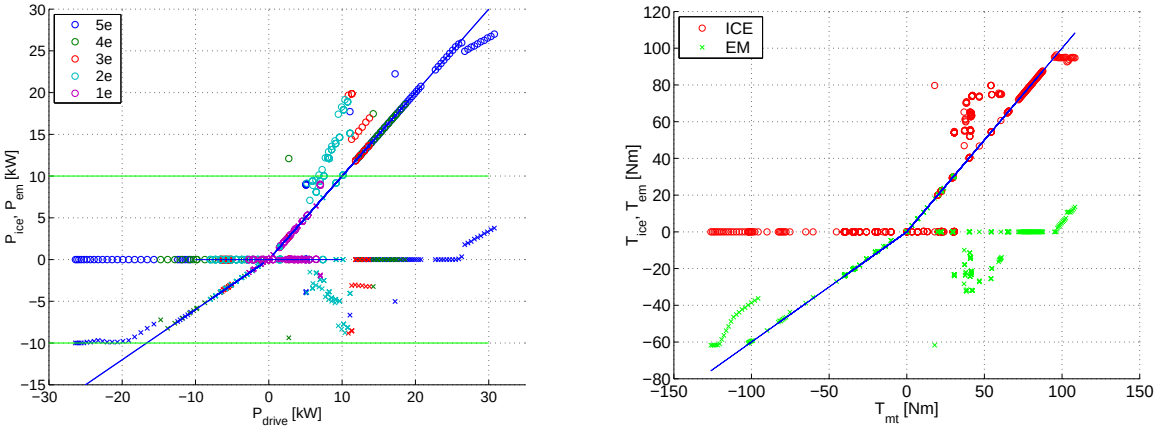

Figure I.9: EM: (left) Until 5 kW: Engine only or Motor only. Now, an engine only region between 15 - 25 kW can be seen. (right) Below 20 Nm, the electro motor delivers all the torque.

I.4 Battery+EM

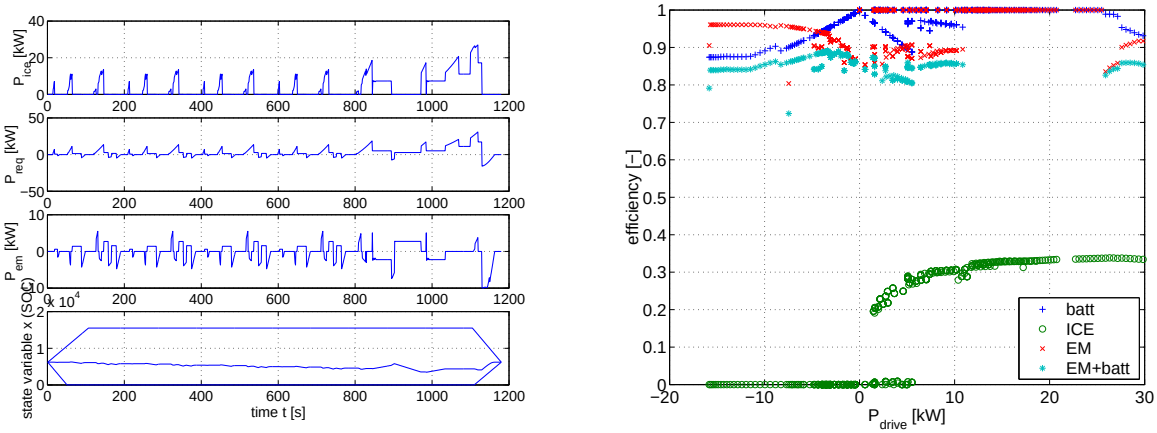

Figure I.10: EM: (left) The power split as function of time (right) Mean efficiencies remain the same: Battery: 95 %, EM: 89 %, battery+EM: 85%

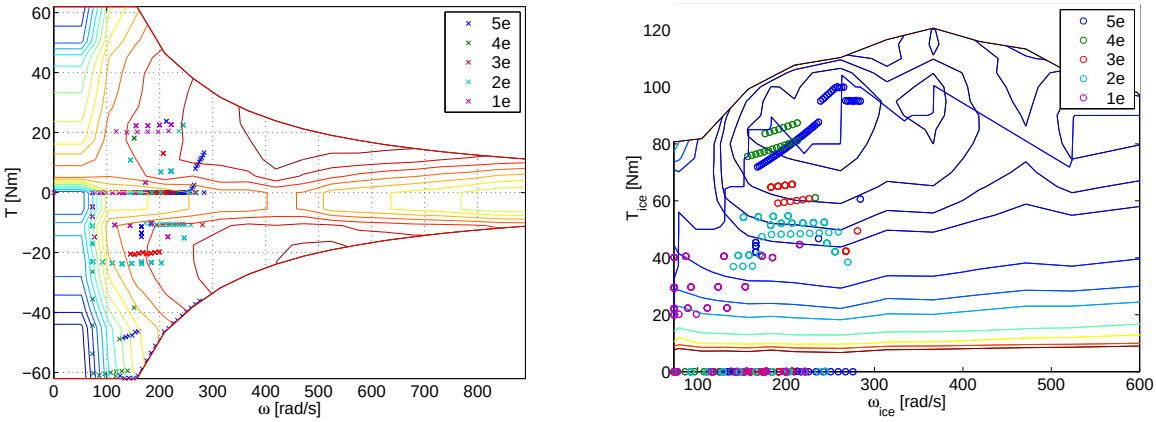

Figure I.11: EM: (left) Motoring and recharging mode take place less often. (right) The operating points for second and third gear have dropped +/- 20 Nm resulting in lower efficiency

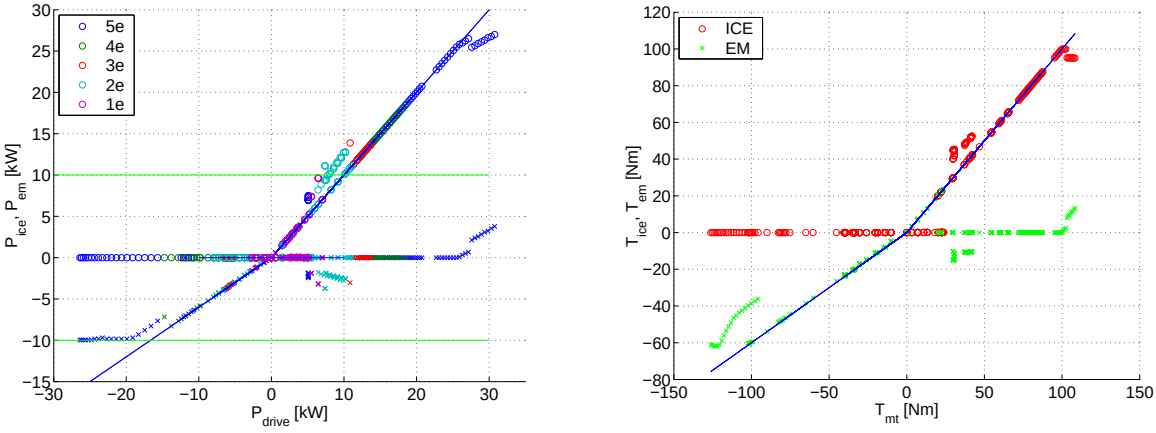

Figure I.12: EM: (left) Less activity in power split. Especially at low driving power, the modes can not defined very well. (right) In the torque split figure, the modes can be defined more easily.

I.5 Honda Civic IMA

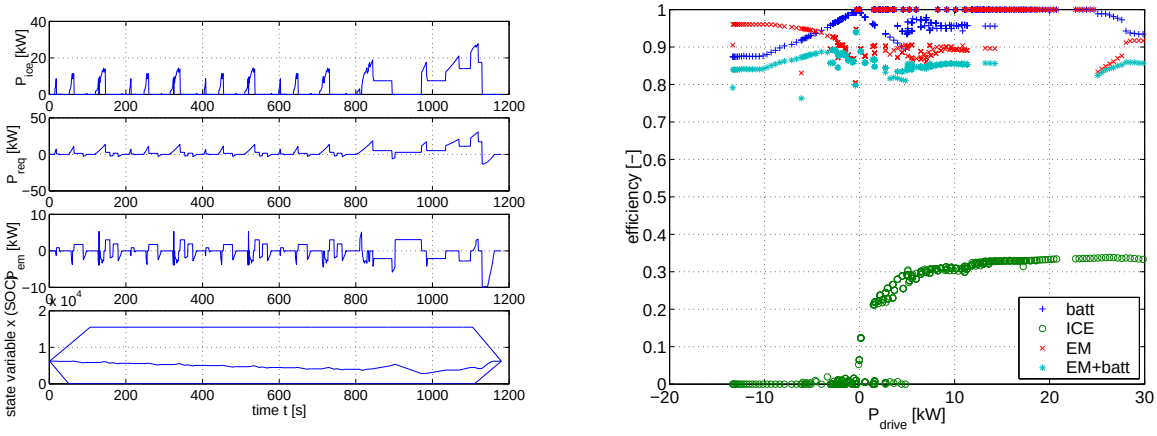

Figure I.13: Honda Civic IMA (left) The power split as function of time (right) The efficiencies of the components remain more ore less the same

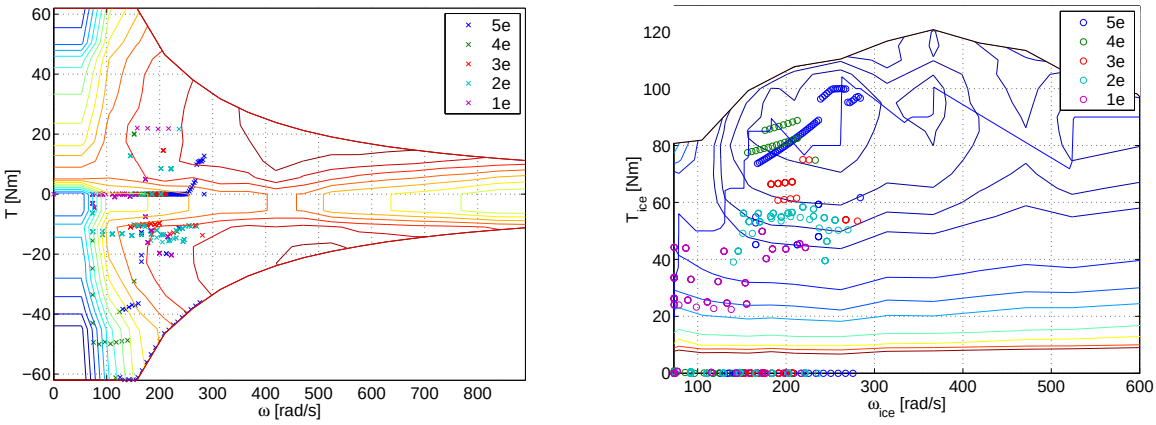

Figure I.14: (left) The recharging mode occurs more often to compensate for the energy used by the auxiliaries and the losses due to drag. (right) The operating points look a bit like the conventional case. However, the are positioned closer to the OOL

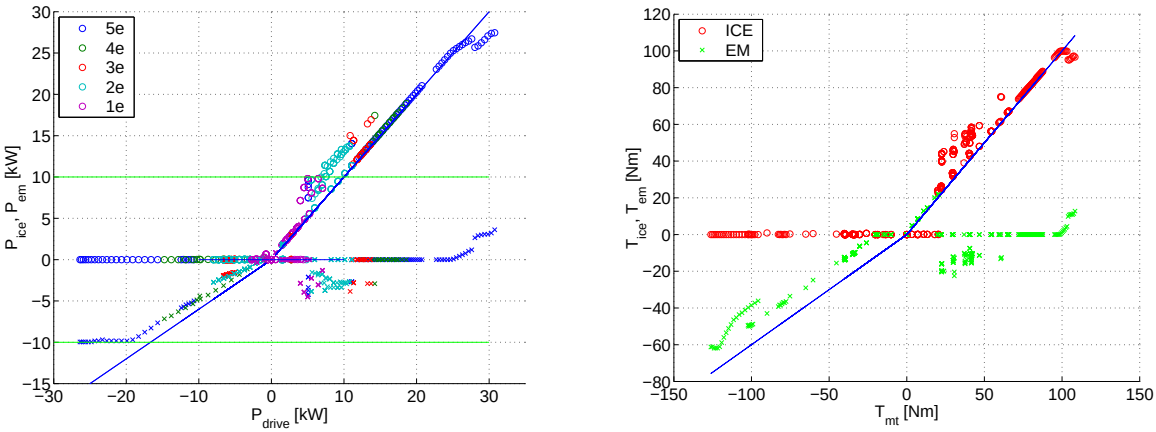

Figure I.15: (left) More recharging can be seen in the power split. (right) The motor only mode still occurs until 20 Nm

Appendix J

Constant Efficiency

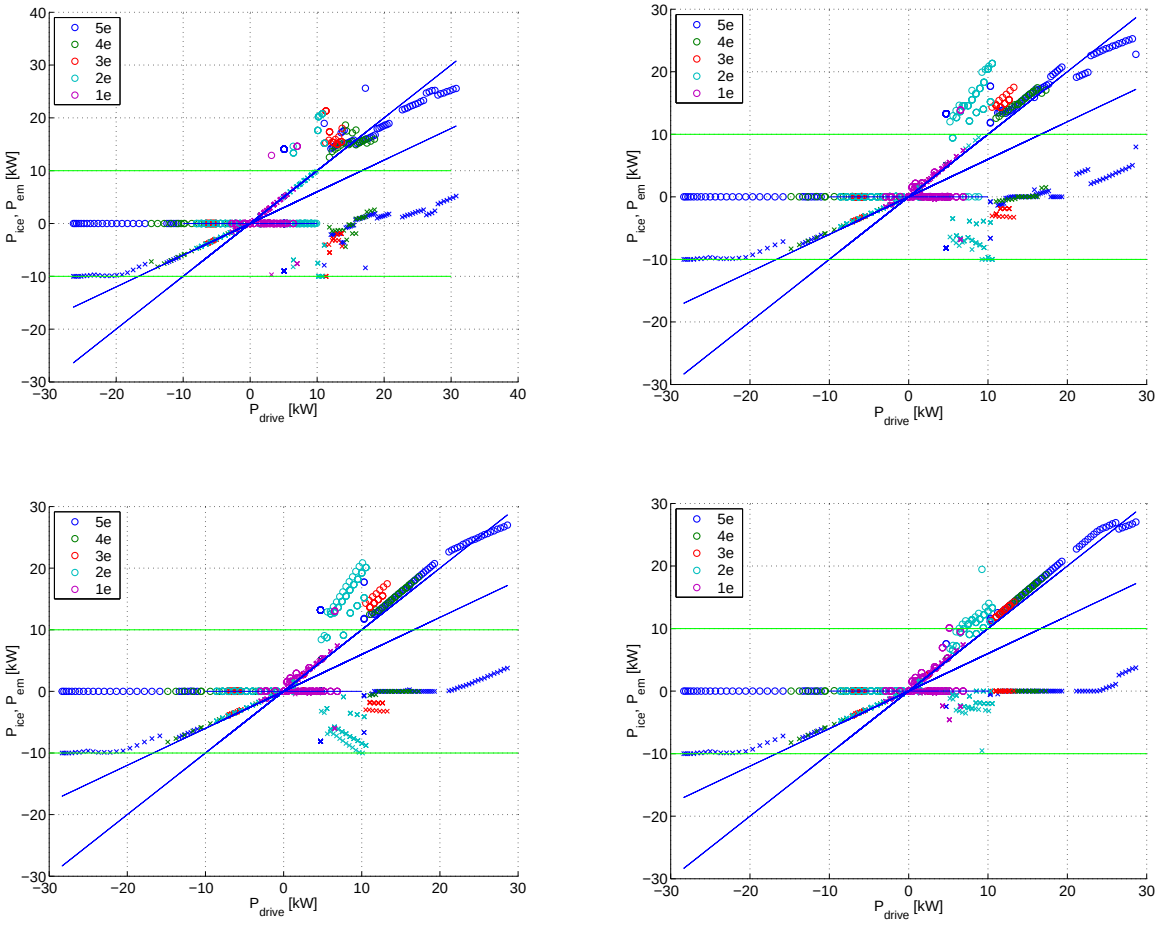

Figure J.1: Top left: $\eta_s = 1$ (Basic), Top Right $\eta_s = 0.95$ (Battery), Bottom left: $\eta_s = 0.9$ (EM), Bottom Right $\eta_s = 0.85$ (Battery+EM